

Gelation and Melting Point Depression in PVDF-based Gel Electrolytes



Raid Khider Salman

School of Physics and Astronomy

The University of Leeds

Submitted in Accordance with the Requirements for the Degree of
Doctor of Philosophy

February 2014

Declaration

The candidate confirms that the work submitted is his own and that appropriate credit has been given where reference has been made to the work of others.

This copy has been supplied on the understanding that it is copyright material and that no quotation from the thesis may be published without proper acknowledgement.

To ... The great Master (Prophet Mohammed)
To ... the sweet heart of love and kind (My Mother)
To ... My lantern in the dark of life (My Father)
To ... who supported me with love and patience in my Foreignness
(My beloved Wife)
To ... Little angles (My Kids)
To ... My Brother and Sisters
To ... My Relatives
To all the good friends
I dedicate this works

Raid

Acknowledgement

In my study here in the UK, I have met a lot of kind people without whom this work would not have been able to come to life.

First and foremost, I would like to give my thanks to my supervisors Dr. Alison Voice and Professor Ian Ward for their guidance and advice, which greatly helped me in producing my thesis to such a high academic quality. I would like to give my highest thanks and gratitude to Professor Peter Olmsted, who supported me during stages of my research when I really needed it, and who was indeed my best support team. My gratitude is also dedicated to the sweethearts Mrs. Glenys Bowles and Mrs. Faith Bonner, for their administration advice and support. My thanks also to Dr. Peter Hine, Dr. Eric Lewis, Dr. Mark Bonner, Mr. Simon Wellings and Dr. Hugh Hubbard, who gave their time to help and support me with the relevant experimental techniques, as well as providing very helpful advice regarding sample preparation and experimental work. I would also like to thank the mechanical and electrical workshop team, who were wonderfully disciplined men and did their best to design and build any part or apparatus needed for the experimental work.

My highest thank to my colleagues, who become my second family in the school during my study, and in particular my roommate Peter Richardson and the other nice guys Daniel Baker, Robin Richardson Raffaella Cabriolu and Asmaa El Sheshiny. Our discussions were really helpful, supportive and constructive for me. My thanks also go to Dr. Manan Ali, for his support during the study.

Lastly, and not least, I would like to thank Dr. Timothy Stevenson and Timothy Comyn in the School of Process, Environmental and Materials Engineering for their great help and for their permission to use their equipment.

Thanks to everybody who has given me aid in this hard, long and stressful journey to acquiring the honour of the PhD.

Abstract

This thesis presents the designs and results of experimental investigations into gelation and melting point behaviour for polymer gel electrolytes. The study used one of the most prominent types of materials in the commercial world—polyvinylidene fluoride-based (PVDF) gel electrolytes—focussing on the effects of gelation temperature and gel composition on the properties of its solid electrolytes. While PVDF was used as the polymer matrix, propylene carbonates (PC) and diethyl carbonate (DEC) were used as solvents.

Lithium tetrafluoroborate (LiBF_4) and lithium bisoxalatoborate (LiBOB) were used as the electrolyte salts. Gelation from molten PVDF solutions was studied isothermally, using 30% PVDF/PC unsalted and 30% PVDF/PC/ LiBF_4 salted gels to investigate the effect of salt addition on gelation behaviour. Crystallisation behaviour and subsequent melting was also investigated. Varying the gel composition involved changing polymer concentration, solvent nature and salt concentration. The measured properties included gel structure and morphology, melting point and ionic conductivity.

The techniques of DMTA, DSC, WAXS, dielectric spectroscopy and optical microscopy were used to investigate gelation behaviour and gelation properties. It was found that gelation time is significantly increased at higher temperatures, and that the addition of salt reduces gelation time at any given temperature whilst extending the gelation process to higher

temperatures. Gelation occurs without crystallisation at high temperatures, whereas it is induced by crystallisation at low temperatures. The sharp cut-off for crystallisation gives two distinct temperature windows, within which gelation occurs via different mechanisms.

The addition of salt has found to raise the gel melting point by about 25°C for 1M LiBF₄, and hence to enhance its thermal stability, which is attributed to the salt affecting the Flory interaction parameter. Salt also reduces crystal size and gel pore size, and this is attributed to the nucleating effect of the salt molecules. The incorporation of up to 40% DEC in the solvent increases the gel melting point by 5 to 10 °C, and is accompanied by a negligible reduction in ionic conductivity, which shows a possible route for further enhancing the properties of the electrolytes.

Abbreviations and Symbols

A_H	Helmholtz free energy
DMTA	Dynamic mechanical thermal analyses
DSC	Differential scanning calorimetry
E_c	Cohesive energy
G'	Storage shear modulus
G''	Loss shear modulus
G_{mix}	Gibbs free energy of mixing
K_B	Boltzmann's constant
$LCST$	Lower critical solution temperature
L_{hkl}	Crystal size
$LiBF_4$	Lithium tetrafluoroborate
$LiBOB$	Lithium Bis(oxalatoborate)
R	Gas constant
T_{gel}	Gelation temperature
T_m	Gel melting temperature
T_m^o	Melting point of pure polymer
U	Internal energy
$UCST$	Upper critical solution temperature
V_{pol}	Molar volume of the polymer
V_{solv}	Molar volume of the solvent
γ	Shear strain

δ	Solubility parameter
δ_d	Dispersed solubility parameter
δ_H	Hydrogen bonding solubility parameter
ΔH_{mix}	Change in the enthalpy of mixing
δ_P	Polar solubility parameter
ΔS	Change in the entropy
v	Volume fraction
σ	Ionic conductivity
T	Shear stress
χ_c	Polymer crystallisation percentage
χ_F	Flory interaction parameter

Contents

Declaration	ii
Acknowledgement	iv
Abstract	vi
Abbreviations and Symbols	viii
Contents	x
Table of Tables	xiii
Table of Figures	xiv
Chapter1. Introduction and Literature Review	1
1.1 Introduction	1
1.1.1 Polymer gel electrolytes	2
1.2 Earlier studies on polymer electrolytes.....	4
1.2.1 PVDF-gel electrolytes	6
1.3 Aims of the study.....	9
Chapter2. Theoretical Background	11
2.1 Introduction	11
2.2 The definition of a ‘gel’ and gelation concepts in polymers	12
2.3 The gelation mechanism	13
2.4 Phase separation	13
2.5 Crystallisation from solution	18
2.6 Polymer solutions and the thermodynamics of gel formation	20
2.6.1 Gelation from solution	20
2.6.2 Fundamental theories of gel formation.....	21
2.6.3 The Flory-Huggins treatment for diluted solutions.....	25
2.7 Polymer solubility	28
2.8 Melting point depression	34
2.8.1 The effects of good and poor solvents on melting depression.....	35
Chapter3. Materials and Methods	37
3.1 PGE components	37
3.1.1 Polymer: polyvinylidene fluoride (PVDF)	37
3.1.2 Solvents	41
3.1.3 Electrolyte salts	42
3.2 Gel compositions.....	43

3.2.1	Unsalted gel preparation	43
3.2.2	Salted gel preparation	44
3.3	Sample preparation	50
3.3.1	The glove box.....	51
3.3.2	Hot presser.....	52
3.4	Rheological studies	53
3.4.1	Introduction	53
3.4.2	Dynamic mechanical thermal analyses	53
3.4.3	Rheological instruments: the RSA II machine	55
3.5	Differential scanning calorimetry	57
3.5.1	Introduction	57
3.5.2	The enthalpy of melting.....	58
3.5.3	Polymer and gel crystallinity.....	61
3.6	Ionic conductivity.....	62
3.6.1	The ionic conductivity of polymer electrolyte cells containing blocking electrodes.....	62
3.7	X-Ray scattering analysis (WAXS).....	66
3.7.1	Introduction	66
3.7.2	Bragg's Law	66
3.8	Optical microscopy.....	69
3.9	Measurement procedures	72
3.9.1	DMTA.....	72
3.9.2	DSC 72	
3.9.3	Ionic conductivity.....	74
3.9.4	WAXS measurements.....	74
3.9.5	Optical microscopy.....	76
Chapter 4.	Isothermal Gelation.....	78
4.1	Introduction	78
4.2	Isothermal formation	79
4.2.1	Gelation investigations using DMTA	79
4.2.2	Gelation investigations using DSC measurements	88
4.2.3	Comparing crystallisation and gelation.....	95
4.2.4	Subsequent melting temperature	97
4.2.5	Isothermal optical microscopy	98
4.2.6	Combining DMTA and optical microscopy	99

4.3 Discussion and conclusions	106
Chapter5. The Effects of Gel Composition.....	108
5.1 Introduction	108
5.2 The polymer concentration effect	108
5.2.1 Gel melting points	108
5.2.2 Thermodynamic interpretation of the effect of polymer concentration on the melting depression.....	118
5.2.3 Ionic conductivity	125
5.3 Effect of solvent quality	126
5.3.1 Gel melting points	126
5.3.2 Thermodynamics of mixing	128
5.3.3 The effect of solvent composition on ionic conductivity	131
5.4 The effect of salt.....	132
5.4.1 Gel melting points	132
5.4.2 Ionic conductivity	134
5.4.3 The effects of salt concentration	134
5.4.4 The effects of gel composition on pore size	136
5.4.5 Wide-angle x-ray scattering.....	138
5.5 Discussion and conclusions	142
Chapter6. Conclusions and Future Work	145
6.1 Introduction	145
6.1.1 Phase separation and crystallisation behaviour	146
6.1.2 The effect of gel composition	147
6.2 Future Work	149
References.....	150

Table of Tables

Table 3-1 PVDF crystal forms and their corresponding attributes[115]	40
Table 3-2 PVDF crystal phases and their corresponding crystal planes.....	41
Table 3-3 Room temperature physical properties of PVDF, PC, DEC and LiBF ₄	46
Table 3-4 PVDF concentrations and equivalent masses	47
Table 3-5 LiBF ₄ concentrations and the corresponding masses.	47
Table 3-6 LiBOB concentrations and the correspond masses.	47
Table 3-7 PVDF concentrations and equivalent masses in an electrolyte solution of PC/LiBF ₄ 1M	48
Table 3-8 composition of PC:DEC mixed solvents gels.	50
Table 4-1 Average values of times of isothermal gelation from DMTA measurements. A dash shows that the experiment was undertaken but no gelation took place.....	87
Table 4-2 Onset times and areas of crystallisation peaks under isothermal conditions. The dashes show an isothermal experiment has been undertaken, but that no crystal peak has been observed.....	93
Table 5-1 The effect of PVDF concentration on the melting point of PVDF/PC/LiBF ₄ 1M salted gel and PVDF/PC unsalted gel.	115
Table 5-2. Hansen solubility parameters at room temperature.	119
Table 5-3 PVDF density and linear parameters [Welch and Miller data][146]	121
Table 5-4 PVDF densities and molar volumes in relation to melting temperatures, acquired from the density extrapolated plot provided by Welch and Miller.....	123

Table 5-5 PC densities and their corresponding molar volumes at the measured melting temperatures.	124
Table 5-6 Flory interaction parameters for salted and unsalted gels, as obtained from the melting depression equation.	125
Table 5-7 PC: PVDF/PC:DEC imperial parameters used to estimate heat of mixing.	130
Table 5-8 Crystal sizes found through WAXS for 30PVDF/PC unsalted gel and 30PVDF/PC/LiBF ₄ 1M salted gel.	142

Table of Figures

Figure 2-1 Free energy of mixing as a function of the volume fraction to show mixing possibilities in binary systems[58].	15
Figure 2-2 Phase diagram showing (a) Lower critical solution temperature LCST and (b) Upper critical solution temperature UCST where $T_1 > T_2 > T_3 > T_4$. [57]	16
Figure 2-3 Phase diagram in which the change in Gibbs free energy is plotted as a function of the polymer concentration. ($T_1 > T_2 > T_3 > T_4$). [59]	17
Figure 2-4 Sketch of binodal and spinodal regions in polymer-solvent systems [60].	18
Figure 2-5 Spherulitic structures produced by lamellae formation and grow radially [64].	23
Figure 2-6 Types of thermoreversible cross-links: (a) point cross-links, (b) junction zones and (c) Fringed micelles [71].	23
Figure 2-7 Illustrates Lattice model for two types of solution; (a) The small molecules solution and (b) The polymeric solution in a solvent (the polymer segments are represented by the black liked circles (sectors) while the solvent molecules are shown in grey circles).	27
Figure 2-8 Schematic of PVDF/PC phase diagram.	33
Figure 2-9 Optical micrographs of (a) nucleation and growth and (b) spinodal decomposition in polymer gels[64].	33
Figure 3-1 PVDF's chemical and structural forms [95]	38
Figure 3-2 The three PVDF crystal forms: α , β and γ [116].	39

Figure 3-3 α , β and γ conformation transitions produced using different processes on PVDF [103, 117].	40
Figure 3-4 Schematic view of the glove box	51
Figure 3-5 Hot pressing plates with gel samples in between.	52
Figure 3-6 DMTA Geometries	55
Figure 3-7 Screw-thread Tube Method used with RSA II.	56
Figure 3-8 The RSA II Machine	57
Figure 3-9 Simplified sketch illustrating the DSC technique.	60
Figure 3-10 Heat transitions measured by the DSC.	61
Figure 3-11 Model of the ionic conductivity cell illustrating: (a) A simulated circuit for PGE (2), with thickness (t) and area (A) inserted between two electrodes (1); and (b) The equivalent circuit for the polymer/electrode interfaces, where C_a is the capacitance of the anode, C_c is the capacitance of cathode, R is the internal bulk resistance of the gel, and C_e is the capacitance of the electrolyte.	63
Figure 3-12 The imaginary component plotted against the real component of the impedance for (a) the ideal electrolyte and (b) a typical gel electrolyte.	64
Figure 3-13 Demonstration of Bragg's diffraction law.	67
Figure 3-14 The principle of optical microscopy principle (left), and a sketch of an optical microscope (right) [140].	70
Figure 3-15 Refractive index ellipsoid or what is known as the 'indicatrix' with the crystal involved in it, to understand the crossed-polarisation principal.	72
Figure 3-16 Ionic conductivity cell.	74
Figure 3-17 Sketch of WAXS diffraction technique measurements.	75
Figure 3-18 Sketch of the hot-stage microscopy.	77
Figure 4-1 Isothermal gelation using DMTA for 30PVDF/PC unsalted gel, showing the time at which gelation occurs ($F'=F''$), at (a) 30°C and (b) 60°C.	81
Figure 4-2 Isothermal gelation using DMTA for 30PVDF/PC unsalted gel, showing the time at which gelation occurs' (a) at 90°C, and no gelation in (b) at 100°C.	82
Figure 4-3 Isothermal gelation using DMTA for 30PVDF/PC/LiBF ₄ salted gel, showing the time at which gelation occurs ($F'=F''$), (a) at 30°C and (b) at 60°C.	83
Figure 4-4 Isothermal gelation using DMTA for 30PVDF/PC/LiBF ₄ salted gel, showing the time at which gelation occurs ($F'=F''$), (a) at 90°C and (b) at 120°C.	84

Figure 4-5 Isothermal gelation using DMTA for 30PVDF/PC/LiBF ₄ salted gel, showing the time at which gelation occurs ($F' = F''$), (a) at 140°C, and no gelation is taking place in (b) at 150°C.	85
Figure 4-6 Time to initiate gelation for 30%PVDF/PC unsalted gels and 30%PVDF/PC/LiBF ₄ 1M salted gels. Onset of gelation is determined for $F' = F''$	86
Figure 4-7 Isothermal DSC traces for 30PVDF/PC unsalted gel from 65–75°C, showing no crystallisation at and above 70°C temperatures. The data are offset and combined from different data files.	90
Figure 4-8 Isothermal DSC traces for 30PVDF/PC unsalted gel from 45–60°C. The data here are offset. The data are offset and combined from different data files.	90
Figure 4-9 Isothermal DSC traces for 30PVDF/PC/LiBF ₄ 1M salted gel from 60–70°C. The data are offset and combined from different data files.	91
Figure 4-10 Isothermal DSC traces for 30PVDF/PC/LiBF ₄ 1M salted gel from 45–55°C. The data are offset and combined from different data files.	91
Figure 4-11 Isothermal DSC traces for 30PVDF/PC/LiBF ₄ 1M salted gel from 90–100°C. Note that there is no crystallisation observed at 95°C or above. The data are offset and combined from different data files.	92
Figure 4-12 Isothermal DSC traces for 30PVDF/PC/LiBF ₄ 1M salted gel from 75–85°C. The data are offset and combined from different data files.	92
Figure 4-13 Time to initial crystallisation under isothermal conditions for 30%PVDF/PC unsalted gels and 30%PVDF/PC/LiBF ₄ 1M salted gels, as determined by DSC.	94
Figure 4-14 Heat of fusion of crystallisation plotted as a function of the isothermal crystallisation temperature.	94
Figure 4-15 Time to initiate crystallisation and gelation for 30%PVDF/PC unsalted gels. The onset of crystallisation is determined by the DSC peak. The onset of gelation is determined by $F' = F''$	96
Figure 4-16 Time to initiate crystallisation and gelation for 30%PVDF/PC/LiBF ₄ 1M gels. The onset of crystallisation is determined by the DSC peak. The onset of gelation is determined by $F' = F''$	96
Figure 4-17 Subsequent melting points plotted as a function of isothermal crystallisation temperature for 30%PVDF/PC unsalted gels and 30%PVDF/PC/LiBF ₄ 1M salted gels.	97

Figure 4-18 Heat of fusion of the melting peak following isothermal crystallisation at T_c for 30%PVDF/PC unsalted gels and 30%PVDF/PC/LiBF₄ 1M salted gels.	98
Figure 4-19 Optical Micrographs of heating from room temperature to 160oC for 30PVDF/PC/LiBF₄ 1M salted gel showing structure evolution isothermally. (The top are normal micrographs while below the crossed-polariser micrographs).	100
Figure 4-20 Optical Micrographs of cooling from 160oC to 110oC for 30PVDF/PC/LiBF₄ 1M salted gel showing no crystallisation occurs at this point. (The top are normal micrographs while below the crossed-polariser micrographs).	101
Figure 4-21 Optical Micrographs of cooling from 160oC to 50°C for 30PVDF/PC/LiBF₄ 1M salted gel showing gelation occurs via crystallisation. (The top are normal micrographs while below the crossed-polariser micrographs).....	102
Figure 4-22 Optical Micrographs of heating from room temperature to 160oC for 30PVDF/PC unsalted gel, showing structure evolution isothermally. (The top are normal micrographs while below the crossed-polariser micrographs).	103
Figure 4-23 Optical Micrographs of cooling from 160oC to 80oC for 30PVDF/PC unsalted gel showing low phase separation but no crystallisation this point. (The top are normal micrographs while below the crossed-polariser micrographs).	104
Figure 4-24 Optical Micrographs of heating from room temperature to 160oC for 30PVDF/PC unsalted gel, showing structure evolution isothermally. (The top are normal micrographs while below the crossed-polariser micrographs).	105
Figure 5-1 Heating (10°C/min) DSC traces for unsalted gel from (a) 20PVDF/PC and (b) 25PVDF/PC.....	110
Figure 5-2 DSC traces for unsalted gel from (a) 30PVDF/PC and (b) 35PVDF/PC.....	111
Figure 5-3 DSC traces for unsalted gel from 40PVDF/PC.....	112
Figure 5-4 DSC traces for salted gel from 20PVDF/PC/LiBF₄ 1M.	112
Figure 5-5 DSC traces for salted gel from (a) 25PVDF/PC/LiBF₄ 1M and (b) 30PVDF/PC/LiBF₄ 1M.....	113
Figure 5-6 DSC traces for salted gel from (a) 35PVDF/PC/LiBF₄ 1M and (b) 40PVDF/PC/LiBF₄ 1M.....	114

Figure 5-7 Melting temperature as a function of PVDF concentration for PVDF/PC unsalted and PVDF/PC/LiBF ₄ 1M salted gels.	116
Figure 5-8 Heat of fusion plotted as a function of PVDF concentration for PVDF/PC and PVDF/PC/LiBF ₄ 1M.....	117
Figure 5-9 Degree of crystallisation of the polymer in the gel as a function of PVDF content for PVDF/PC and PVDF/PC/LiBF ₄ 1M.....	117
Figure 5-10 PVDF densities plotted as a function of temperatures at a range from 180–200°C. Note that the data has been extrapolated from room temperature measurements, which gives the densities within the experimental melting points.....	122
Figure 5-11 Density of PC plotted as a function of the temperature [118]. Note the extrapolated data used to find out ρ value at the experimental melting points.	124
Figure 5-12 Flory interaction parameters plotted as a function of the PVDF content for the unsalted and salted gel.....	125
Figure 5-13 Room temperature ionic conductivity versus PVDF concentration for PVDF/PC/LiBF ₄ 1M gels. The samples were made in the glove box and slow-cooled.	126
Figure 5-14 Melting temperature (onset) versus DEC:PC ratio (percentage ratio of DEC to PC) in 30%PVDF/PC:DEC/LiBF ₄ 1M salted and 30%PVDF/PC:DEC unsalted gels.	127
Figure 5-15 Heat of mixing predicted for 30PVDF/PC and 30PVDF/DEC, showing the thermodynamic interactions between each solvent and the polymer.	130
Figure 5-16 Interaction parameter plotted as a function of temperature for PVDF-PC and PVDF-DEC.	131
Figure 5-17 Room temperature ionic conductivity versus DEC content (percentage of total solvent) in PC:DEC/LiBF ₄ 1M liquids and 30%PVDF/PC:DEC/LiBF ₄ 1M gels.	132
Figure 5-18 Melting temperature (onset) versus salt concentration for 30%PVDF/PC/LiBF ₄ gels.....	133
Figure 5-19 Melting point as a function of the salt concentration for 30%PVDF/PC/LiBF ₄ and 30%PVDF/PC/LiBOB. To compare the effect of two types of salts on the melting point of PVDF-based gels.	134
Figure 5-20 Room temperature ionic conductivity versus salt concentration for PC/LiBF ₄ liquids and 30%PVDF/PC/LiBF ₄ gels.....	135
Figure 5-21 Comparison of ionic conductivity values in the salted gel samples, depending on the salt type.	135

- Figure 5-22 Room temperature optical micrographs illustrating the effect of salt on pore size for (a) 30PVDF/PC (unsalted gel) and (b) 30PVDF/PC/LiBF₄ 1M (salted gel). Both optical spectrographs used a magnification power of 500X. 137**
- Figure 5-23 WAXS patterns for 30PVDF/PC/LiBF₄ 1M salted gel and 30PVDF/PC unsalted gel. The dotted lines in the graph are provided to compare the peaks found in the unsalted gel with the lack of peaks in the salted one. 140**
- Figure 5-24 A comparison of the melting curves in the salted and unsalted gels, showing the multi peaks that are present in the unsalted gel with the single peak in the salted gel. 140**
- Figure 5-25 A comparison between (a) unsalted and (b) salted fit peaks, showing the three peaks that were found in the unsalted gel compared to the single peak that was found in the salted gel. 141**

Chapter1. Introduction and Literature Review

1.1 Introduction

The use of gels for everyday life products has received a large amount of interest in different areas of material science as a result of both their high mechanical and thermal stability and the flexibility that they provide, which means that they can be utilised in a wide variety of applications. Polymer gel electrolytes are one of the most important types of polymer gels due to their potential to be used in applications considered to be vital in current and future everyday life. So, what are polymer gel electrolytes? What makes them this important? And what methods are there for improving their properties and hence enhancing the performance of the applications in which they are used? This chapter aims to answer these questions and more through a comprehensive general review of polymer gel electrolytes together with a more focused review of a specific type of them, PVDF-based gel electrolytes.

The chapter starts by providing a general definition of polymer gel electrolytes and showing their importance for different applications. This first section also discusses some other types of polymer electrolytes, providing an example of each type. An inclusive literature review on the subject of polymer gel electrolytes is then undertaken, and the role that PVDF-based gel electrolytes play in its latest employments is described. Finally, the chapter outlines the main aims of the study and introduces the techniques that will be used to achieve them.

1.1.1 Polymer gel electrolytes

Polymer gel electrolytes (PGEs) are innovative materials that have a potentially wide range of applications, such as rechargeable batteries, smart cards, fuel cells, super capacitors, sensors and display devices [1–3]. In polymer gel electrolytes, the polymer network envelops the electrolyte liquid (salt and solvent), and prevents it from escaping. In other words, it plays the role of a matrix that can trap large amounts of solvent, thus providing the gel with the properties of a solid although it is more than 50% liquid. The salt provides free mobile ions, while the solvent's role is to dissolve and dissociate the salt and to allow the free mobile ions to move within the electrolyte system, and can thus be considered as a medium for the mobile ions[4]. Therefore, for polymer gel electrolyte materials to have effective characteristics, they must have high specifications that offer thermomechanical stability together with an effective ionic conductivity. This means that the polymer matrix, for instance, should be of low density, with a high dielectric constant and a low glass transition temperature [5]. The solvent, on the other hand, must possess a high dielectric constant, a high boiling point and a low viscosity, in order to allow the ions to move easily inside the gel system [6, 7]. Meanwhile, electrolyte salts must have a large number of anions and a low dissociation energy to allow the salt to dissociate easily.

Another advantage of using polymer gel electrolytes is that the polymer can be used to separate the electrodes of a battery in order to prevent short-circuits [8, 9]. PVDF is often preferred over other polymers by researchers looking for polymer matrixes for polymer gel electrolyte applications

because its mechanical, thermal and electrochemical stability meet the above characteristics [5, 10–13]. Despite all these merits, however, adding solvent to the PVDF during gel preparation may affect these properties through changing its structure, morphology and crystallisation [3, 14]. Polymers dissolve in different solvents in different ways, depending on the nature of the solvent [15–17]. However, regardless of the solvent type, the polymer-dissolving process has a thermodynamic nature [16–18], and therefore making safe and high efficiency polymer gel electrolyte-based products (such as rechargeable batteries) requires an extensive understanding of the polymer dissolution mechanism (i.e. polymer-solvent interactions). This can be achieved by developing an appreciable level of knowledge about the thermodynamics of polymer-diluent systems.

This study investigates PVDF gelation and crystallisation mechanisms in different solvent systems and salts. The parameters that will be considered comprise polymer concentration, solvent composition, salt concentration and salt nature. Solvents with varied polarities and viscosities propylene carbonate PC and diethylene carbonate DEC were selected, and salts were selected on the basis of their tendency to dissociate in solvent. The salts selected were Lithium tetrafluoroborate LiBF_4 and lithium bisoxalatoborate LiBOB. The techniques to be used are DSC, to measure crystals' melting temperatures and the re-crystallisation of the gel under different parameters; DMTA, to investigate the gelation phenomena with and without the incorporation of salt; and ionic conductivity, to understand how these parameters affect ionic conductivity. In addition to the advantages outlined above, PVDF-based gel electrolytes were also

selected for this study because of their influential position in the commercial world, with many applications, such as electrical and electronic products, requiring materials with a high thermomechanical stability for high performance.

1.2 Earlier studies on polymer electrolytes

Studies on polymer electrolytes began in 1973, when Fenton et al. began experimenting with the use of polyethylene oxide-based polymer electrolytes [19]. These electrolytes were developed until the 80s, at which time they were first employed within the field of technology. The development of polymer electrolytes produced three main types: solid polymer electrolytes, composite polymer electrolytes and gel polymer electrolytes [20].

The first type of polymer electrolyte to be developed was the poly(ethylene oxide) PEO, which is a dry solid-state polymer electrolyte. One of the benefits of PEO is that it can dissolve salt without a solvent, which means that it can be cast into thin films with solid-state durability without using a solvent. Despite its useful mechanical properties, PEO is not ideal for using for technological devices due to its low conductivities (10^{-8} – 10^{-4} S.cm⁻¹) at temperatures between 40–100°C, which make it unsuitable for using in devices that function at room temperature [21, 22].

The second type of polymer electrolyte developed was the composite polymer-based electrolyte. This was made with a polymer matrix filled with electrochemical fillers such as Al₂O₃, BaTiO₃, and TiO₂ [23–25], the main

feature of which is to produce ionic conductivity and maintain high stability within the electrode interfaces [26].

The third type of electrolyte material developed was the gel-based electrolyte or polymer gel electrolyte, which exhibit both elastic and viscous behaviours, depending on temperature and/or mechanical loads [27]. Among several polymers, poly(acrylonitrile) PAN, poly(methyl methacrylate) PMMA and poly(vinylidene fluoride) PVDF represent good polymer matrices for this type. Gel electrolytes were first successfully studied in detail in 1985, when PMMA was used for gelation purposes by Lijima and Toyoguchi [28]. Later, Appetecchi et al. [29] reported that the complex of PMMA and lithium salt affects electromechanical stability. The disadvantage of PMMA-based electrolytes is that stronger interactions may occur between the polymer chains and the conducting electrolyte at higher polymer concentrations, which can lead to a large drop in conductivity and a rise in the activation energy of conduction. Moreover, it has been found that the addition of PMMA increases viscosity and hence reduces conductivity. However, PMMA electrolytes show good thermal stability in the temperature range -110°C to $+240^{\circ}\text{C}$, which gives PMMA a strong advantage in terms of its practical applications over other polymers used in this field.

PAN-based electrolytes have been studied by Watanabe et al. [30, 31], who found that this polymer simply functions as a matrix which holds the electrolyte liquid and provides mechanical stability to the system without affecting the ion-transport mechanism. In PAN-based gels, it has been found that reducing water from the system increases the ion transference

numbers between 0.5–0.7 (this is the number of Lithium free ions that move across the porous medium to the total number of ions) [32].

Since gel is generally composed of two phases (solid polymer and solvent), the thermodynamics of gelation is of interest for optimising gel composition. In 1982, Kuwahara et al. [33] claimed that phase separation could be induced in polymers through changes in pressure, temperature and/or solvent concentration. These foundations have been confirmed by Lal and Bansil [34], who studied the kinetics of spinodal decomposition in polystyrene-cyclohexane (PS-CH) solutions using small angle light-scattering. Their study revealed that when the sample was quenched to a temperature below the spinodal temperature, a growth rate in the power law fashion was observed. In their study, Lal and Bansil [34] used time- and angle-resolved light scattering to investigate phase separation activity at low pressure. In 2004, Lee et al. [35] subjected a model of polymer solution to a linear spatial temperature gradient in a numerical study of temperature-induced phase separation kinetics and found that gradient temperature jumps can induce anisotropic structures and morphologies.

1.2.1 PVDF-gel electrolytes

PVDF has frequently been used as a polymer host for polymer gels and polymer gel electrolytes [3, 8, 14, 36–39]. There are two reasons for using this polymer in the electrolyte system: first, because of its electrochemical stability, which is due to its electron-withdrawing functional group; and second, because it has a high dielectric constant, which reduces or eliminates any sub-reaction with salt or solution (allowing Li-ions to move

without chemical reaction), meaning that salt will dissolve in the solution and increase the density of charge carriers inside the polymer matrix [10, 13]. Studies on poly(vinylidene fluoride)-based gel electrolytes showed that they have good mechanical stability and display significant ionic conductivity at room temperature. PVDF has been found to undergo gelation in three distinct mechanisms, which depend on the processes used and/or the gel's contents. For instance, Kim et al. [40] who dissolved PVDF in PC at 90°C and cooled the molten gel gradually to the room temperature. Prior study by Cho et al. [41] showed similar behaviour of liquid-liquid demixing in PVDF-based gels when dissolved in γ -butyrolactone in the same processes. The second mechanism is the solid-liquid phase separation, which has been shown in [41] following the liquid-liquid phase separation at the late stage of gelation.

However, Tazaki et al. [42] found that crystallisation-induced gelation can be achieved by cooling PVDF solutions directly from 180°C to 30°C in a water bath for 12h under a different gelation process. In this study, PVDF was dissolved in aliphatic and cyclic ketones with γ -butyrolactone as ester, and it was found that the gelation in γ -butyrolactone was slower than it was in other aliphatic ketones, while no gelation was observed in DMF or DMSO. Another phase separation by spindal decomposition was observed in PVDF-based gels by Hong et al. [43]. By dissolving PVDF in TG at 180°C and then quenching the solution to room temperature, they found that PVDF gels in this solvent through liquid-liquid phase separation via different mechanisms, which depend on the spinodal transition point, T_s .

In another study, a new gelation mechanism was found by using different

grades of PVDF [44]. In this case, 3 grades of PVDF were dissolved in acetophenone and ethyl benzoate at 175°C for 20min and cooled rapidly to room temperature. This study showed that percolation induced this type of gelation. Zhang et al. [45] used different solvents including propylene glycol carbonate (PGC), dimethyl phthalate (DMP), diphenyl ketone (DPK), and dibutyl phthalate (DBP) to study the gelation of PVDF in these solvents. They reported the formation of crystallisation-induced gelation in most systems (PVDF-DMP, PVDF-DBP and PVDF-PGC), while PVDF-DPK showed gelation by liquid-liquid phase separation.

Polymer gel electrolytes have been researched at the University of Leeds since the 1990s, and thermoreversible polymer gel electrolytes were studied in depth by a number of researchers there in 1994 [3]. This study used dynamic modulus G' and ionic conductivity σ , which have been utilised for investigating the effect of salt on the structure of the gel. Wide-angle x-ray diffraction (WAXD) measurements were also applied to the samples to study the effect of salt on the crystalline phases of the PGE system. The gel samples were made from poly(vinylidene fluoride) PVDF, as a polymer matrix mixed with dimethylformamide DMF, and tetraethylene glycol dimethyl ether (tetraglyme) TG solvents, with different weight ratios of the polymer and solvent being mixed with lithium-based electrolyte salt. It was found that G' decreases with increases in strain amplitude, but remains constant when the strain rate is increased. It has also been shown experimentally that 30% by weight of PVDF is the best amount to add to the electrolyte solvent in order to obtain ionic conductivities in the range of 10^{-3} – 10^{-2} S.cm⁻¹.

In 1997, Voice et al. [14] studied the structure of poly(vinylidene fluoride) PVDF polymer gel electrolytes. Their samples were made from PVDF/TG, with a mechanical modulus of up to 100 KPa. Using DSC measurements, they found that polymer crystallinity increases with salt concentration, whilst DMTA showed that the mechanical modulus simultaneously decreases.. Ward et al. [8] found that, in addition to its use as an electrolyte material, PGE can also be used as a separator for binding the cell laminate together and forming a rechargeable cell without the need for a case. That led to the development of rechargeable cells with thicknesses less than 0.1 mm, and energy densities up to 170 W.h. Kg⁻¹.

In spite of all the above studies, there appears to be no comprehensive research that investigates gelation in the PVDF-based gel both with and without the presence of commercially effective electrolyte salts such as LiBF₄ and LiBOB. Furthermore, no study has examined the effect of gel composition on the melting depression of the PVDF gel system.

Thus, the literature review on gelation and melting depression of PVDF gel electrolytes has shown that very few studies have been undertaken in this area. Therefore, this thesis will undertake both quantitative and qualitative research with the aim of contributing to a better understanding of this topic.

1.3 Aims of the study

This thesis has two major aims. The first is to study and understand the gelation behaviour of PVDF-based gels. To do so, the isothermal gelation and crystallisation of the gel from a molten solution will be investigated

through DSC and DMTA measurements of two types of gels 30PVDF/PC unsalted and 30PVDF/PC/LiBF₄ salted gels. DSC will be used to observe isothermal crystallisation, while DMTA will be used to investigate isothermal gelation. In addition to these two techniques, optical microscopy will be used to observe the two above activities within thermal conditions that are similar to those that will be used for the prior two techniques. The purpose of these investigations is to develop a good level of understanding about the gelation mechanism.

The second aim of this thesis is to study the effect of gel components on PVDF's properties. DSC will also be used in this part of the study, but this time to measure the melting point of pre-formed gel by heating it at a slow rate (10°C/min) and observing the resulting traces until the melting peaks are obtained, so that the melting point and the heat of fusion can be determined. The gel components will be varied in order to understand the effects of polymer concentration, solvent quality, salt concentration and salt quality on the gel. The parameters to be investigated in addition to the melting point are ionic conductivity, wide-angle x-ray scattering and optical microscopy, which will be used to investigate the effect of salt on gel pore size.

The data acquired from both investigation sets will provide knowledge that contributes to improving the quality of the rechargeable batteries that can be manufactured, on the one hand, and help to develop a better understanding of these materials in academic fields, on the other.

Chapter2. Theoretical Background

2.1 Introduction

In this chapter, the physical aspects of polymer gels and gelation behaviour will be discussed. This will involve first providing an extensive overview of gel terminology, and classifying types of gels in relation to the nature of their junctions and their mechanical properties. In order to develop a good understanding of their gelation mechanisms, the fundamentals of thermodynamic phase separation and spinodal decomposition will be outlined and explained. Crystallisation from the polymeric solutions will also be discussed, as this, along with phase separation, can be considered to be one of the gelation-inducing mechanisms.

The second part of this chapter contains a brief discussion of melting depression in polymer gels and the thermodynamic concepts relating to this process. The effect of good and poor solvents on melting depression represent two important sections in this part of the chapter.

This chapter also reviews the major theories that are used to interpret the above phenomenon relating to the gelation mechanism. The Flory-Huggins theory and Hansen solubility parameters will be the key for the final interpretation of the activities above [46].

2.2 The definition of a 'gel' and gelation concepts in polymers

Although it is hard to provide an exact definition for the term 'gel', many researchers in this field have tried to give a summary-style analysis of it, in terms of its properties. For instance, Almdal et al. [47] defined a gel as a material that is composed of two or more components, of which at least one is a liquid. Similarly, Sperling [48] considers the gel system to be one in which a swollen network forms in a solvent, where the solvent is dissolved in the polymeric network, but not vice versa. These definitions were expanded by Rogovina et al. [49], who proposed that a gel is a three dimensional polymer network with chemical or physical junctions (comprising covalent or non-covalent bonding) in a liquid medium.

Polymeric gels can be classified into two types [50]: thermoreversible gels, which exhibit thermoreversible behaviour when thermal transfer occurs between solid-like and liquid-like phases; and permanent gels, which typically do not have the ability to recover their original state after they have been heated. Thermoreversible gels develop transient physical junctions when they form, which provide thermal stability for the polymeric network below the melting point (the temperature at which the physical bonding breaks up). Permanent gels, on the other hand, form a covalently bonded network in solvent.

2.3 The gelation mechanism

Gelation in polymer solutions is the process via which the material is converted from a viscous liquid into a soft solid material. This may preferably occur under thermal treatment. Polymer gel can be produced by several methods, depending on the inducing process, which may involve either temperature variation, as seen in protein gelation [51]; phase separation, as seen in block copolymers [52]; ionomer formation [53, 54]; and/or crystallisation [55]. However, phase-separation is commonly used to produce the polymer gels used in many practical applications, such as conductive gels. Crystallisation is also a method that is desirable for producing such gels, since it generates better stiffness in them, which provides a stand-alone gel system. As the crystallisation and phase separation methods are the best and most commonly used ones for producing polymer gel electrolytes, both will be described in detail in the forthcoming sections.

2.4 Phase separation

Phase separation can be considered as one of the most important phenomena in thermodynamics of polymer solutions, since it highly affects their properties as well as the ultimate structure. Many processes encountered in polymer science and engineering such as polymerisation, purification, modification and post processing depend on phase separation process. All solutions that are composed of two or more components can undergo phase separation induced by temperature or pressure, in which

the homogeneous mixtures are distinctively separated into two different phases.

Phase separation boundaries can be illustrated for any polymer solution by a phase diagram showing the change in free energy of mixing ΔG_{mix} as a function of polymer concentration v [56]. The main condition for components in a solution to be mixed and form one homogeneous stable phase, is that the change in free energy must be negative. i.e. [57];

$$\Delta G_{mix} = \Delta H_{mix} - T\Delta S_{mix} < 0 \quad \text{Equation 2-1}$$

where, ΔH_{mix} and ΔS_{mix} are the change in enthalpy and entropy respectively. T is the temperature. The other condition for miscibility is that the second derivative of the free energy with respect to composition must be positive; i.e.

$$\left[\frac{\partial^2 \Delta G_{mix}}{\partial v_i^2} \right]_{T,P} > 0 \quad \text{Equation 2-2}$$

where v_i is the volume fraction of the component i.

When the free energy is plotted as a function of volume fraction (see Figure 2-1), it can be shown that there are three possibilities for mixing of the binary systems; total mixing, when the system is totally mixed and in stable state; the partial mixing region, in which the system is in partially miscible state and the last possibility, when $\Delta G_{mix} > 0$, when no mixing can take place.

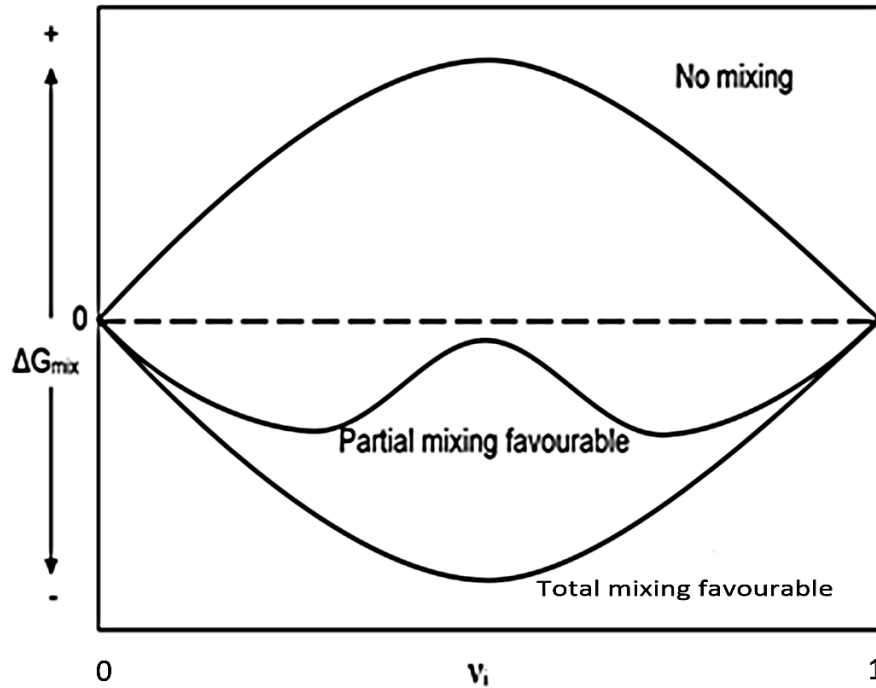


Figure 2-1 Free energy of mixing as a function of the volume fraction to show mixing possibilities in binary systems[58].

Fig 2.2 shows the binodal line, which is the locus of $\frac{\partial \Delta G_{mix}}{\partial v_i} = 0$ and the spinodal line, which is the locus of $\frac{\partial^2 \Delta G_{mix}}{\partial v_i^2} = 0$. Two possibilities can exist for partial miscibility; the first one in which the binodal and spinodal lines meet at low temperature as shown in Figure 2-2 (a), leading to phase separation at higher temperatures and miscibility at low temperature, known as lower critical solution temperature (LCST). The other phase separation behaviour can be observed when the binodal and spinodal lines meet at high temperature, in which phase separation takes place at low temperature, and miscibility at high temperature. This situation is known as upper critical solution temperature (UCST) and is shown in Figure 2-2 (b). The latter behaviour is more likely to occur in polymer-solvent systems.

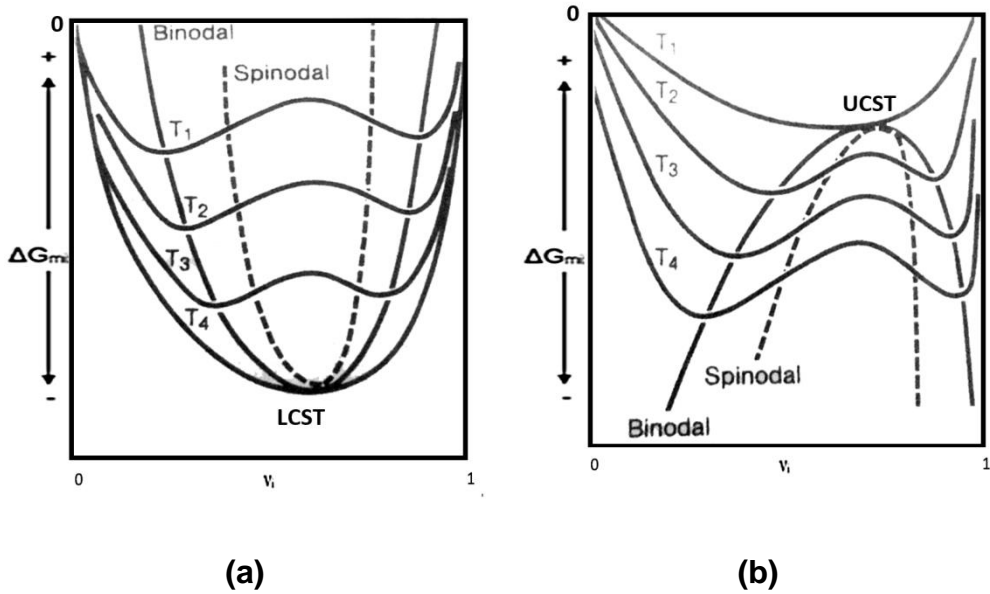


Figure 2-2 Phase diagram showing (a) Lower critical solution temperature LCST and (b) Upper critical solution temperature UCST where $T_1 > T_2 > T_3 > T_4$. [57]

Referring to Figure 2-3 makes this discussion much easier. In this figure, the free energy phase diagram has been related to the temperature-composition phase diagram and all phase boundaries are clearly illustrated. In this diagram, phase separation starts when the temperature is reduced from T_1 to T_2 , causing transfer from the stable state to a metastable state which can be found in the binodal region. In the binodal region, depending on the polymer concentration, the polymeric solution turns to either a polymer-rich phase which dominates the region with the presence of liquid-rich pockets; or it may turn to a liquid-rich phase, in which a discrete polymer-rich clusters are found swimming in a continuous liquid-rich medium. These two states form by nucleation and growth and are illustrated in Figure 2-4. Within the spinodal decomposition region the system spontaneously separates into 2 distinct phases due to the difference in molecular weight.

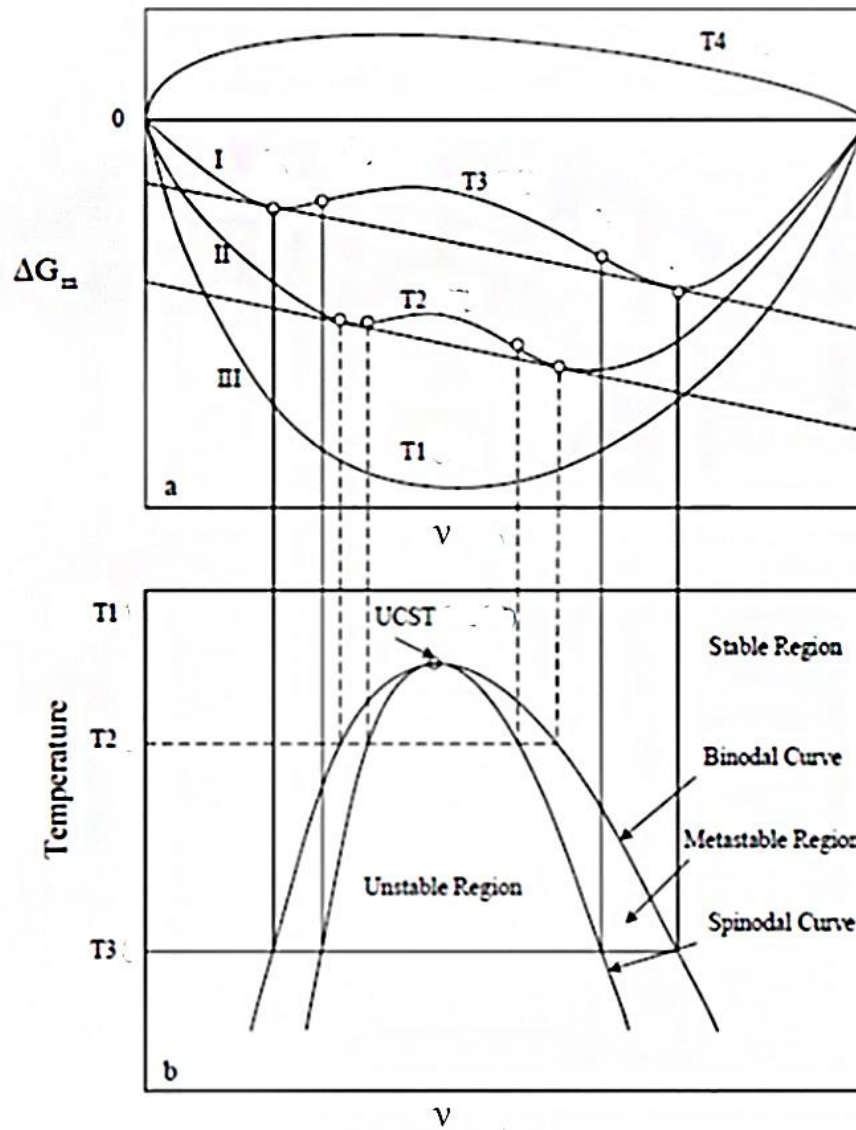


Figure 2-3 Phase diagram in which the change in Gibbs free energy is plotted as a function of the polymer concentration. ($T_1 > T_2 > T_3 > T_4$). [59]

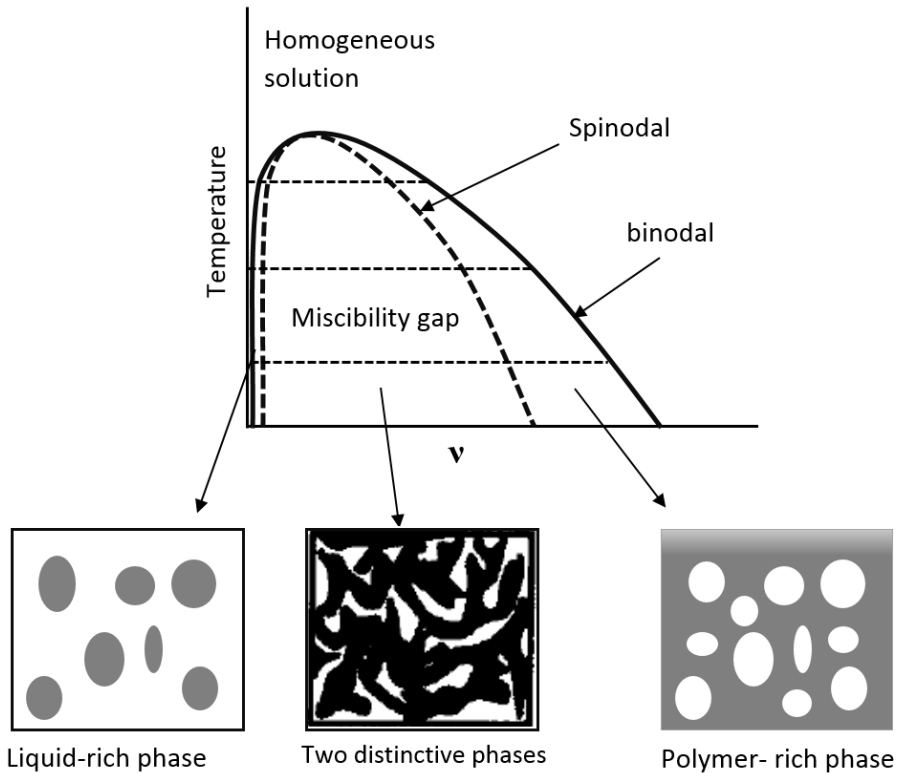


Figure 2-4 Sketch of binodal and spinodal regions in polymer-solvent systems [60].

2.5 Crystallisation from solution

Crystallisation in polymers and polymeric solutions refers to the process through which the molecular chains undergo partial alignment. This can be achieved when the chains pack together as a result of being induced by a thermodynamic parameter, forming an ordered region known as a lamella. Lamellae can grow radially to form spherical structures called spherulites (see Figure 2-5) [64]. Crystallisation can occur as the result of different inducements, such as solvent evaporation, mechanical stretching and cooling from the melt. The crystallisation of the molten polymer from its solution through cooling is of importance here, due to its relation with the

main subject of this study.

Crystallisation that occurs in solutions via the reduction of the solvent usually happens with precipitates, typically at temperatures below their melting points [65]. However, crystallisation from molten solutions typically occurs when the solution is cooled to a temperature range between the melting points of the two components. Most polymers are amorphous in their nature, but folding in polymeric chains is thermodynamically favourable in polymer solidification. Thus, chains tend to fold together, forming ordered regions within approximately one micrometre. However, these regions cannot grow uniformly due to the presence of the entangled regions that hinder their progress. Therefore, cooling polymers from their molten states can produce crystalline regions alongside amorphous regions, leading to what is called a semicrystalline polymer [66, 67]. The crystallisation point is normally below the melting point, T_m , and above the glass point, T_g .

Crystallisation from solution may be different, however, in that it depends on how diluted the solution is, as well as on how concentrated the solvent is in the solution. The polymer chains in dilute solution are separated into segments surrounded by the solvent. When the solution is concentrated (e.g. by the evaporation of the solvent or increasing the concentration of the polymer), an interaction between the molecular chains that is induced by this concentration can encourage crystallisation similar to that produced from the melt [68]. Crystallisation from solution may also lead to a higher degree of crystallinity. When the polymer is crystallised from the melt in the presence of a diluted environment, this causes a confined crystallisation to

occur, which leads to a spherulitic morphology that can be similar to the above, but with a few morphological differences resulting from the space in which the spherulites are formed.

2.6 Polymer solutions and the thermodynamics of gel formation

2.6.1 Gelation from solution

For diluted systems, gelation depends on the polymer concentration and/or the type of solvent used in the solution. A polymeric gel is a polymeric network containing solvent. Although this definition seems to be a bit different from the definition mentioned in the prior section, considering the condition of the solvent involvement in the polymeric network returns us to the prior definition of Almdal in section 2.2. According to this, two approaches can be used to describe polymer gel formation from diluted systems. Under the first one, a polymeric gel is produced by forming a polymeric network in a solvent in which the polymeric chains are relaxed. The rubber elasticity theory is used for interpreting such gels [69]. The second method proposes that a previously cross-linked polymer is subsequently swollen in a solvent, and such a gel follows the Flory-Rehner theory [70].

Physical gels are highly affected by the number and strength of the bonds, since the physical cross-links may involve dipole-dipole interactions, traces of crystallinity, multiple helices, and so on. However, in such gel systems,

the number of cross-links depends on time, pressure, and temperature. Physical gels are typically thermoreversible i.e. the physical bonds break at high temperatures and reform at lower temperatures. Thermoreversible gels may be formed either in point crosslinks, in which gel networks are bonded at single points; in junction zones, in which the chains interactions execute over a part of their length; or they may form fringe micelles junctions. Figure 2-6 shows the three types of thermoreversible cross-links [71].

Solvent exudes from some gels, producing syneresis, and two types of syneresis occurs in them [72]: (a) The χ -type, which results from poor thermodynamics of mixing and causes a phase separation between polymer and solvent—spinodal decomposition is frequently involved in this type, causing a turbid appearance; and (b) The n -type, in which a rise in cross-link density causes the solvent to exude. In this latter case, the equilibrium swelling level decreases, but the polymeric gel still forms one phase with the solvent, producing a gel with a clear appearance. In both types, different amounts of fluid remains can surround the gel.

2.6.2 Fundamental theories of gel formation

The property of complete recoverability after a high deformability of elastic rubber shows that the gel's behaviour is very similar to polymeric networks in diluted environments. Therefore, the rubber elasticity theory is the best available theory for interpreting the formation of gel networks in solvents, and can be used to partially explain the thermodynamic activities involved in the formation of this type of gel [73–75]. In order to interpret gelation in

solvents, the rubber elasticity theory locates two conditions under which the gel can be treated as being elastic or rubber-like: the first is that the polymer chains must be highly flexible (e.g. in highly concentrated polymeric solutions); and the second that the polymeric chains must be joined in a network structure. In this theory, the deformation of the sample resulting from chain extension is related to the reduction in entropy [76–78], and this assumption led to calculating the number of polymer chain conformations in the space. These conformations are reduced when the chain is extended, and finish with only one conformation when the chain is rod-like. The thermodynamic approach to rubber elasticity can be illustrated by the Helmholtz free energy A_H :

$$\Delta A_H = \Delta U - T\Delta S \quad \text{Equation 2-3}$$

$$T\Delta S = \Delta U - \Delta A_H \quad \text{Equation 2-4}$$

Here, U is the internal energy, T is the temperature and S is the entropy.

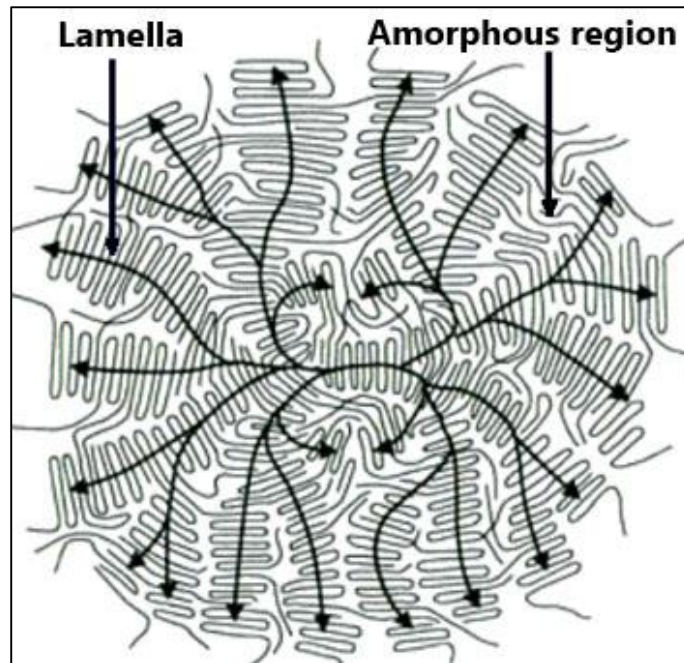


Figure 2-5 Spherulitic structures produced by lamellae formation and grow radially [64].

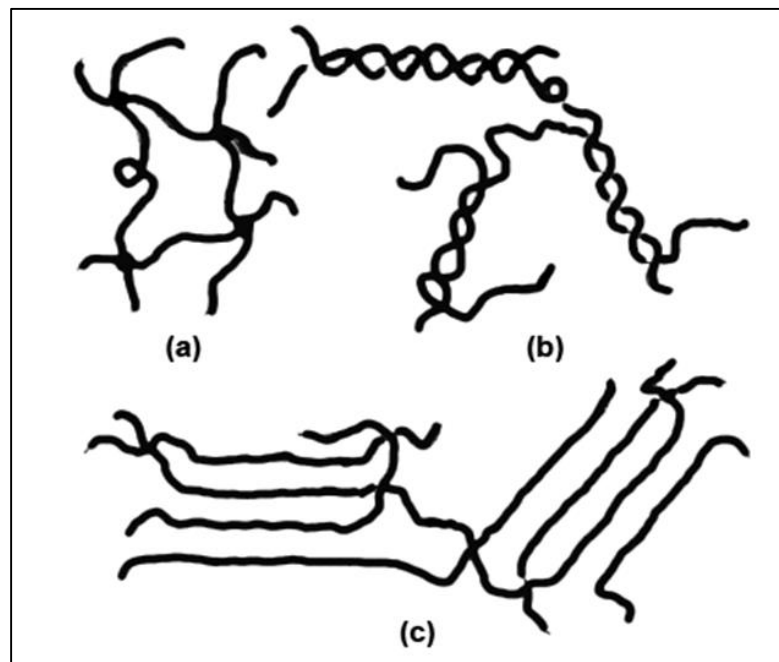


Figure 2-6 Types of thermoreversible cross-links: (a) point cross-links, (b) junction zones and (c) Fringed micelles [71].

External work is needed when the chain is stretched, therefore this operation is considered to be nonspontaneous, and $T\Delta S$ must be negative.

However, the temperature is higher than absolute zero at all times, so T can never be negative. Thus, the change in entropy, ΔS , must be negative. This indicates that the elastomer is in a more stable (ordered) state when it is stretched—i.e. when it is naturally entangled. In contrast, when the tension is removed, the chain spontaneously regains its original shape, implying that the change in free energy, ΔA_H , is negative. Referring to Equation 2-3, it can be seen that this means that ΔS must then be positive and increased, since the second term, ΔA_H , will be positive regardless. Although this equation provides a good interpretation of some polymeric gels behaviour, it focuses only on the entropic part of the interactions [79], and it is thus necessary to find a theory that takes all the possible thermodynamic interactions into account.

When a prior cross-linked polymer immersed is into a thermodynamically good solvent, it is driven by an entropic mixing force. Another elastic retractive force then develops, which increases as the volume causing the deformation to the polymer chains rises. This leads to a reduction in entropy, which is caused by the lessening of the probability of extended chain configurations occurring. Therefore, when these two opposite forces are equal, the system should be in a state of equilibrium [80].

Frenkel produced the first theory based on this phenomena [81, 82], and this was later developed as a general theory by Flory and Rehner [70, 83]. The Flory-Rehner theory is based on two distinguishable characteristics taken from other solids that are related to the elastomers: first, their ability to absorb a large amount of solvent without dissolving; and second, the elastic deformation that elastomers undergo with small stresses. According

to Flory and Rehner's hypothesis, two components of free energy are accompanied by swollen networks interactions: the free energy of mixing ΔG_{mix} and the free energy of elastic deformation ΔG_{el} . Therefore, the total change in the free energy, ΔG , of swelling can be given by [84]:

$$\Delta G = \Delta G_{mix} + \Delta G_{el} \quad \text{Equation 2-5}$$

Both the theories above suggest undertaking thermodynamic treatments from different points of view, according to the gel formation approach. However, these theories both lack thermodynamic interaction parameters. However, the Flory-Huggins theory provides better interpretations for the polymer cross-linked in a solvent. This theory will now be discussed.

2.6.3 The Flory-Huggins treatment for diluted solutions

Flory-Huggins theory provides a good treatment for diluted solutions, since it involves the entropic term in calculating the free energy of mixing [17, 86-88]. The principle of this theory is based on expanding the concept of the classical entropy of mixing of the ideal solution to the non-ideal solution (such as the polymeric solutions), through the statistical thermodynamics. It also, presents the enthalpic part of the interactions of the mixing, which is essential in regarding with the regular polymer solution. The entropy of mixing ΔS_{mix} , can be determined, according to statistical thermodynamics using the following equation;

$$\Delta S_{mix} = k \ln \Omega \quad \text{Equation 2-6}$$

where k is Boltzmann's constant and Ω is the number of possible space configurations which the molecules may occupy.

The lattice model (shown in Figure 2-7), can be used to illustrate Ω . Figure 2-7 (a) shows a lattice contains two different types of small molecules N_1 and N_2 with identical sizes. For this type of molecules, Ω can be given as;

$$\Omega = N_o! / N_1! N_2! \quad \text{Equation 2-7}$$

where, N_o is the total number of molecules ($N_o = N_1 + N_2$). Using $\ln N! = N \ln N - N$ (Stirling approximation), and substituting this into Equation 2-6 yields;

$$\Delta S_{mix} = k[(N_1 + N_2) \ln(N_1 + N_2) - N_1 \ln N_1 - N_2 \ln N_2] \quad \text{Equation 2-8}$$

However, when the polymer with x chain segments is mixed with the solvent (see Figure 2-7 (b)), the entropy of mixing then can be given by;

$$\Delta S_{mix} = -k[N_1 \ln v_1 + N_2 \ln v_2] \quad \text{Equation 2-9}$$

which represents the total entropy, where, v_1 and v_2 are the volume fractions of solvent and polymer, respectively.

i.e.,

$$v_1 = \frac{N_1}{N_1 + xN_2}$$

$$v_2 = \frac{xN_2}{N_1 + xN_2} \quad \text{Equation 2-10}$$

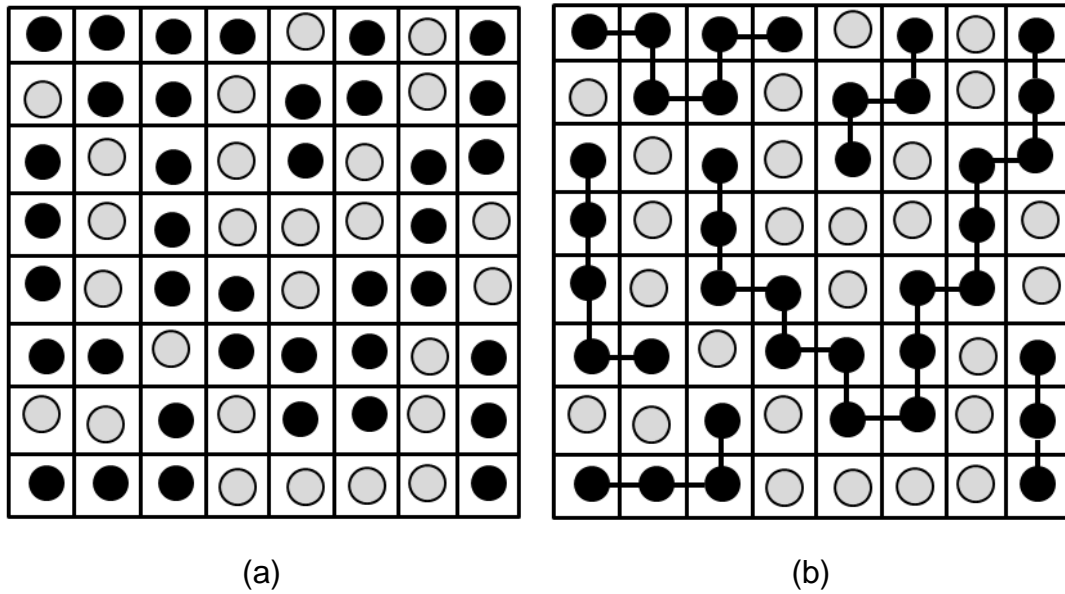


Figure 2-7 Illustrates Lattice model for two types of solution; (a) The small molecules solution and (b) The polymeric solution in a solvent (the polymer segments are represented by the black liked circles (sectors) while the solvent molecules are shown in grey circles).

Flory- Huggins theory suggests χ_F the interaction parameter, which is a unitless quantity can represent the enthalpy of mixing as follows[17, 88];

$$\chi_F = \frac{\Delta H_{mix}}{kTN_1v_2} \quad \text{Equation 2-11}$$

or

$$\Delta H_{mix} = \chi_F kTN_1v_2 \quad \text{Equation 2-12}$$

Therefore, combining Equation 2-12 with Equation 2-9 can give the free energy of mixing for the polymeric solutions from the rubber elastic theory point view ΔG_{mix} .

$$\Delta G_{mix} = kT(N_1 \ln v_1 + N_2 \ln v_2 + \chi_F N_1 v_2) \quad \text{Equation 2-13}$$

As shown above, the first and second terms in Equation 2-13 represent the entropic contribution (which are negative due to the fractional volume concentrations) while the last term expresses the enthalpic contribution. As explained in Section 2.4, ΔG_{mix} must always be negative in order to keep the mixture in one phase.

2.7 Polymer solubility

Polymer solubility can be defined as the ability for the polymer to be dissolved in a solvent. When a polymer is mixed with a solvent, it undergoes several steps before dissolving and forming a homogenous solution. Dissolving starts by the polymer swelling due to the solvent diffusion. This process is highly affected by the sample size and temperature[89]. Diffusion increase then leads to segments breaking apart and floating within the solvent molecules. Polymer solubility theory has been founded in 1936 by Joel H. Hildebrand and Scott[90], who used the concept of cohesive energy density to predict the ability of dissolving. According to this theory, the degree of interaction of solubility between materials can be estimated numerically by introducing a parameter called solubility parameter δ , which can be given as a function of the cohesive energy E_c of the solvent vaporisation. The cohesive energy, can be defined as the internal energy needed to eliminate the intermolecular forces per mole of a material. Cohesive energy density is the energy released when all intermolecular forces (physical links) in a volume unit are broken.

According to the definitions above solubility parameter can be given by;

$$\delta = \left(\frac{E_C}{V_M} \right)^{\frac{1}{2}} \quad \text{Equation 2-14}$$

where V_M is the molar volume of the substance. Cohesive energy is one of the free energy forms, which can be written according to the Helmholtz free energy form as;

$$\Delta E_C = \Delta H - RT \quad \text{Equation 2-15}$$

Therefore, Hildebrand solubility parameter can be given by the following equation;

$$\delta = \left[\frac{\Delta H - RT}{V_M} \right]^{1/2} \quad \text{Equation 2-16}$$

Where; ΔH is the enthalpy of vaporisation, R gas constant, T temperature and V_m is the molar volume. As can be seen from the equation above, the solubility depends on the temperature and the molar volume. Therefore, the solubility in most of materials changes at elevated temperatures; similarly the higher molar volume material (such as polymers) requires a lower solubility parameter to be used. This parameter can give simple predictions of phase equilibrium for most of the materials. However, this parameter can be used only for non-polar or slightly polar systems. It also cannot be used for the polydispersed systems, which shows that Equation 2-5 has a lot of limitations. In 1966, Charles M. Hansen proposed three

components of solubility parameters that can predict Hildebrand parameter in more comprehensive way. Each component can deal with different activity in the solution, which is caused by either; dispersed force, polar force and/or hydrogen bonding. Hansen parameters can be given by the equation[91];

$$\delta_t^2 = \delta_d^2 + \delta_p^2 + \delta_h^2 \quad \text{Equation 2-17}$$

Where, δ_t is the total solubility parameter, δ_d , δ_p and δ_h are the dispersion, polar and hydrogen bonding components respectively.

According to Hansen et.al, each one of these components is a function of temperature according to the following differential equations [92];

$$\frac{\delta_D}{dT} = -1.25\alpha\delta_D \quad \text{Equation 2-18}$$

$$\frac{\delta_P}{dT} = -0.5\alpha\delta_P \quad \text{Equation 2-19}$$

$$\frac{\delta_H}{dT} = -\delta_H(1.22 \times 10^{-3} + 0.5\alpha) \quad \text{Equation 2-20}$$

Where α is the coefficient of thermal expansion.

Considering Equation 2-16, and using Equation 2-12 with converting the molecular form (Nk) form to the molar form (R), Flory interaction parameter can be related to the solubility parameters by the equation [93, 94];

$$\chi_F = \frac{V_1}{RT} (\delta_{\text{solvent}} - \delta_{\text{polymer}})^2 \quad \text{Equation 2-21}$$

where, V_1 is the molar volume of the solvent, δ_{solvent} and δ_{polymer} are Hansen solubility parameters for the solvent and polymer respectively. χ_F is an indicator for the solvent ability to dissolve or mix with the polymer or other solvent.

Equation 2-21 predicts only $\chi_F > 0$ due to the square of the difference in solubility parameters. Therefore, this equation is suitable only for non-polar interactions in which only weak Van der Waals interactions can take place and no strong polar forces or hydrogen bonds are considered. However, in polymeric solutions all such interactions may occur and have evident effect on the phase behaviour. Flory-Huggins has solved this problem by using an empirical expression for χ_F , according to equation 2.22.

$$\chi_F = A + \frac{B}{T} \quad \text{Equation 2-22}$$

In Equation 2-22, the parameter A represents the entropic part meanwhile B represents the enthalpic part of the mixture, which incorporates the combined effect of interactions and volume changes. It can be shown from this equation that the sign of B has a major effect on χ_F and hence on the free energy of mixing ΔG_{mix} according to equation 2.15. If B is positive

($B > 0$), χ_F decreases with the increase of temperature, which in turn makes ΔG_{mix} more negative (according to Equation 2-13) enhancing miscibility at higher temperatures. In this case, we have upper critical solution temperature, and this behaviour has been observed in this study. Conversely, when $B < 0$, this causes ΔG_{mix} to be less negative when temperature is increased, which reduces the miscibility and causes lower critical solution temperature LCST, above which phase separation occurs. Figure 2-2 in section 2.4 illustrated these two behaviours.

Gels in this work are made by cooling polymer-solvent solutions to room temperature [12, 61, 62]. Figure 2-8 represents an example of how a gel forms in a composition of 30%PVDF/PC. At T_1 the system exists as a homogeneous solution. At T_2 the solution becomes unstable and separates into a polymer-rich phase and a solvent-rich phase. At T_3 crystallisation can take place by nucleation and growth while the system is in the binodal region, where structures as illustrated in Figure 2-4 can be observed. However, if the sample is quenched from the homogeneous phase to temperatures below T_4 spinodal decomposition can take place and structures like Fig 2.8b can be obtained.

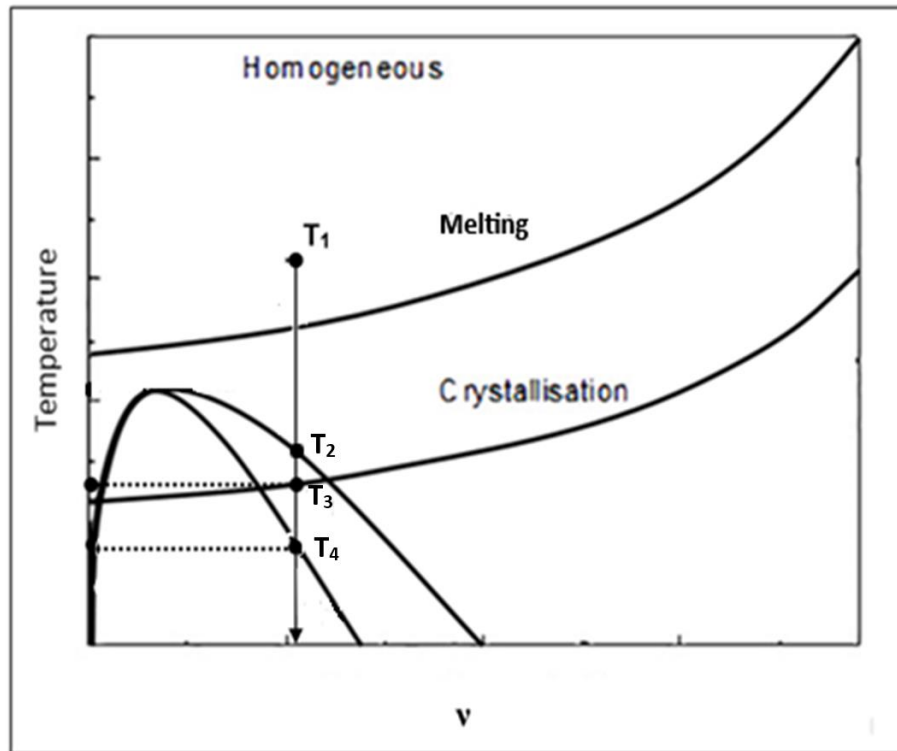


Figure 2-8 Schematic of PVDF/PC phase diagram.

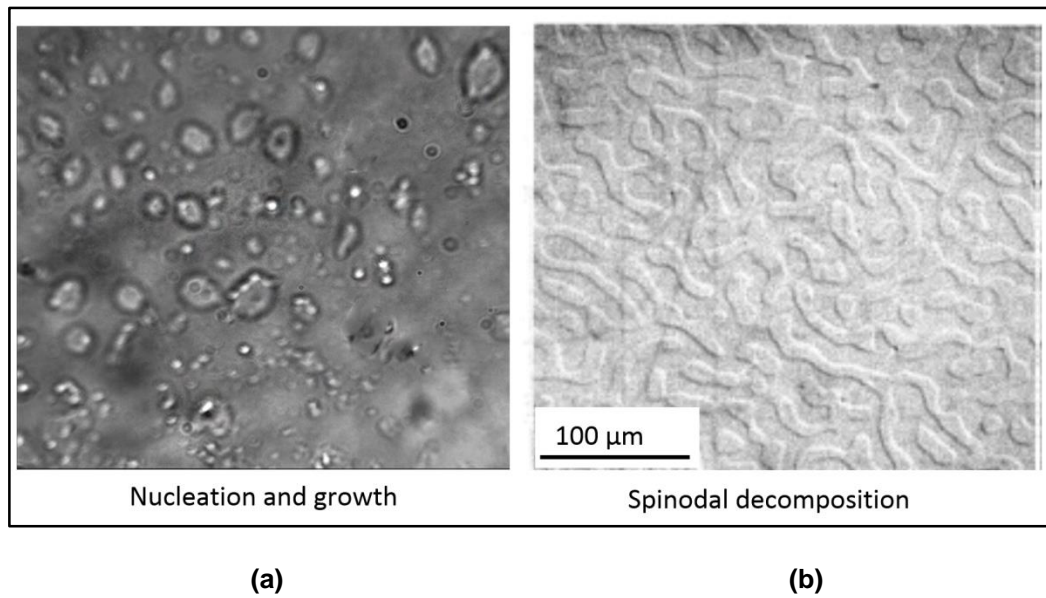


Figure 2-9 Optical micrographs of (a) nucleation and growth and (b) spinodal decomposition in polymer gels[64].

2.8 Melting point depression

The melting point depression is the reduction in the crystallisation melting temperature in semi-crystallised polymers. This reduction may occur due to non-crystallisable impurities, such as solvents or plasticisers. It has been found that the crystallisation melting points of polymers are depressed when they are dissolved in solvent. This happens when adding a solvent to a polymer causes disruption in the intracrystalline forces, which leads to reducing the free energy of the mixture, thus producing a significant decrease in melting temperature. Adding solvent may also increase the mobility of polymer chains and may reduce the thickness of lamellae as well. Melting point depression is very important here, since it provides valuable information about polymers' changes in crystallinity in the presence of dilution agents. In systems such as gel polymer electrolytes, the determination of melting depression is necessary for investigating the thermal stability of devices such as rechargeable batteries, as well as the materials used within them.

According to Flory [87], the melting point depression of semi-crystalline polymers can be calculated using the following equation:

$$\frac{1}{T_m} - \frac{1}{T_m^0} = \frac{RV_{pol}}{\Delta H_f^0 V_{solv}} (v_{solv} - \chi v_{solv}^2) \quad \text{Equation 2-23}$$

Here, T_m is the observed melting point of the diluted polymer; T_m^0 and ΔH_f^0 are the melting point and the enthalpy of fusion of the pure polymer,

respectively; R is the gas constant; V_{pol} and V_{solv} are the molar volume of the polymer repeat unit and the solvent, respectively; and v_{solv} is the volume fraction of the solvent. This equation can be used to predict the interaction parameter when the other parameters are known.

2.8.1 The effects of good and poor solvents on melting depression

In the current discussion, a 'good solvent' is one that can easily dissolve the solute (either the polymer or the electrolyte salt). As previously noted, the solubility parameters play the major role in this profile. A good solvent does not refer to one that has higher solubility parameters, but it does refer to one that has solubility properties matching or close to the solute's solubility properties. There is thus a solvent dedicated to the solute for each solution, otherwise little or no dissolving can take place. The reason for this from the physical point of view is that small differences between the values of the solubility parameters leads to low interaction parameters at a constant temperature (as shown by Equation 2-21), which means that a low potential is needed to dissolve the solute. This converse of this is true for poor solvents, whose solubility parameters significantly differ from the solute, and hence require higher energies to dissolve them. Since crystallisation from the molten solution is highly dependent on both temperature and solvent quality, it is expected that such poor solvents will contribute to increasing the melting point, since their effects are limited at high temperatures (see Equation 2-21). Meanwhile, good solvents will affect the melting point even at low temperatures as a result of their

solubility properties, which reduce intermolecular forces and hence depress melting points.

Chapter3. Materials and Methods

3.1 PGE components

Polymer gel electrolytes are composed of a polymer, an organic solvent and an electrolyte salt. The polymer can be used as a matrix that keeps the electrolyte solution in i.e. that prevents it from escaping or leaking. The solvent is used to dissolve the polymer and the salt (i.e. it dissociates the salt components and frees the conducting ions). The salt, which is a lithium-based one, provides the free ions necessary for conduction after it has been broken into parts by the polar solvent.

3.1.1 Polymer: polyvinylidene fluoride (PVDF)

Poly(vinylidene fluoride) PVDF ($\text{CF}_2\text{-CH}_2$)_n is a semi-crystalline fluoropolymer with an almost 70% crystalline structure that can form thermoreversible gels when it is dissolved in a suitable solvent. Its high mechanical, thermal and chemical stabilities have led PVDF to be chosen as a polymer host for polymer gel electrolytes [3, 14, 37, 38, 92–94]. Figure 3-1 shows the structural and chemical formulae of PVDF. In PVDF, the C-F bond is highly polar, which supports a high dielectric constant (8.4) and provides better dissociation, releasing Li^+ ions that are used as charge carriers in rechargeable batteries. Therefore, PVDF attracts the interest of researchers and battery manufacturers alike [13].

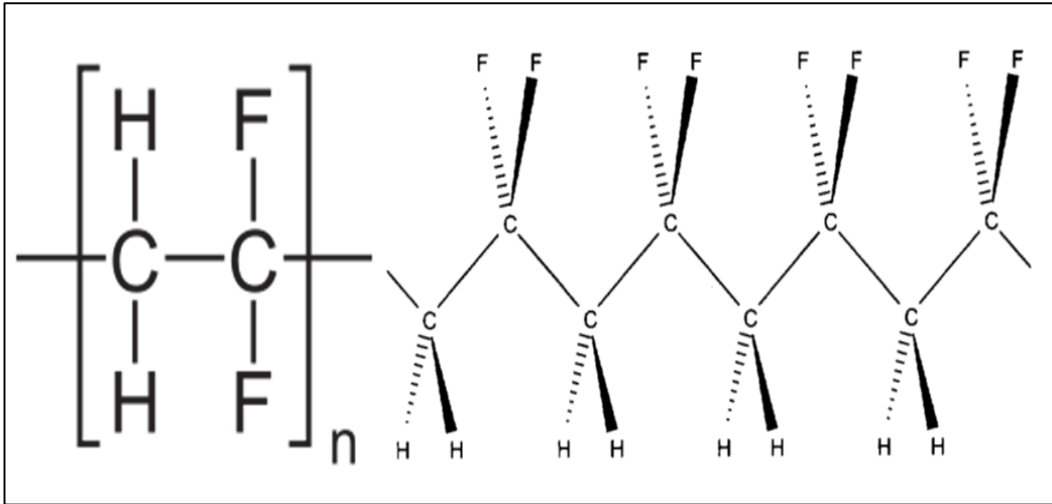


Figure 3-1 PVDF's chemical and structural forms [95]

PVDF crystallises through several different phases, which can be affected by the conditions and the processing of the polymer. These include the nonpolar α -phase (form II), with TGTG' conformation as trans (T) or gauche (G) linkages, where G' is gauche with 120° conformation difference; the polar β -phase (form I), with Trans TTTT conformation; and the γ -phase (form III) the semipolar phase with TTTGTTG' conformation (see Figure 3-2). The different crystal phases are associated with a variety of properties [96–103], and each phase can be obtained in a different process, as shown in Figure 3-3. The high-polar phase β (form I), for instance, can be obtained by cooling PVDF from melting using a pressure of approximately 350MPa. Other processes that can be applied to the non-polar form II (α -phase) to obtain form I involve applying extensive stretching to it [104–108], subjecting it to gamma irradiation [109] or subjecting it to a strong electric field [110]. Moreover, the γ -phase can be obtained from both phases β and α by annealing the solid polymer at a high temperature [111, 112]. More details about the transformations of the PVDF crystal forms are illustrated

in Figure 3-3. Table 3-1 shows the unit cell systems of the different polymorphs of PVDF, while Table 3-2 illustrates the crystal planes of PVDF's different crystal phases according to two references [113, 114]. A number of studies [112–115] have provided detailed analyses of these crystal forms (see Table 3-1 and Table 3-2).

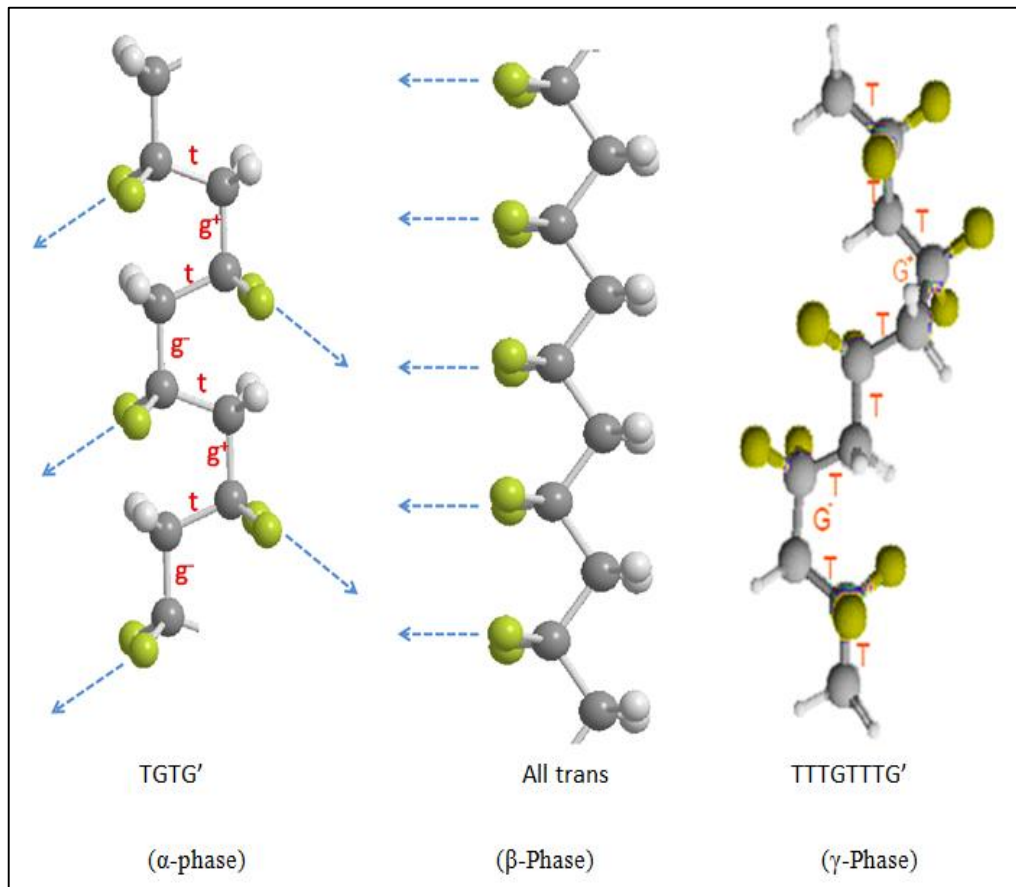


Figure 3-2 The three PVDF crystal forms: α , β and γ [116].

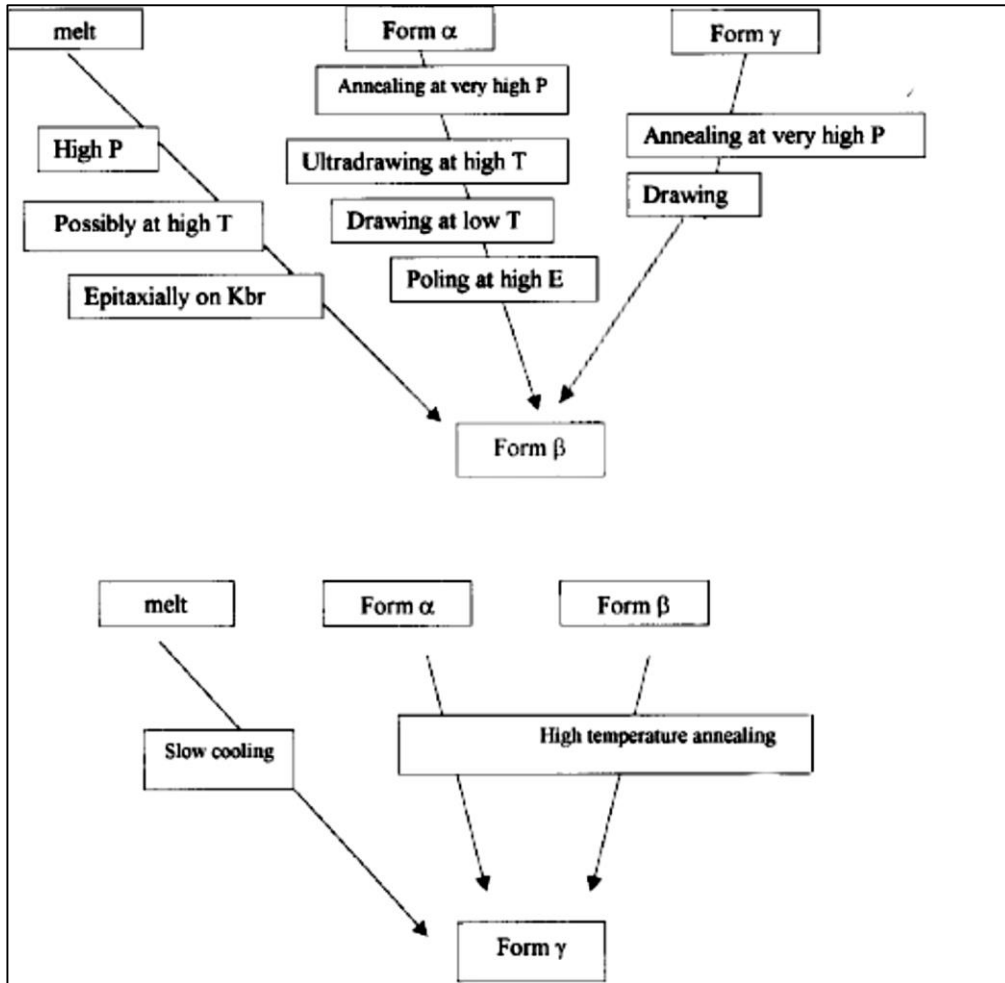


Figure 3-3 α , β and γ conformation transitions produced using different processes on PVDF [103, 117].

Table 3-1 PVDF crystal forms and their corresponding attributes[115]

Property	Crystal Phase		
	α	β	γ
Crystal system	Monoclinic	Orthorhombic	Monoclinic
Lattice constants	$a=4.96 \text{ \AA}$	$a=8.58 \text{ \AA}$	$a=8.66 \text{ \AA}$
	$b=9.64 \text{ \AA}$	$b=4.91 \text{ \AA}$	$b=4.93 \text{ \AA}$
	$c=4.62 \text{ \AA}$	$c=2.56 \text{ \AA}$	$c=2.58 \text{ \AA}$
	$\beta=90^\circ$		$\beta=97^\circ$

c =fibre direction

Table 3-2 PVDF crystal phases and their corresponding crystal planes

2θ (°)		Phase
<i>Satapathy et al. [113]</i>	<i>Gregoreo et al. [114]</i>	
18.4 (020)	18.3 (020)	α (<i>non-Polar</i>)
19.9 (110)	19.9 (110)	
26.6 (021)	26.56 (021)	
20.7 (200)	20.26 (200)	β (<i>Polar</i>)
20.8 (110)	20.26 (110)	
20.3 (101)	20.04 (α and β)	γ (<i>Polar</i>)

3.1.2 Solvents

3.1.2.1 Propylene carbonate (PC)

Propylene Carbonate (PC) ($C_4H_6O_3$) is an odourless and colourless organic solvent that can be used to dissolve PVDF and lithium salts such as $LiBF_4$ and LiBOB in polymer gel electrolytes. PC has been used for such processes due to its high dielectric constant (64.92), which allows it to dissolve the polymer and dissociate the salt [118]; its high boiling point (241°C), which gives it thermal stability and reduces the evaporation rate in thermoreversible gel production and use; and its low viscosity (at room temperature), which provides good mobility for the charge carriers in the electrolyte gel system [118–120]. Despite all these virtues, it is not advisable to use PC as the only solvent in rechargeable batteries due to its

determinant effect on electrodes, such as graphite passivation. However, mixing PC with ethylene carbonate (EC) or diethyl carbonate (DEC) can effectively solve this problem [121, 122].

3.1.2.2 Diethyl carbonate (DEC)

Diethyl carbonate (DEC) ($C_5H_{10}O_3$) is a colourless liquid. Although it is considered to be a poor solvent due to its extremely low polarity ($\epsilon=2.84$) [123], it also has a very low viscosity (0.749 mPa.s at room temperature) [124], which makes it desirable to use as a co-solvent in rechargeable batteries along with good solvents, such as propylene carbonate (PC) and ethylene carbonate (EC) [125].

3.1.3 Electrolyte salts

3.1.3.1 Lithium tetra (fluoroborate) ($LiBF_4$)

Lithium tetrafluoroborate ($LiBF_4$) is one of the most common salts that is used in polymer gel electrolyte applications. In aprotic solvents such as PC, $LiBF_4$ can be dissociated by extracting Li^+ cations, which can work as charge carriers in rechargeable batteries.

3.1.3.2 Lithium bis(oxalate)borate ($LiBOB$)

Lithium bis(oxalate)borate ($LiBOB$) (C_2O_4)₂ is also used in rechargeable batteries as the electrostatic force between the Li^+ ion and the BOB^- ion is weaker than the forces between Li^+ and BF_4^- ions, which means that $LiBOB$ is easier to dissociate in organic solvents than $LiBF_4$, and thus releases

more Li^+ ions than it. Therefore, ionic conductivity in polymer gel electrolytes that contain LiBOB is greater than in polymer electrolytes that have LiBF_4 as lithium ion providers [126].

3.2 Gel compositions

PVDF 1015 provided by Solvay-Solef was used as a polymer matrix for polymer gel electrolytes in this study, with propylene carbonate (PC) and diethyl carbonate (DEC) from Sigma-Aldrich being used as solvents to dissolve the polymer and the salt. Lithium tetrafluoroborate (LiBF_4) and lithium bis(oxalate)borate (LiBOB) from Aldrich (Cat.:24,476–7) was used as an ionic salt. All gels and electrolytes were prepared in an oxygen-free nitrogen-filled glove box to protect them from moisturing. Table 3-3 shows the properties of the polymer, the solvents and the ionic salts.

3.2.1 Unsalted gel preparation

3.2.1.1 30%PVDF/PC unsalted gel preparation

Unsalted gel was prepared by mixing 3g of PVDF with 7g of PC (equivalent to 5.834ml at room temperature). The mixture was stirred well in a glass tube using a metal spatula and then heated at 160°C until melted. It was then stirred again to expel the bubbles and was left to cool and gel. The polymer content of these PGEs is defined as the mass of polymer to the combined mass of polymer and solvent (regardless of any salt content).

3.2.1.2 PVDF/PC at different polymer concentrations

Different amounts of PVDF were mixed with 7g of PC to produce a range of

unsalted polymer gel electrolytes with different polymer concentrations. The gels were then prepared using the same procedures outlined in section 3.2.1.1. PVDF masses were determined using Equation 3-1, where C_{PVDF} is PVDF fractional concentration, and m_{PVDF} and m_{PC} are masses of PVDF and PC respectively. Table 3-3 shows PVDF concentrations and their equivalent masses.

$$m_{PVDF} = \frac{C_{PVDF} \times m_{PC}}{(1 - C_{PVDF})} \quad \text{Equation 3-1}$$

3.2.2 Salted gel preparation

3.2.2.1 30%PVDF/PC/LiBF₄

To make the electrolyte solution, different concentrations of LiBF₄ were mixed with 7g of PC in a glass tube, then the mixture was stirred at room temperature using magnetic stirrer bars until the salt had dissolved and the mixture had become clear and transparent. The PVDF was then dissolved in this electrolyte solution, stirred well using a spatula, and heated until dissolved. The mixture was left to cool and form the polymer gel electrolyte. Table 3-5 shows the concentrations of LiBF₄ with corresponding masses. These masses have been calculated as follows:

Taking the conventional definition of molarity, the mass of salt to be made up to 1L of solvent ($m_{\text{salt/L}}$) is given by the equation:

$$m_{\text{salt/L}} = M_{\text{salt}} * C \quad \text{Equation 3-2}$$

where M_{salt} is the molar mass in g, and C is the concentration of salt in mole per litre. The volume of salt needed to be dissolved in 1L ($V_{\text{salt/L}}$) is

given by the equation:

$$V_{salt/L} = \frac{m_{salt/L}}{\rho_{salt}} \quad \text{Equation 3-3}$$

Where ρ is the salt density, Hence the total amount of solvent in cm^3 needed per litre of solution ($V_{solv/L}$) assuming no change in volume on dissolution of the salt in the solvent is given by the equation:

$$V_{solv/L} = 1000 - V_{salt/L} \quad \text{Equation 3-4}$$

The mass of solvent per litre is given by the equation:

$$m_{solv/L} = \rho_{solv} \times V_{solv/L} \quad \text{Equation 3-5}$$

where ρ_{solv} is the density of the solvent. The total PC mass for these gel samples was 7g, and thus the salt masses (m_{salt}) can be scaled down accordingly as follows:

$$\frac{m_{solv/L}}{m_{salt/L}} = \frac{7}{m_{salt}} \quad \text{Equation 3-6}$$

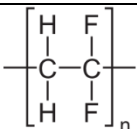
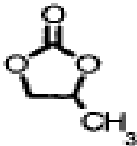
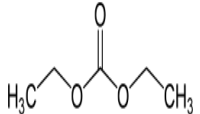

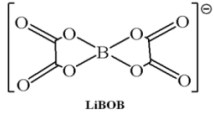
3.2.2.2 30%PVDF/PC/LiBOB

The procedure for making 30%PVDF/PC/LiBF₄ outlined in section 3.2.2.1 was also used to make 30%PVDF/PC/LiBOB polymer gel electrolytes with different concentrations of LiBOB. Table 3-6 shows LiBOB concentrations and their corresponding masses.

3.2.2.3 PVDF/PC/LiBF₄ 1M, different polymer concentrations

The procedure outlined in section 3.2.1.2 was also used to make PVDF/PC/LiBF₄ 1M with different polymer concentrations, using polymer mass calculations. The new PVDF-based gels were prepared by dissolving different amounts of PVDF in a glass tube containing an electrolyte solution composed of 5.834ml PC with 1 molar concentration of LiBF₄.

Table 3-3 Room temperature physical properties of PVDF, PC, DEC and LiBF₄

Material	Property (unit)	value	
PVDF - (-CH ₂ -CF ₂ -) _n -		Molecular weight Mw (g/Mol)*	570,000
		Density (g/cm ³)	1.78
PC C ₄ H ₆ O ₃		Density at 25°C (g/cm ³) ^[118]	1.19993
		Melting Point (°C)	-55
		Boiling Point (°C)	240
		Dielectric constant ^[118]	64.96
		Viscosity η (mP.s) ^[118]	2.512
DEC C ₅ H ₁₀ O ₃		Density (g/cm ³) ^[124]	0.9691
		Dielectric constant ^[127]	2.84
		Viscosity η (mP.s) ^[124]	0.749
		Melting Point (°C)	-43
LiBF ₄ LiBF ₄		Boiling Point (°C)	126–128
		Density (g/cm ³)**	1.6
		Molar mass (g)	93.74
LiBOB LiB(C ₂ O ₄) ₂		Density (g/cm ³)**	1.7
		Molar mass (g)	193.79

* Solvay official website:

** Measured in Leeds due to absence of any data in the literature (±0.1).

Table 3-4 PVDF concentrations and equivalent masses

PVDF concentration (%)	PVDF mass (g)	PC mass (g)
20	1.750	7
25	2.333	7
30	3.000	7
35	3.769	7
40	4.667	7

Table 3-5 LiBF₄ concentrations and the corresponding masses.

Salt Concentration M	mass of PC g	mass of LiBF ₄ g
0.2	7	0.111
0.4	7	0.224
0.6	7	0.340
0.8	7	0.459
1.0	7	0.581

Table 3-6 LiBOB concentrations and the correspond masses.

Concentration M	mass of PC g	mass of LiBOB g
0.2	7	0.231
0.4	7	0.474
0.6	7	0.728
0.8	7	0.995
1.0	7	1.276

Table 3-7 PVDF concentrations and equivalent masses in an electrolyte solution of PC/LiBF₄ 1M

PVDF concentration (%)	PVDF mass (g)	PC mass (g)	LiBF ₄ mass (g)
20	1.750	7	0.581
25	2.333	7	0.581
30	3.000	7	0.581
35	3.769	7	0.581
40	4.667	7	0.581

3.2.2.4 PVDF/PC: DEC/LiBF₄ with variations in PC:DEC ratio

When making gels with mixed solvents, the total volume of solvent was kept constant, and the ratio of the two solvents was defined as a volume ratio. This procedure involved producing liquid electrolytes by dissolving LiBF₄ (at a concentration of 1M) in a mixture of PC:DEC with volume ratios from 100:0 to 65:35 in glass tubes, then stirring the solution until the salt dissolved. Solvent masses were calculated so that the total solvent volume remained (as previously) at 5.834cm³. 3g of PVDF was then added to each ionic solution and the mixture heated to 160°C for 15min. The masses of the salt solution were then calculated as follows.

The mass of PC needed to make 30%PVDF/PC/LiBF₄ is 7g. So the volume of this amount is given by the equation:

$$V_{PC} = \frac{m_{PC}}{\rho_{PC}} = \frac{7}{1.19993} = 5.834cm^3 \quad \text{Equation 3-7}$$

where m_{PC} and ρ_{PC} are the mass and room temperature density of PC respectively.

This volume is used as the total volume of the two solvents (V_{sol}) in the following calculations:

$$V_{Sol} = V_{PC} + V_{DEC} = 5.833 cm^3 \quad \text{Equation 3-8}$$

Letting R be the volume ratio of PC:DEC:

$$\frac{V_{PC}}{V_{DEC}} = R \quad \rightarrow \quad V_{PC} = R * V_{DEC} \quad \text{Equation 3-9}$$

where V_{PC} and V_{DEC} are the room temperature volumes of PC and DEC respectively.

Substituting Equation 3-9 in Equation 3-8 gives:

$$V_{Sol} = R * V_{DEC} + V_{DEC} = 5.833 cm^3 \quad \text{Equation 3-10}$$

Hence:

$$V_{DEC} = \frac{5.833}{R + 1} cm^3 \quad \text{Equation 3-11}$$

and

$$V_{PC} = \frac{5.833 * R}{R + 1} cm^3 \quad \text{Equation 3-12}$$

The equivalent masses can then be obtained as follows:

$$m_{PC} = V_{PC} * \rho_{PC} \quad (g) \quad \text{Equation 3-13}$$

$$m_{DEC} = V_{DEC} * \rho_{DEC} \text{ (g)} \quad \text{Equation 3-14}$$

Table 3-8 shows the concentrations and masses of solvents, salt and polymer used to prepare this type of mixed solvent PGE.

Table 3-8 composition of PC:DEC mixed solvents gels.

PVDF	PC:DEC	V_{PC}	V_{DEC}	m_{PC}	m_{DEC}	LiBF₄(1M)
Mass (g)	Volume Ratio	(cm³)	(cm³)	(g)	(g)	(g)
3	100:00	5.834	0.000	7.000	0.000	0.581
3	95:05	5.542	0.292	6.650	0.283	0.581
3	90:10	5.250	0.583	6.300	0.565	0.581
3	85:15	4.959	0.875	5.950	0.848	0.581
3	80:20	4.667	1.167	5.600	1.131	0.581
3	75:25	4.375	1.458	5.250	1.413	0.581
3	70:30	3.792	2.042	4.550	1.978	0.581
3	65:35	3.500	2.333	4.200	2.261	0.581

3.3 Sample preparation

In spite of the variations in test conditions that were required for some samples to be processed, all the gel samples were originally prepared in the same environment—an oxygen-free nitrogen-filled glove box. This was used to reduce moisture, which affects the properties of some of the materials used, such as the electrolyte salts. The samples were then processed according to the test conditions. The techniques that were used for preparing and processing the gels will now be provided in the following sub-sections.

3.3.1 The glove box

An MBraun Labmaster 130 Glove Box was used for preparing gel samples. This is a box with high strength glass walls that is used to keep the materials inside under a pressure slightly higher than one atmosphere at low humidity (~5%), see Figure 3-4 below. The gel was prepared inside the glove box because some materials (e.g. lithium salts) are very hygroscopic, and gels need to be made in a water-free environment.

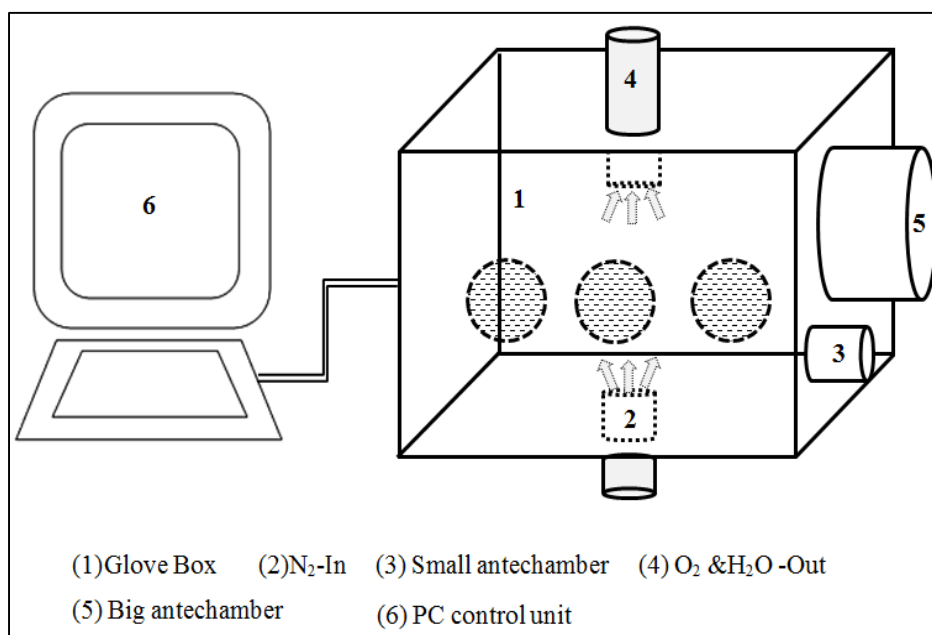


Figure 3-4 Schematic view of the glove box

3.3.2 Hot presser

A hot presser is used to make thin films within a ~50 micron thickness for use in morphological investigations in optical microscopy and WAXS (Wide Angle X-Ray Scattering). It can also be used to make thin samples (~2 mm thickness) for the parallel plate method used for rheological measurements. This tool consists of two square cross-sectional shaped metallic plates with a screw at each corner, as shown in Figure 3-5. Hot pressing is done by heating the two metallic plates to 160°C, and inserting a piece of gel between them that will be melted using separators to give the required thickness, as shown below. After the gel has been melted and flattened, the two plates are screwed together using four screws, in order to let the sample cool at the desired thickness.

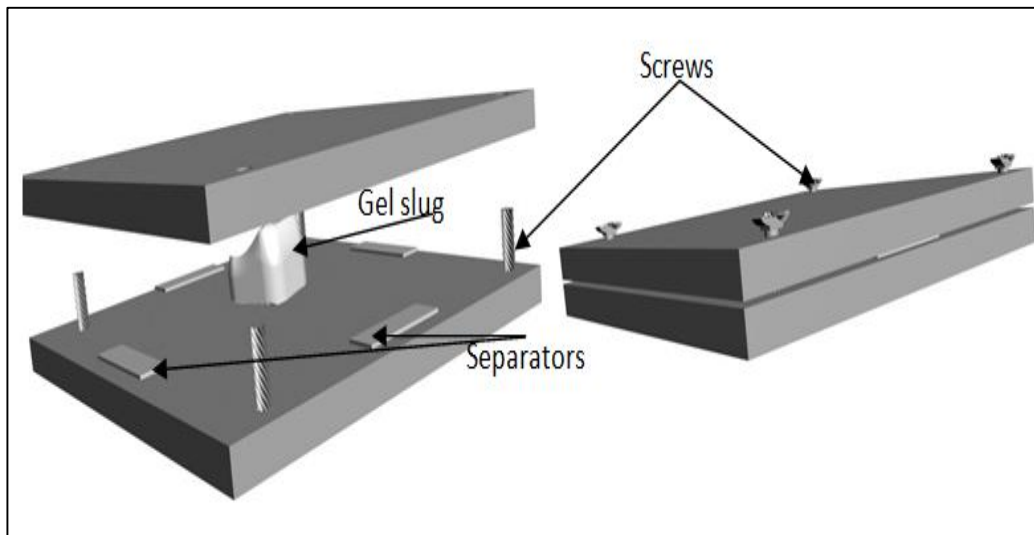


Figure 3-5 Hot pressing plates with gel samples in between.

3.4 Rheological studies

3.4.1 Introduction

The term 'rheology' refers to the science of the deformation and flow of matter under applied force, while 'rheometry' refers to the tools and devices that are used to measure and determine rheological data [128]. Rheological experiments were undertaken in this research in order to help determine the gelation mechanism.

3.4.2 Dynamic mechanical thermal analyses

Dynamic mechanical thermal analyses (DMTAs) are techniques that are typically used to analyse and measure the rheological properties of materials under thermal conditions. DMTA gives clear information about phase transitions, viscosity, tensile and/or shear modulus... etc.

In spite of the diversity of DMTA machines, the working principle is always virtually the same, involving the application of an oscillating deformation and the resulting force being measured [129].

The applied deformation (e) is given by:

$$e = e_o \sin(\omega t) \quad \text{Equation 3-15}$$

And the resulting force is given by:

$$F = F_o \sin(\omega t + \delta) \quad \text{Equation 3-16}$$

where ω is the angular frequency (in $\text{rad}\cdot\text{sec}^{-1}$) and δ is the phase angle.

In this research, non-standard geometry was used to allow the measurement of the mechanical properties in both the sol and gel phases. The results are presented to show the components of the force, both when it is in-phase and out of phase with the applied deformation, so that the relative weighting of the elastic and viscous responses can be seen. The results are shown as F' and F'' , where:

$$F' = F_o \cos(\delta) \quad \text{Equation 3-17}$$

And

$$F'' = F_o \sin(\delta) \quad \text{Equation 3-18}$$

The DMTA machine used different geometries depending on material types. For instance, a concentric cylinder was used to measure fluids, while rectangular torsion was used to measure solids. Similarly, cone and parallel plates were used to measure rubbery and gel materials. Figure 3-6 below illustrates these different geometry systems.

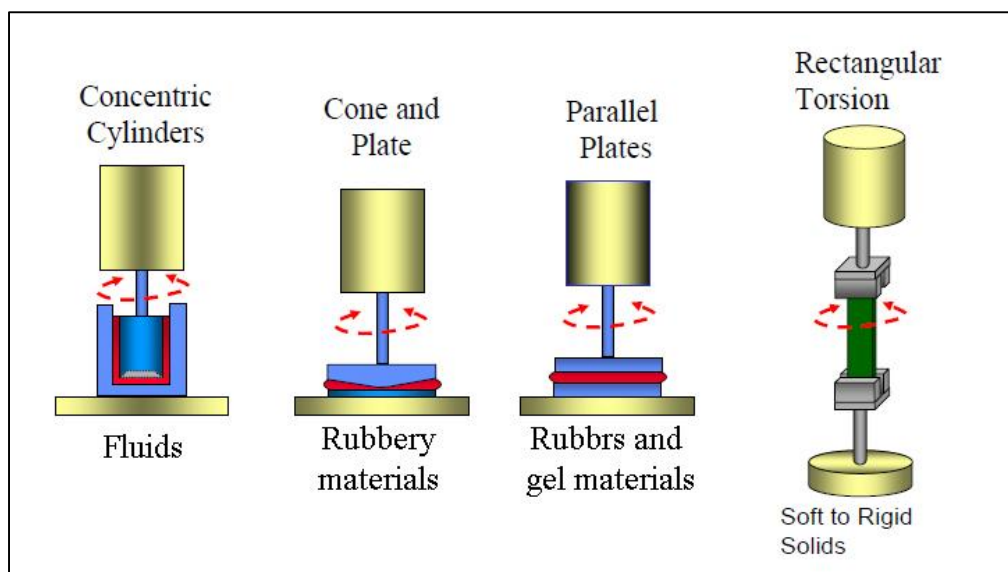


Figure 3-6 DMTA Geometries

3.4.3 Rheological instruments: the RSA II machine

The Rheometric Solid Analyser RSA II was used to measure the shear modulus behaviour that occurred with temperature increases. The machine was modified to measure the shear modulus of solid gel and its viscous solution, having been originally designed to measure tensile and compression moduli for solid polymers. This modification was required so that the solid gel (with $G' \sim 10^5$ Pa) could be measured with the same instruments after it had undergone its viscous molten transition (when $G' \sim 10^2$) through containing the gel in a glass tube. Thus, using this modification, the gel could be measured in both states at the same time and under the same conditions.

The modification of the machine involved replacing the tensile grips with a screw thread and tube (see Figure 3-7), and this was first performed by Voice et al. [14]. The process involves chopping the gel into small pieces of

3-4mm, inserting the pieces into a tube, and heating them they have melted. The screw thread is inserted into the tube of the molten gel, as shown in Figure 3-7, then fixed to the transducer from the top, whilst it is constrained at the bottom by fixing it to the motor. The sample is then rapidly cooled to the desired isothermal condition and measurements are taken to show the sample's mechanical responses over time.

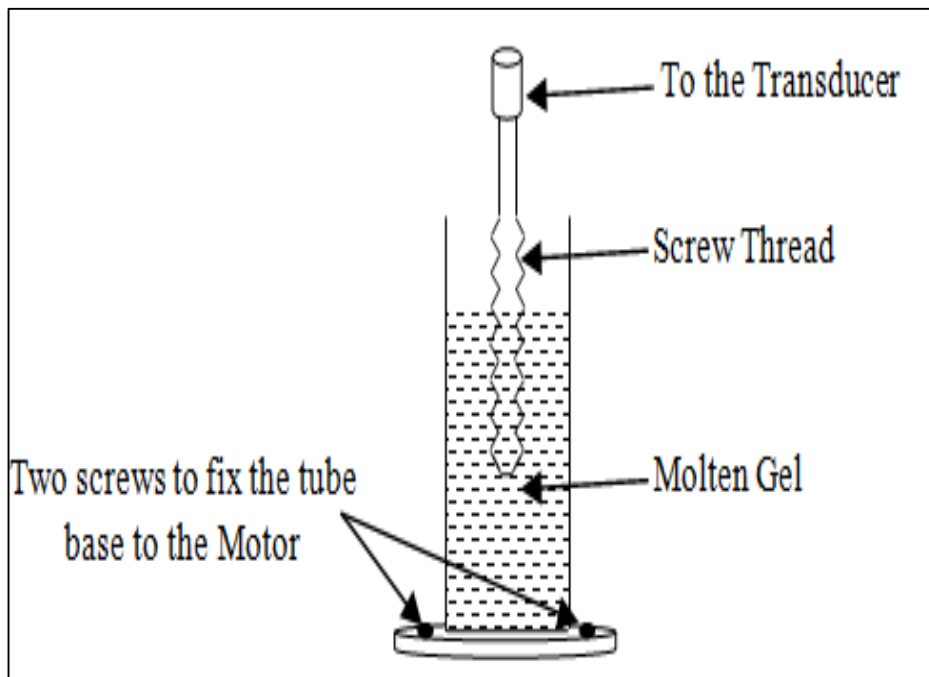


Figure 3-7 Screw-thread Tube Method used with RSA II.



Figure 3-8 The RSA II Machine

3.5 Differential scanning calorimetry

3.5.1 Introduction

Differential Scanning Calorimetry (DSC) is one of the techniques that can be used for investigating thermal transitions of polymers and gels through melting, crystallisation and glass transition. This instrument measures the difference in the amount of heat that is required to increase the temperature between a sample and the reference. The device is sketched in Figure 3-9 below. As shown, the DSC system consists of a DSC chamber, which in turn consists of two wells in which the measured sample and reference (empty pan) are mounted. The sample and reference are then heated by the electrical furnace that is connected to the bottom of the wells. During the heat flow, the sample and reference are kept at the same temperature. Any difference in the amount of heat absorbed or released by

the sample and the reference is measured as a function of the temperature. When the sample undergoes thermal transition, it exhibits endothermic or exothermic peaks (see Figure 3-10), which can be analysed on the computer using the specified software [130–132]. Before measurements are made, it is essential that the instrument is calibrated using an indium standard sample with an onset melting temperature of 156.6°C and a heat of fusion of 28.45J.g⁻¹. DSC measurements typically run under a constant pressure, and therefore heat flow varies equivalently with the enthalpy changes, which can be calculated as follows:

$$\left(\frac{dQ}{dt}\right)_p = \frac{dH}{dt} \quad \text{Equation 3-19}$$

where, dH/dt is the heat flow, measured in J.sec⁻¹. The heat flow difference between the sample and the reference is calculated as follows:

$$\Delta \frac{dH}{dt} = \left(\frac{dH}{dt}\right)_{sample} - \left(\frac{dH}{dt}\right)_{reference} \quad \text{Equation 3-20}$$

which can be used to interpret the resulting peaks. When $\Delta \frac{dH}{dt}$ is positive (i.e. $\left(\frac{dH}{dt}\right)_{sample} > \left(\frac{dH}{dt}\right)_{reference}$), this means that the heat absorbed from the sample is higher than that of the reference, and hence the device shows endothermic transition. When $\left(\frac{dH}{dt}\right)_{sample} < \left(\frac{dH}{dt}\right)_{reference}$ (i.e. $\left(\Delta \frac{dH}{dt}\right)$ is negative), this will appear on the monitor as an exothermic peak.

3.5.2 The enthalpy of melting.

In the DSC programme, the enthalpy of transition, ΔH , can be calculated as a function of the transition point and the peak area, i.e. the enthalpy of

melting or crystallisation can be found as follows:

$$\text{Peak area} = \int \frac{dQ}{dt} dT \quad \text{Equation 3-21}$$

where T is the temperature, and the heat rate is the time variation of temperature.

i.e. heat rate = dT/dt .

$$\therefore \text{Peak area} = \text{heat rate} \cdot \int dQ \quad \text{Equation 3-22}$$

Hence,

$$\text{Peak area} = \text{heat rate} \times \Delta Q \quad \text{Equation 3-23}$$

But,

$$\Delta Q = m \cdot \Delta H \quad \text{Equation 3-24}$$

Substituting ΔQ value from Equation 3-24 into Equation 3-23 gives;

$$\text{peak area} = m \cdot \Delta H \cdot \text{heat rate} \quad \text{Equation 3-25}$$

Thus,

$$\Delta H = \frac{\text{Peak area}}{m \times \text{heat rate}} \quad \text{Equation 3-26}$$

Where m is the mass of the gel (g). Equation 3-26 shows that the peak area depends on the heating rate. Therefore, one should take care to choose a suitable heating rate when running DSC measurements. Typically, heating rates are between 2 to 20°C per minute. This work used 10°C/min for all samples.

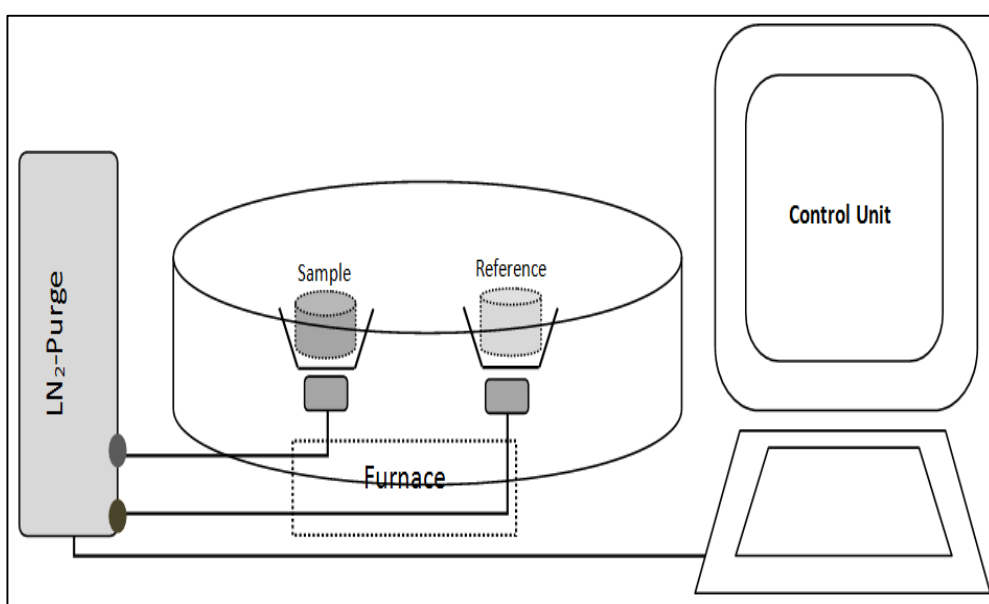


Figure 3-9 Simplified sketch illustrating the DSC technique

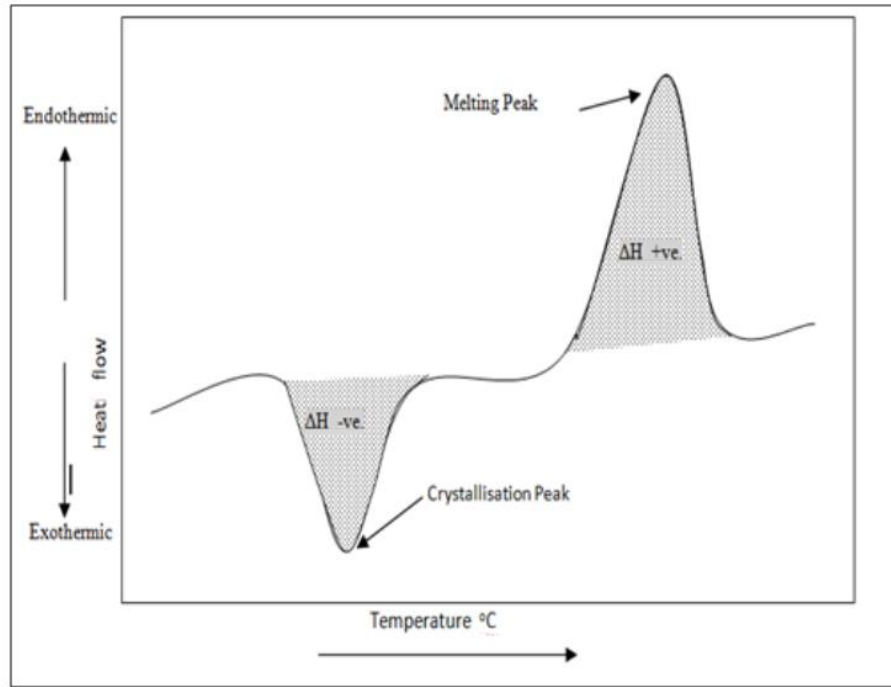


Figure 3-10 Heat transitions measured by the DSC.

3.5.3 Polymer and gel crystallinity

The latent heat of melting (enthalpy of melting ΔH) that is obtained using Equation 3-26 can be used to find out how much crystallinity there is in the polymer (or gel). This can be done by measuring the ratio between the latent heat of melting for the gel (ΔH) and the latent heat of the pure polymer (100% crystalline polymer) (ΔH^*) [133], which is denoted by χ_{gel} . I.e.:

$$\chi_{gel} = \frac{\Delta H}{\Delta H^*} \quad \text{Equation 3-27}$$

The crystallinity of the polymer, χ_{pol} , is then worked out as follows:

$$\chi_{pol} = \frac{\chi_{gel}}{m_{pol}/m_{gel}} \quad \text{Equation 3-28}$$

where m_{pol}/m_{gel} is the mass of polymer to the mass of the whole gel ($m_{gel} =$

$m_{\text{pol}} + m_{\text{solvent}} + m_{\text{salt}}$). The ΔH^* of PVDF is 104.7 J/g [134].

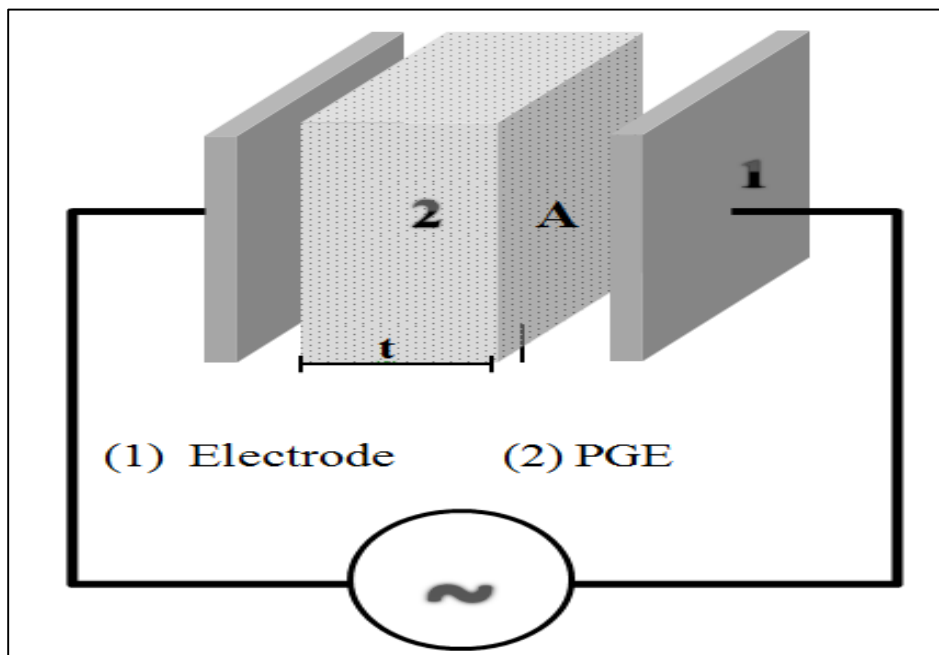
3.6 Ionic conductivity

3.6.1 The ionic conductivity of polymer electrolyte cells containing blocking electrodes.

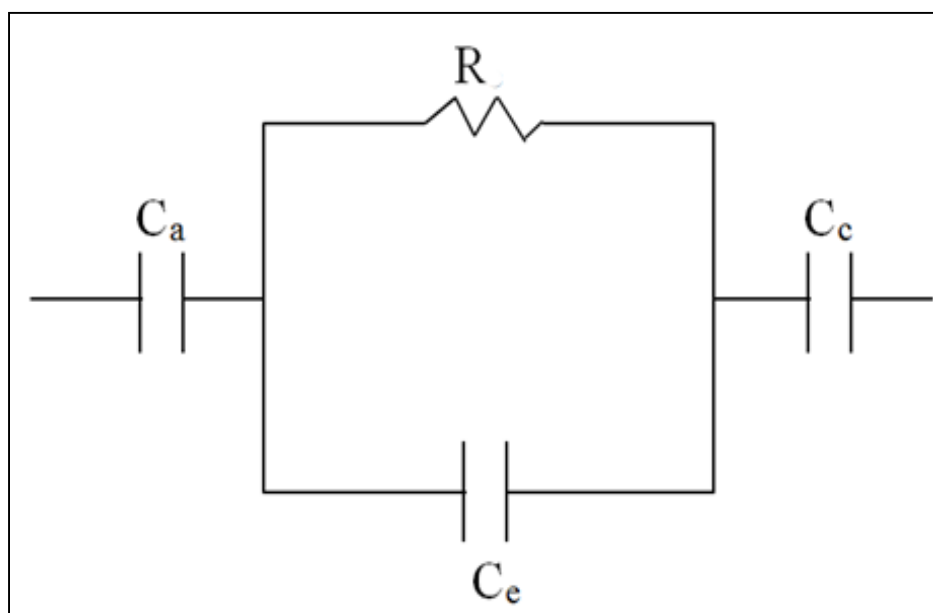
Dielectric spectroscopy can be used to determine the ionic conductivity of the polymer gel through applying an A.C. voltage and observing the change in the impedance through a range of frequencies. This technique is commonly referred to as the impedance spectroscopy. It was theorised by J.R. MacDonald [135] and established experimentally by Sorensen and Jacobsen [136]. The major characteristic of a polymer electrolyte cell containing blocking electrodes is that no reactions occur between the mobile species and the electrodes. Therefore, the electrodes of the cell are made from inert metal. To understand the ionic conduction in such electrolyte/electrode systems, let us consider an idealised lithium ion conducting polymer with platinum blocking electrodes. If an A.C. voltage with a variant frequency was applied to the cell, the resulting circuit could be simulated in the way sketched in Figure 3-11(b) below. The electrodes would become alternatively positively and negatively charged, and thus the sinusoidal electric field across the electrolyte would drive the lithium ions back and forth in phase with the applied voltage. (In Figure 3-11(b), the resistor, R, represents the migration of the lithium ions.)

Another detectable effect of the applied voltage on the electrolyte polymer would be the polarisation of the immobile polymer chains, which can be

represented by the capacitor C_e .

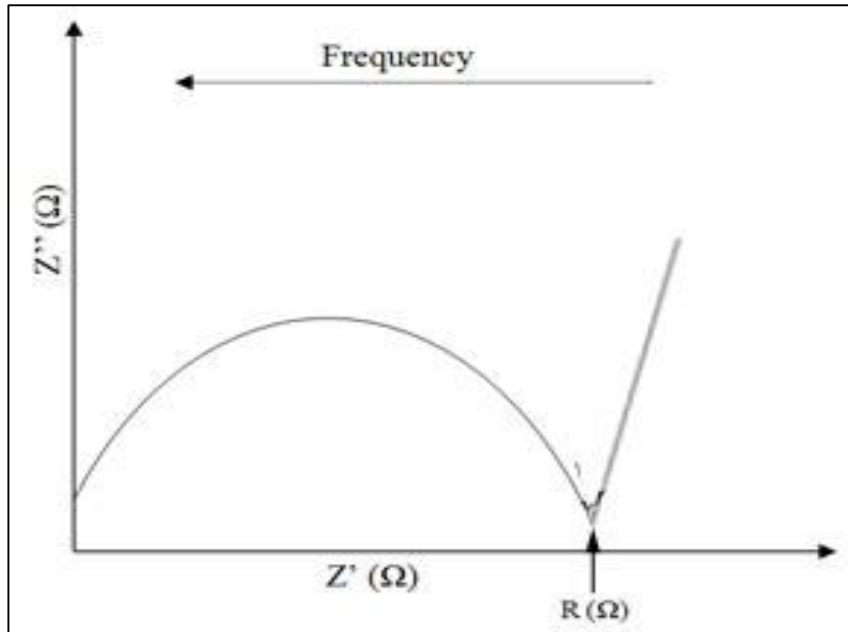


(a)

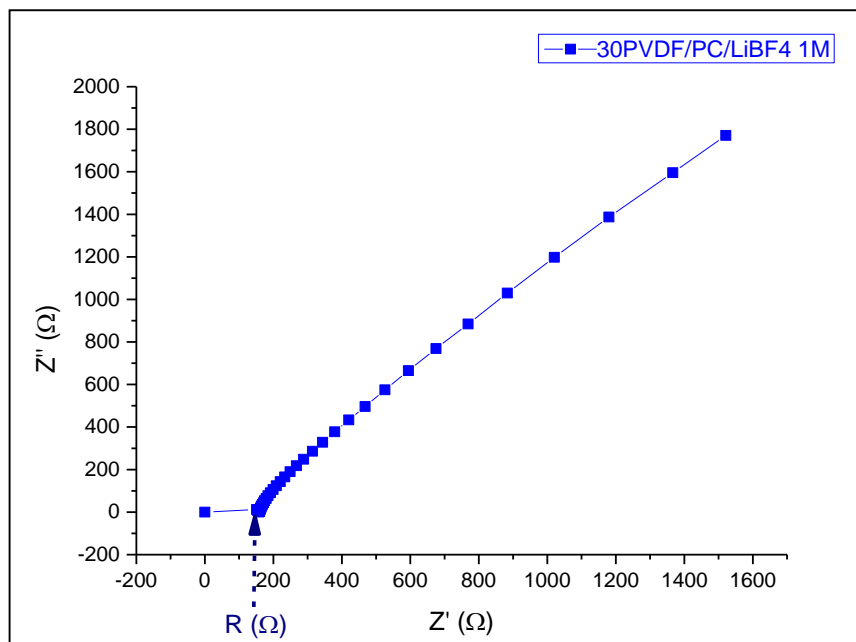


(b)

Figure 3-11 Model of the ionic conductivity cell illustrating: (a) A simulated circuit for PGE (2), with thickness (t) and area (A) inserted between two electrodes (1); and (b) The equivalent circuit for the polymer/electrode interfaces, where C_a is the capacitance of the anode, C_c is the capacitance of cathode, R is the internal bulk resistance of the gel, and C_e is the capacitance of the electrolyte.



(a)



(b)

Figure 3-12 The imaginary component plotted against the real component of the impedance for (a) the ideal electrolyte and (b) a typical gel electrolyte.

The driven ions would then be alternatively accumulated and depleted at each electrode due to the alternating field, causing a very thin electrode/electrolyte interface. This would behave as a capacitor with a high capacitance, and would be considered to be the capacitance of the anode interface, C_a , and the cathode interface, C_c . The semicircle in Figure 3-12 represents the electrolyte contribution at a high frequency, while the spike at the low frequency is due to the blocking electrode/electrolyte interface. The resistance, R , of the PGE is the value of the Z' when $Z''=0$, which is typically 10^2 to 10^3 ohms.

In the above discussion, only the ideal behaviours of the cell and the electrode/electrolyte interface were considered. In the real cell, however, the complex plot is noticeably different from the idealised plot, as shown in Figure 3-12 (b). In this case, the semicircle is broadened, and is hard to detect, and electrode spike is non-vertical. This may be due to the surface layers on the electrodes, long-term ion migration issues, the inhomogeneity in the electrolyte and the microscopically rough electrode surfaces. The measured resistance, R , can be related to the ionic conductivity in Equation 3-29 for a uniform cross-section of a homogeneous substance (like that shown in Figure 3-12(a)), with thickness t and area A , and is given by the equation:

$$\sigma = \frac{t}{RA}$$

Equation 3-29

where σ is the ionic conductivity measured in S/cm.

3.7 X-Ray scattering analysis (WAXS)

3.7.1 Introduction

X-rays are electromagnetic waves with wavelengths of 0.1-0.2 nm. X-ray diffraction occurs due to the reaction of bands of x-ray beams with atoms and/or molecules. It has been found that x-rays are scattered in different directions from any material that they are targeted at. When the scattered beams from the whole crystal structure interfere with each other, this produces a diffracted beam that is reflected in one direction and can be picked up by a detector [137]. The principle of interaction between x-rays and material particles (atoms and/or molecules) has been used to investigate the crystal structure of materials. There are two methods used for doing this, depending on the spacing between the crystal planes. When the wavelength of x-ray λ is smaller than the structure spacing, the beam is scattered at small angles ($\theta \leq 5^\circ$), and hence the method used to investigate such structures is that of Small Angle X-Ray Scattering (SAXS). If λ is larger than the structure spacing, the resulting beam is scattered at greater angles ($\theta > 5^\circ$), and the method is Wide Angle X-Ray Scattering (WAXS).

3.7.2 Bragg's Law

A diffracted beam produces a high intensity when Bragg's condition is instantiated. Bragg's condition occurs when the reflected beams from one crystal plane are in the same phase with the reflected beams from the next

plane. This may cause constructive interference, and the wavelength, λ , of any two incident beams reflected from the two successive planes separated by d -spacing is equal to the path difference between them. Bragg's Law can be derived by considering Figure 3-13, which shows incident beams contacting planes with d -spacing. The first beam is reflected from the upper plane at angle θ , while the second one continues to the next plane and is reflected at the same angle θ . Given that the two beams are equal in their wavelengths, and reflect in the same phase, we can calculate the difference in their paths [138].

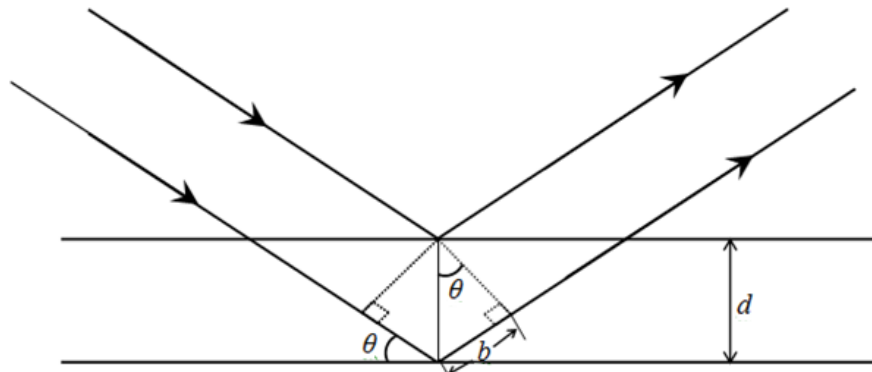


Figure 3-13 Demonstration of Bragg's diffraction law.

$$\sin\theta = \frac{b}{d}$$

Equation 3-30

$$\text{Path difference} = 2b$$

The condition required for constructive interference to take place is that the difference between the incident beams be in $n\lambda$ wavelength, where n is an integer.

I.e.

$$2b = n\lambda \quad \text{Equation 3-31}$$

Therefore

$$n\lambda = 2d\sin\theta \quad \text{Equation 3-32}$$

This is Bragg's Law of diffraction.

WAXS refers to the measurement technique that uses wide angle x-ray scattering diffraction. This technique is usually used to measure the diffracted x-ray beam from the crystalline structure in order to investigate the crystal conformations of polymers. It can aid in the examination of the crystalline structures of crystal planes with smaller separating distances that produce scattering angles 2θ of larger than 5° . On the other hand, the SAXS (small-angle x-ray scattering) x-ray diffraction technique is used for investigating structures within spacings of within nanometres, which give scattering angles 2θ close to 0° [139]. Another property that can be determined from the x-ray spectroscopy is that of crystal size, which can be determined by using the Scherrer equation:

$$L = \frac{\lambda}{\beta \cos \theta}$$

Equation 3-33

where λ is the x-ray wavelength, β is the full width at half the maximum of WAXS detected peak, and θ is Bragg's angle.

3.8 Optical microscopy

Optical microscopy can be used to visually investigate polymer structure. Typically, it involves the use of a visible light microscope with a system of lenses set up to provide illuminated magnified images of samples. Optical microscopes have many shapes and designs that vary with different manufacturers and because of the purposes for which they were developed. However, they all work according to the same principle—they collect light from a sample using a very high-powered magnified lens, called an objective lens, to form a real image. This real image is then magnified by a second lens or group of lens called an eyepiece. Figure 3-14 provides a simple image on the left that represents the principle of optical microscopy in the magnification process [140], and a simple sketch of an optical microscope on the right.

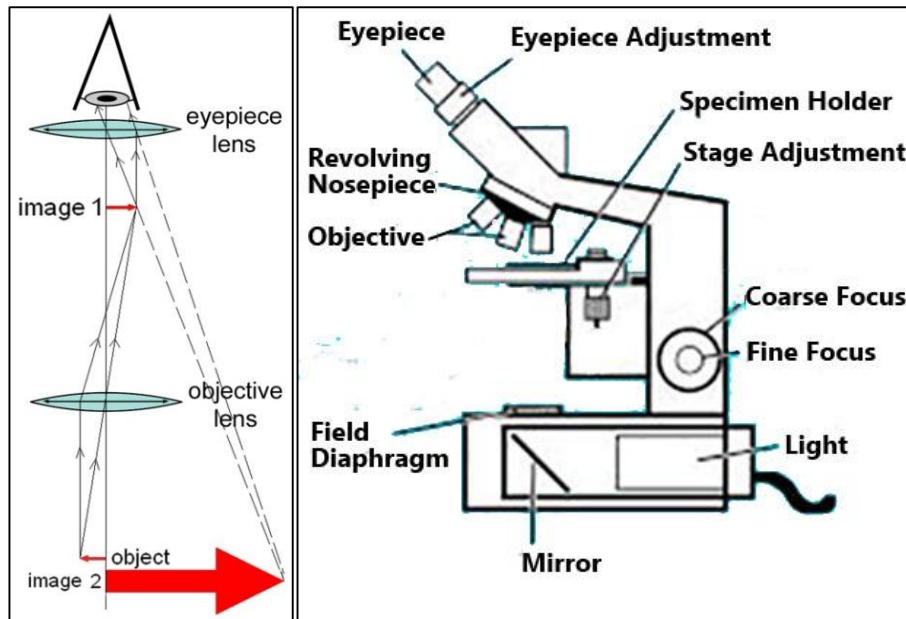


Figure 3-14 The principle of optical microscopy principle (left), and a sketch of an optical microscope (right) [140].

Modern microscopes are usually compound microscopes with exchangeable objective lenses to adjust the magnification. They produce a high quality image at large magnifications and reduce chromatic deviation in comparison to the more simple dissecting microscope. Furthermore, they provide more magnification setups than dissecting microscopes.

Structures investigated in optical microscopy must be no less than $1\mu\text{m}$ across in order for accurate information on them to be obtained. This is because the limitation in resolution is half the wavelength of the light used ($\sim 250\text{nm}$). It is also difficult to recognise the structures in transparent samples (even though they are of suitable sizes) because of their lack of absorption capability in both non-crystalline and crystalline regions, which leads to a poor contrast between them. Polarised light can be used to solve this problem, which involves placing a polariser below the sample and an analyser above so that the analyser is at right angles to the polariser.

Cross-polarising can be understood by understanding the propagation of light through a crystal. When polarised light with a light wave of electric vector D is applied to the sample, the refractive index n of a crystal depends on the direction of this vector (the polarisation direction) in relation to the crystal axes. Figure 3-15 shows the difference in the refractive index with the direction of the incident and the polarised waves. The crystal is shown as a shaded ellipse placed inside an indicatrix represented by the ellipsoid with the x_1 , x_2 and x_3 axes in, and with a radii proportional to n . When polarised light with the D -vector is transmitted through the crystal, then only two possibilities can occur. One happens when D is parallel with the vertical axis (x_3), and the other happens when D is perpendicular to the refractive index ellipsoid (i.e. x_1 or x_2). This causes a contrast in the analysed lights according to the resulting difference in the refractive indices that can be detected by either the eyepiece or by a digital camera fixed to the top of the microscope.

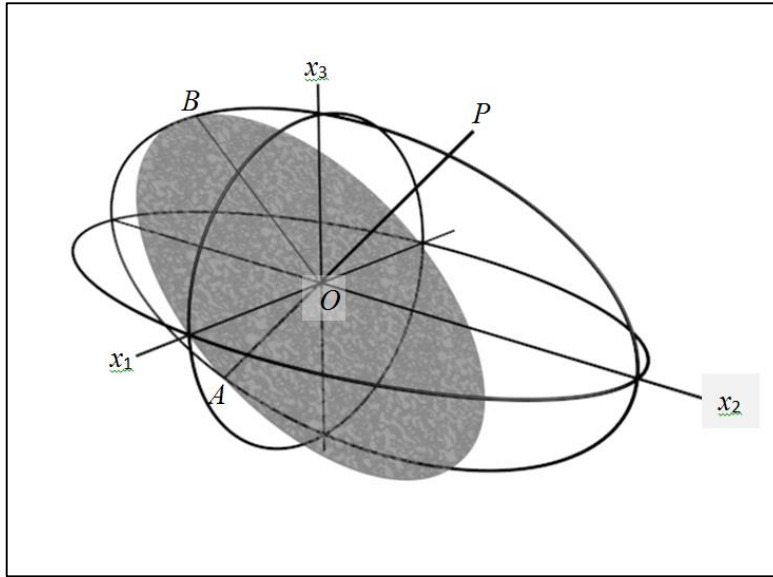


Figure 3-15 Refractive index ellipsoid or what is known as the 'indicatrix' with the crystal involved in it, to understand the crossed-polarisation principal.

3.9 Measurement procedures

3.9.1 DMTA

The Rheometric Solid Analyser RSA II was used to investigate the isothermal gelation point of the PGE samples using the screw thread modification apparatus illustrated in section 3.4.3. The samples were heated until melt at 160°C, and then rapidly cooled to a given temperature, at which it was observed until gelation point was acquired. A frequency of 1Hz and a strain amplitude of 0.15mm were used.

3.9.2 DSC

A PERKIN ELMER differential scanning calorimeter was used to investigate the gel's melting point and the crystallinity of the polymer gel electrolytes. DSC measurements were also used to investigate the isothermal crystallisation and subsequent melting of salted and unsalted

gels. Gel samples with masses between 8–12mg were chopped and put into sealed aluminium pans.

3.9.2.1 Isothermal crystallisation measurements

These tests were used to study the isothermal crystallisation and subsequent melting points of the polymer gel samples. The samples were annealed at 160°C for ~5min to melt the gel and erase any thermal history. The gel was then cooled rapidly (at 500°C/min) to the required isothermal temperature, and the data recorded with time. After each isothermal crystallisation, the sample was again heated to 160°C at 10°C/min, this time to obtain the subsequent melting temperature.

3.9.2.2 Melting temperature investigations

For these investigations, samples were measured in order to examine the effect of study parameters such as salt, solvent and polymer content on the PVDF's melting point, the gel's degree of crystallinity, and the polymer's degree of crystallinity (polymer fraction crystallinity). Each sample was heated from 20°C to 140°C using a heat rate of 10°C/min. PYRES software was used to observe and control the measurements, as this has the ability to analyse and manipulate the resulting curves. Using this software, the curves were fitted to determine the melting temperature and the heat of fusion through integrating the area under the melting curve.

3.9.3 Ionic conductivity

Molten gel was poured into a cell to prepare ionic conductivity samples in the glovebox, as shown in Figure 3-16, and the top metal plate was pressed down securely to ensure a good electrical contact. The gel was then left to cool down in the cell before the measurements were taken.

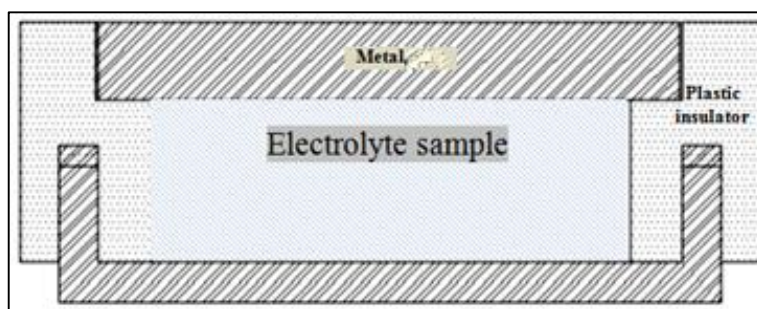


Figure 3-16 Ionic conductivity cell

A Novocontrol Frequency Analyser was used to test the samples at room temperature. An AC voltage was used, $V_{\text{rms}} = 1$ Volt, with a range of frequencies from 10^6 Hz to 10^1 Hz. The graphs of real versus complex impedances Z' and Z'' were plotted to obtain the resistance for each sample, R (where $Z'' \sim 0$) (see Figure 3-12).

3.9.4 WAXS measurements

DRONEK4- AXES HUBER Wide Angle X-ray diffraction apparatus was used to investigate changes in the crystal phase and size in gel with and without the addition of salt. The gel samples in this test were prepared as thin films with thicknesses of ~ 0.8 mm and surface areas of ~ 225 mm² via hot pressing (see section 3.3.2). The samples were then mounted to the machine using a metallic slide with a hole in its centre to allow the x-ray to

pass through the sample. The slide containing the gel film was then inserted into the slot in front of the x-ray path and fixed before the measurements were made. The system generated 40kV and 30mA to produce the x-ray. After the gel was fixed in front of the x-ray's path, measurements were taken by subjecting the sample to the x-ray in a wide range of angles 2θ between $5\text{--}45^\circ$, with an angle step of 0.1° , and data was collected for 1min at each step. By fitting Gaussian peaks, the separate X-ray peaks could be characterised. Figure 3-17 sketches the WAXS technique. The crystal planes were calculated from the reflection angles using Bragg's Law, while the crystal size, L , was detected using the Scherrer equation.

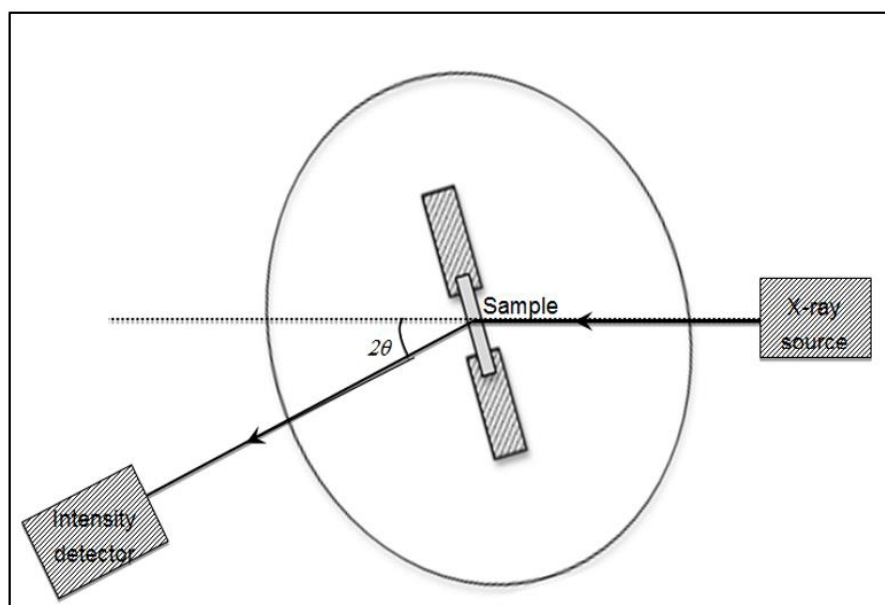


Figure 3-17 Sketch of WAXS diffraction technique measurements

3.9.5 Optical microscopy

Optical microscopy samples were prepared using two different approaches that were appropriate to the different natures of the tests. The first method used pre-made gel samples (both salted and unsalted samples that had been cooled in the glove box as mentioned above) that were hot pressed (see section 3.3.2). A small piece of gel was inserted between the hot plates of the press, which were pre-heated to 160°C. The hot presser was then left with the molten gel inside it until it cooled (which took about 4h), before being removed and measured. The gels were hot-pressed to form thin films of ~40µm thickness, and these samples were used to investigate the effect of salt on the pore size of the polymer gel.

The second method involved using a novel apparatus called a 'hot-stage' microscope. This apparatus (shown in Figure 3-18) consists of a metal base with a hole at its centre to allow light beams to pass through the sample to the observer. The stage contains two air flow paths, which provide compressed cool air that can cool the sample to the required temperature very quickly. The hot stage uses an electrical heater with a thermocouple attached to a small pin near the sample. In this test, gel samples were taken directly from the pre-made gel container (there being no need for hot pressing as the sample was going to be melted). The sample was covered by a transparent thin polyester film with a melting temperature of 250°C in order to protect the liquid from evaporating when the gel was melted. The gel was then melted at 160°C and cooled back to the required temperature so that the isothermal structure formation could be observed.

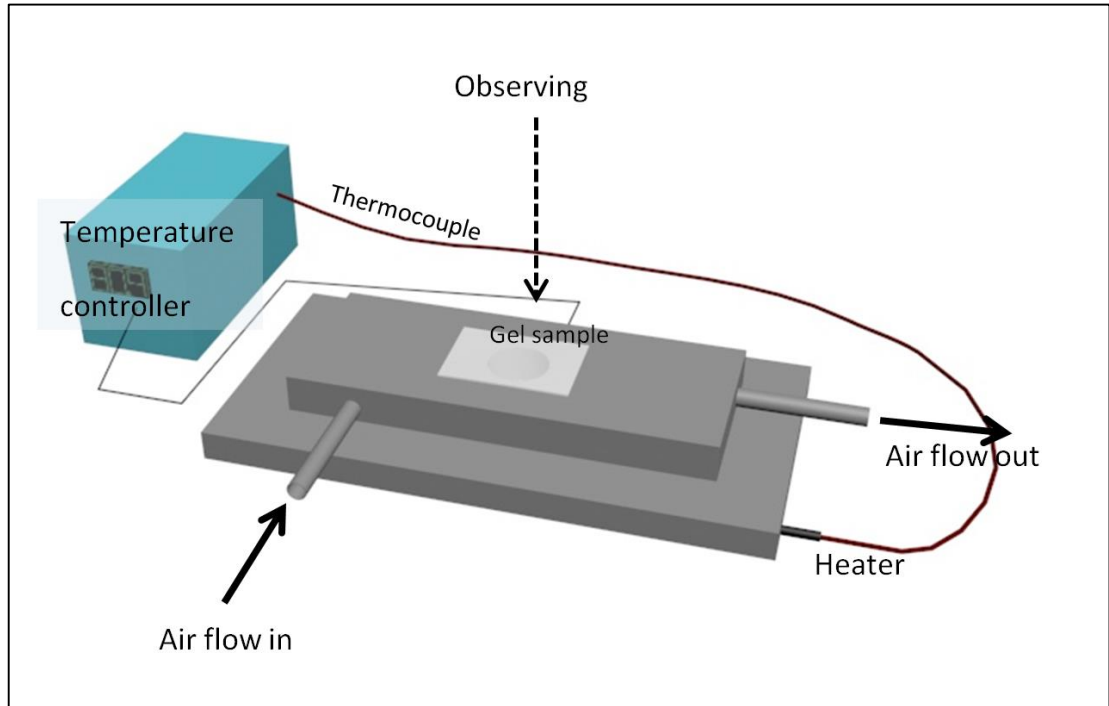


Figure 3-18 Sketch of the hot-stage microscopy

Chapter4. Isothermal Gelation

4.1 Introduction

This chapter presents and discusses the results regarding the gelation mechanisms that occurred and the structures of the gel that were formed through cooling the PVDF-based gels. The discussion includes the data that was collected from the differential scanning calorimetry DSC. Isothermal techniques were used to investigate the crystallisation of the molten gels using a DSC machine, and DMTA measurements were used for collecting gelation points isothermally from different temperatures. That is, the procedure from which the data were collected involved cooling molten gel samples rapidly to a specific temperature and then allowing them to form gels isothermally. Their formation was then studied using either a DSC machine or DMTA measurements. The data from the two techniques were then analysed and discussed individually, before they were combined together and compared to acquire key information about the mechanism of gelation.

The structure of the gel was investigated using optical microscopy and wide-angle x-ray scattering WAXS. Room temperature optical microscopy and room temperature WAXS were initially used to investigate the gel morphology and polymorphs respectively, with and without the addition of salt. Further study involved using a hot-stage optical microscope to observe phase separation as the molten material cooled. Investigations

using the optical microscope helped to reveal the nature of the phase separation, with cross-polarisers being used to show any spherulitic structures that formed.

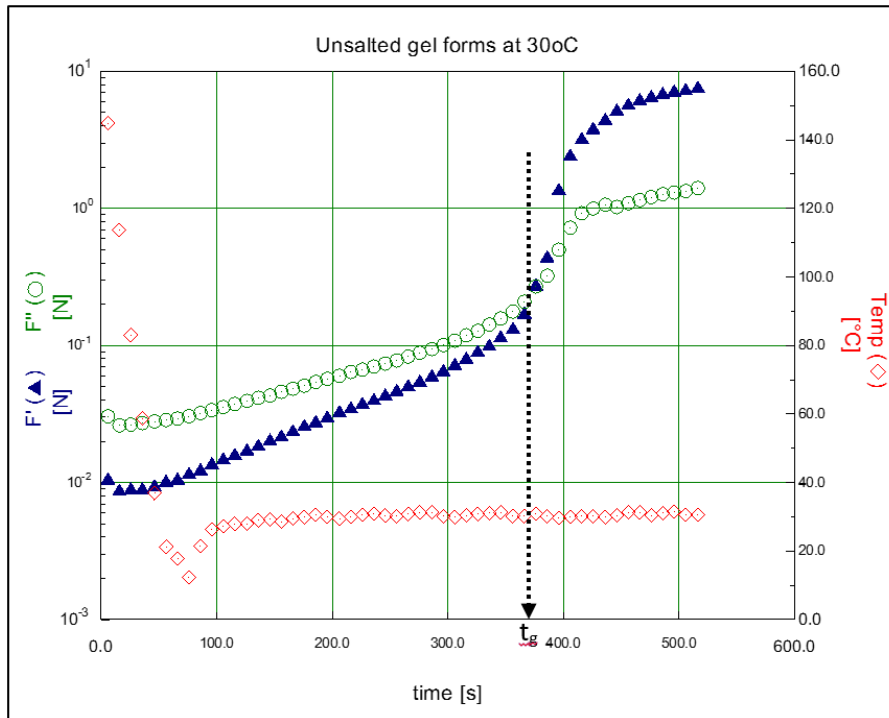
4.2 Isothermal formation

4.2.1 Gelation investigations using DMTA

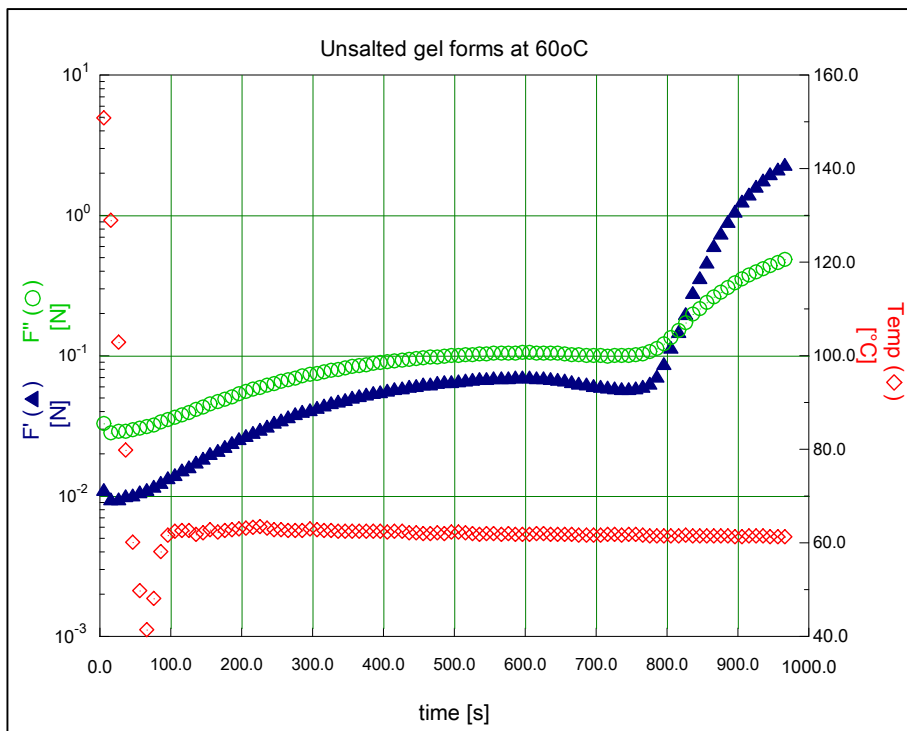
DMTA measurements were used to investigate gel formation through measuring the response of the sample to shear force during isothermal phase transition from the melt state to the gel state. The screw-tube technique described in section 3.4.3 was used to carry out these investigations for both salted and unsalted gels. Figure 4-1 and Figure 4-2 show the isothermal rheological data for the unsalted gels over a range of temperatures, including a point above which no gelation was observed. Figure 4-3, Figure 4-4 and Figure 4-5 show similar traces for the salted gels at different temperatures. Table 4-1 summarises the data acquired from the DMTA measurements.

Figure 4-6 shows the gelation time, plotted as a function of temperatures at which gelation took place isothermally for both salted and unsalted gels. It shows that gelation is rapid for both salted and unsalted gels at low temperatures, with unsalted gels taking a slightly longer time to gel. It also shows that unsalted gels do not form above 100°C, whereas salted gels keep forming at temperatures up to 150°C. Time of gelation (t_{gel}) was determined as the point where the storage and loss components of shear forces cross over, i.e. $F' = F''$. As mentioned in section 3.4.2, when gel is in a

molten state, the loss modulus is higher than the storage. Therefore, the gel shows a resistance to shear force when it transfers from the molten viscous state to the solid state, and hence the storage modulus comes over the loss modulus. The point at which this transition occurs is considered to be the gelation point, and hence the time at which gelation occurs is supposed to be called as the gelation time. As the gelation temperature is increased, the time to gel also increases. The gelation time's dependency on the gelation temperature in PVDF thermoreversible gels has also been reported by Cho et al. [41], who observed similar behaviours in gel behaviour to those seen in the current research in relation to phase separation during earlier stages of gelation. Guojie et al. [141] also reported the electrolyte salt having a similar effect on the gelation time to those found in this study, and attributed the reduction in the time of gelation with the addition of salt to the variations in the local junctions of the polymer. They suggested that when the gel forms in the presence of salt, the salt quickly nucleates the chains, causing shorter but increased numbers of junctions, leading to less gelation and lower gelation times.

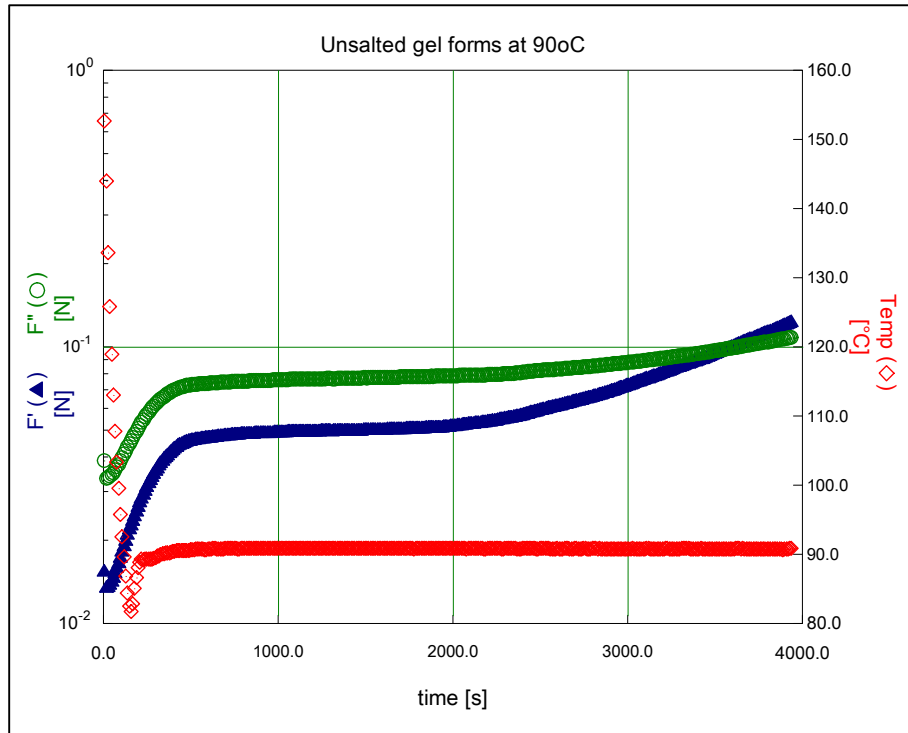


(a)

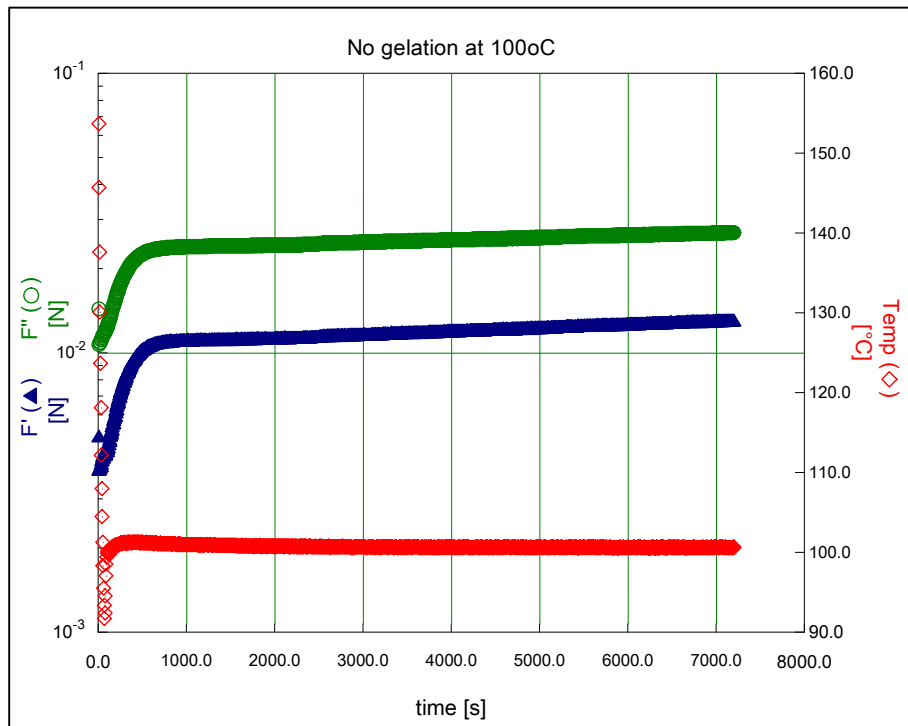


(b)

Figure 4-1 Isothermal gelation using DMTA for 30PVDF/PC unsalted gel, showing the time at which gelation occurs ($F'=F''$), at (a) 30°C and (b) 60°C.

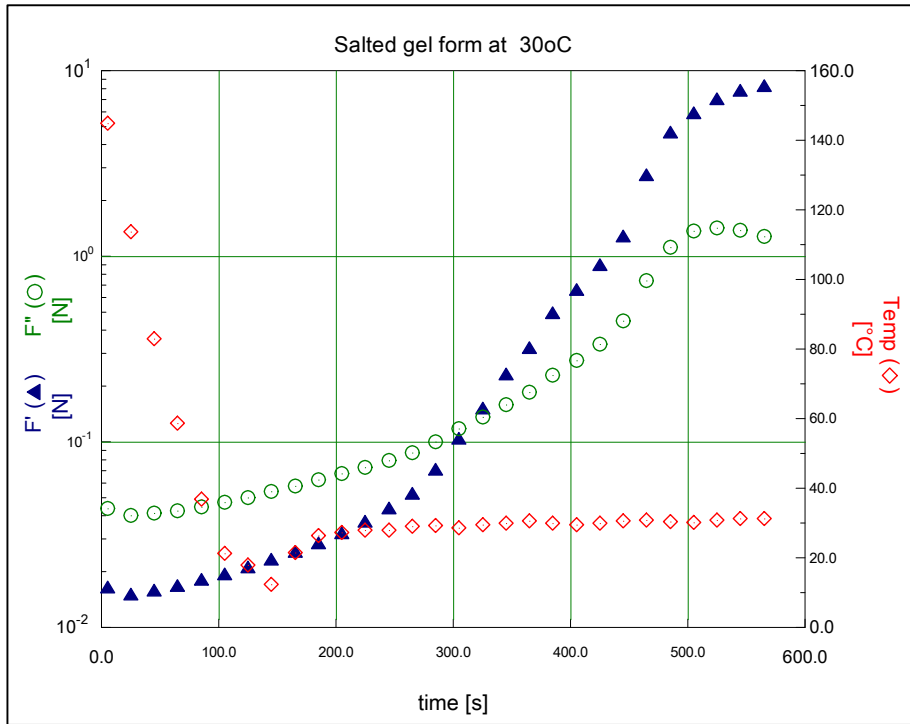


(a)

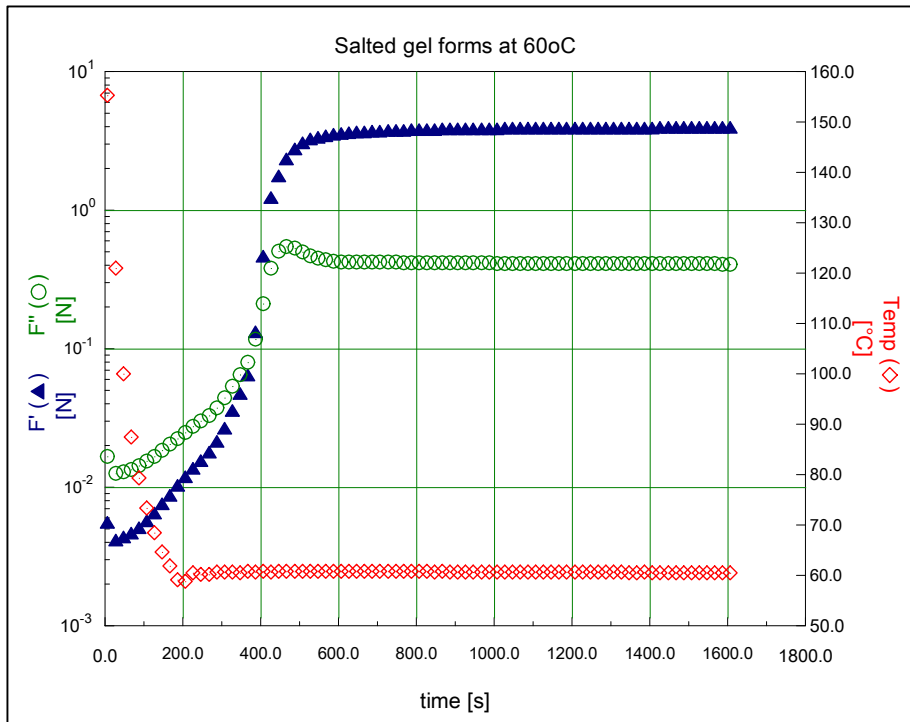


(b)

Figure 4-2 Isothermal gelation using DMTA for 30PVDF/PC unsalted gel, showing the time at which gelation occurs' (a) at 90°C, and no gelation in (b) at 100°C.

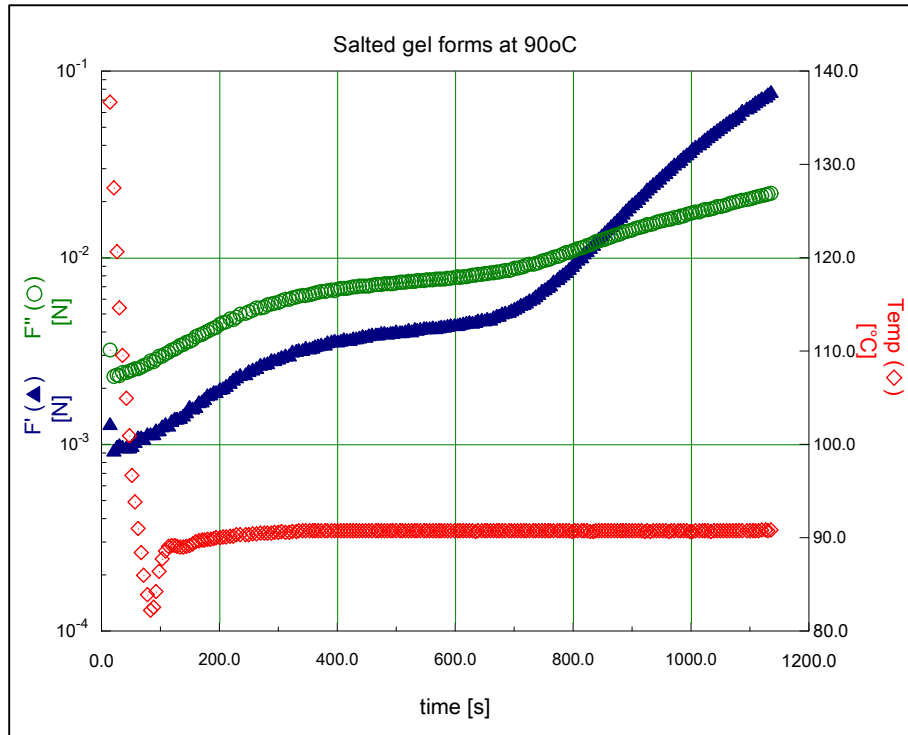


(a)

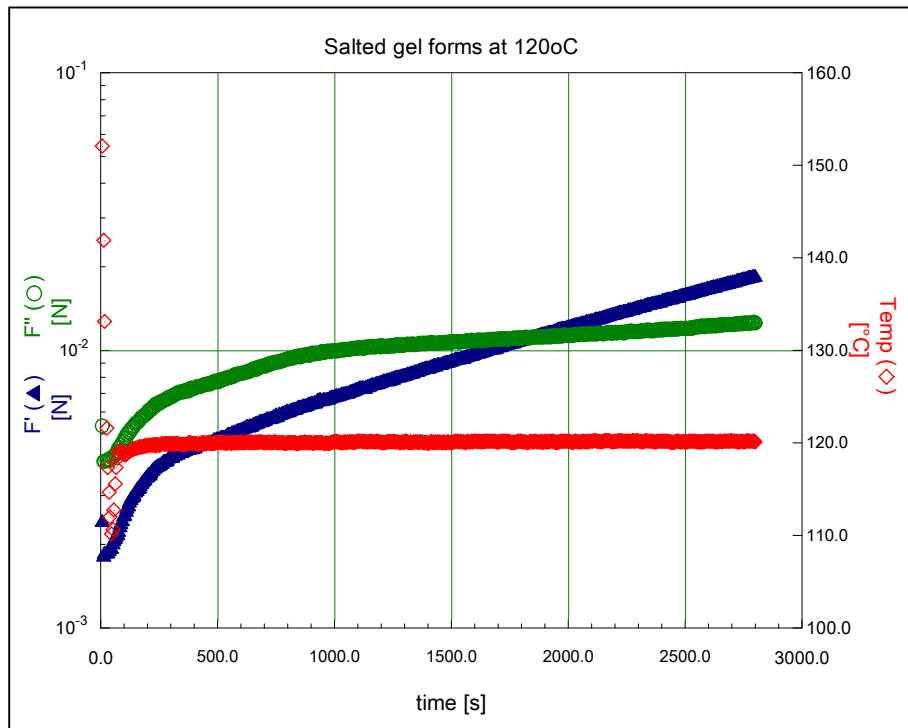


(b)

Figure 4-3 Isothermal gelation using DMTA for 30PVDF/PC/LiBF₄ salted gel, showing the time at which gelation occurs ($F'=F''$), (a) at 30°C and (b) at 60°C.

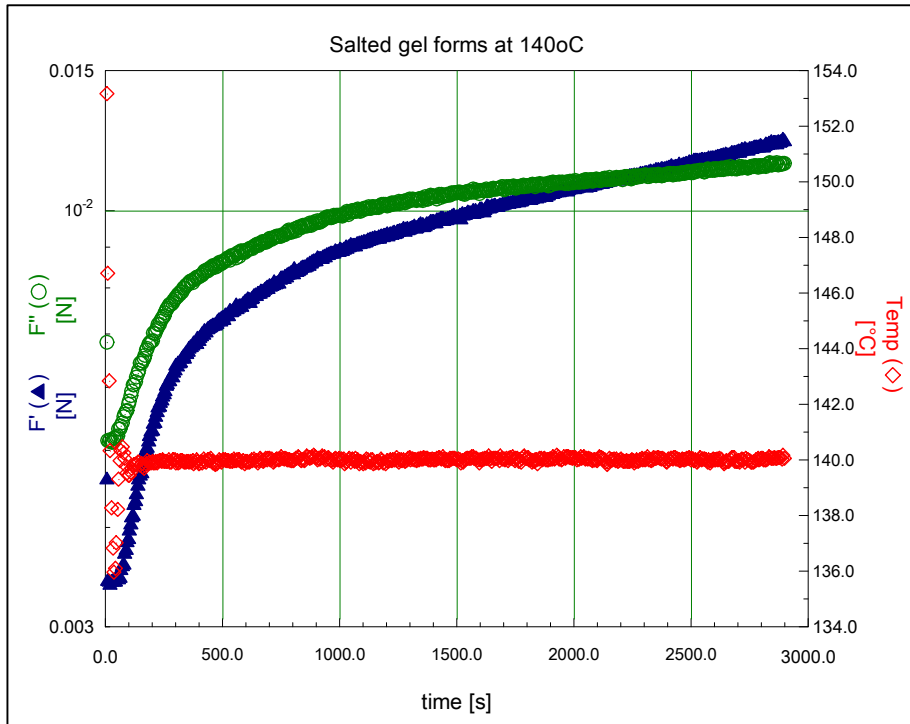


(a)

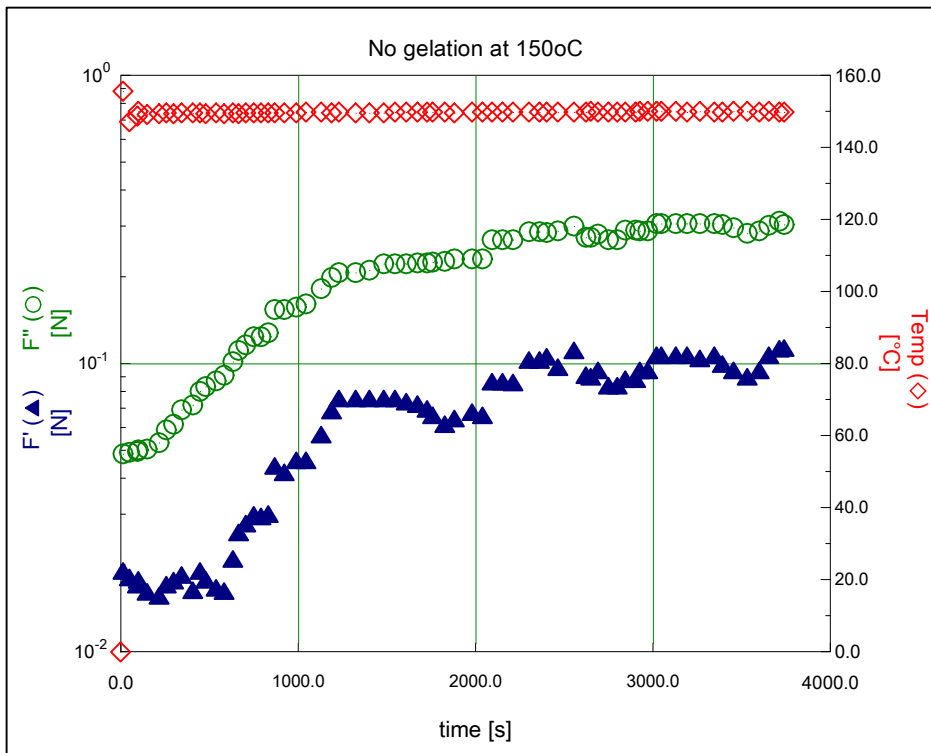


(b)

Figure 4-4 Isothermal gelation using DMTA for 30PVDF/PC/LiBF₄ salted gel, showing the time at which gelation occurs ($F' = F''$), (a) at 90°C and (b) at 120°C.



(a)



(b)

Figure 4-5 Isothermal gelation using DMTA for 30PVDF/PC/LiBF₄ salted gel, showing the time at which gelation occurs ($F' = F''$), (a) at 140°C, and no gelation is taking place in (b) at 150°C.

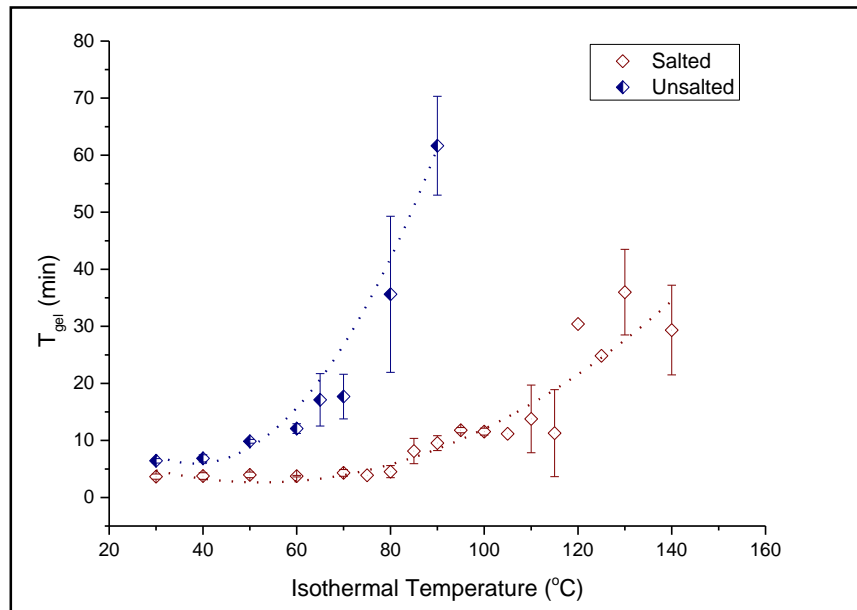


Figure 4-6 Time to initiate gelation for 30%PVDF/PC unsalted gels and 30%PVDF/PC/LiBF₄ 1M salted gels. Onset of gelation is determined for $F' = F''$.

Table 4-1 Average values of times of isothermal gelation from DMTA measurements. A dash shows that the experiment was undertaken but no gelation took place.

T_{gel} (°C)	Time (min)	T_{gel} (°C)	Time (min)
	At $G'=G''$		At $G'=G''$
	Unsalted		Salted
30	6	30	3.66
40	7	40	3.76
50	10	50	3.96
60	12	55	3.74
65	17	60	4.467
70	18	65	4.31
80	36	75	3.90
90	62	80	4.53
100	-	85	8.14
110	-	86	9.53
		95	11.8
		100	11.6
		105	11.2
		110	13.8
		115	11.3
		120	30.4
		125	24.8
		130	36.0
		140	29.3
		150	-
		160	-

4.2.2 Gelation investigations using DSC measurements

Isothermal DSC measurements were made (in the way that was outlined in chapter 3) for 30PVDF/PC unsalted gel and 30PVDF/PC/LiBF₄ 1M salted gel in order to investigate the crystallisation behaviour of the gels at different temperatures. The DSC curves in Figure 4-7 and Figure 4-8 represent isothermal crystallisation from the unsalted gels, whilst those in Figure 4-9, Figure 4-10, Figure 4-11 and Figure 4-12 represent isothermal crystallisation from the salted gels. Table 4-2 summarises the results of the isothermal crystallisation process for the two types of gel that were collected and analysed within the different experiments. Figure 4-13 shows the increase in crystallisation time with increasing isothermal temperature. It also shows that the salted gels crystallised more rapidly than the unsalted ones, and that they also form crystals at higher temperatures than the unsalted gels. However, as can be seen in Table 4-1, the heat of fusion (ΔH) is significantly reduced at higher crystallisation temperatures (see Figure 4-14).

The DSC traces in Figure 4-8 and the analysed data in Figure 4-13 show that the unsalted gel takes longer to crystallise than the salted gel at low temperatures. However, salted gels show crystallisation at higher temperatures where no crystallisation can be observed in the unsalted gels. This can be confirmed by comparing Figure 4-8 and Figure 4-7 with Figure 4-10 and Figure 4-9, in which the exothermic peaks for the salted gels show slight differences from those for the unsalted gels at low temperatures. The deeper and sharper peak seen for salted gels concords with the high nucleation rates taking place at earlier stages of

crystallisation. The peaks for unsalted gels show less depth, but are broader within the same range of temperatures, which renders less nucleation but high growth rates. However, at elevated temperatures, both types of gels show similar peaks, even though they occur at different points, which indicates similar nucleation and growth behaviour in these regions. Figure 4-14 shows that the heat of fusion released from both salted and unsalted gels drops significantly with the increase in temperature, with salted gels showing higher values of ΔH , and hence greater crystallinity.

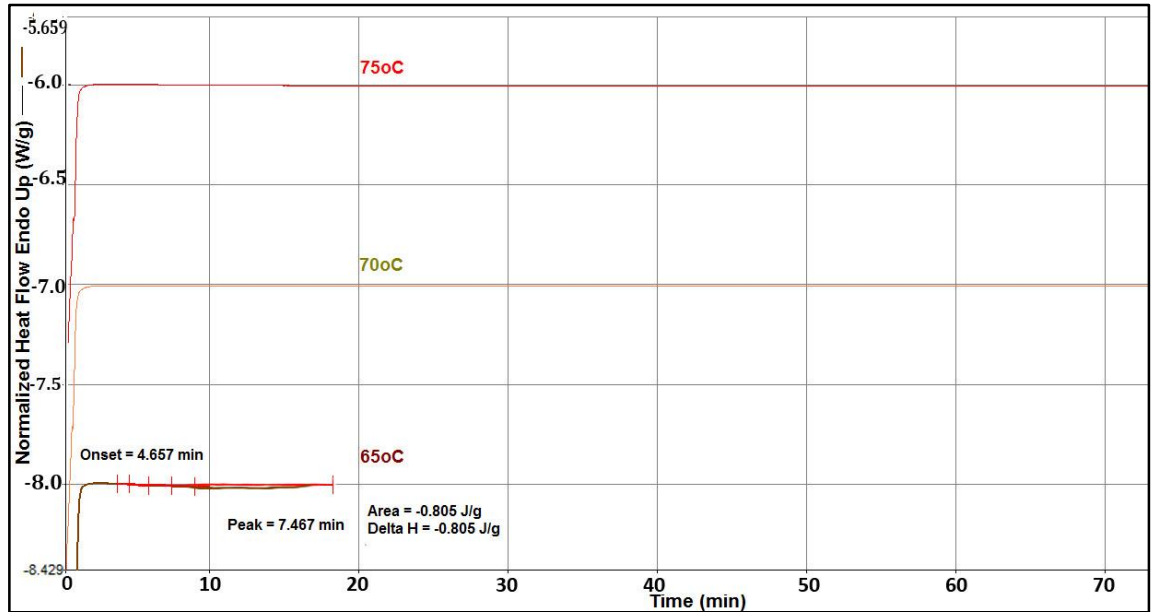


Figure 4-7 Isothermal DSC traces for 30PVDF/PC unsalted gel from 65–75°C, showing no crystallisation at and above 70°C temperatures. The data are offset and combined from different data files.

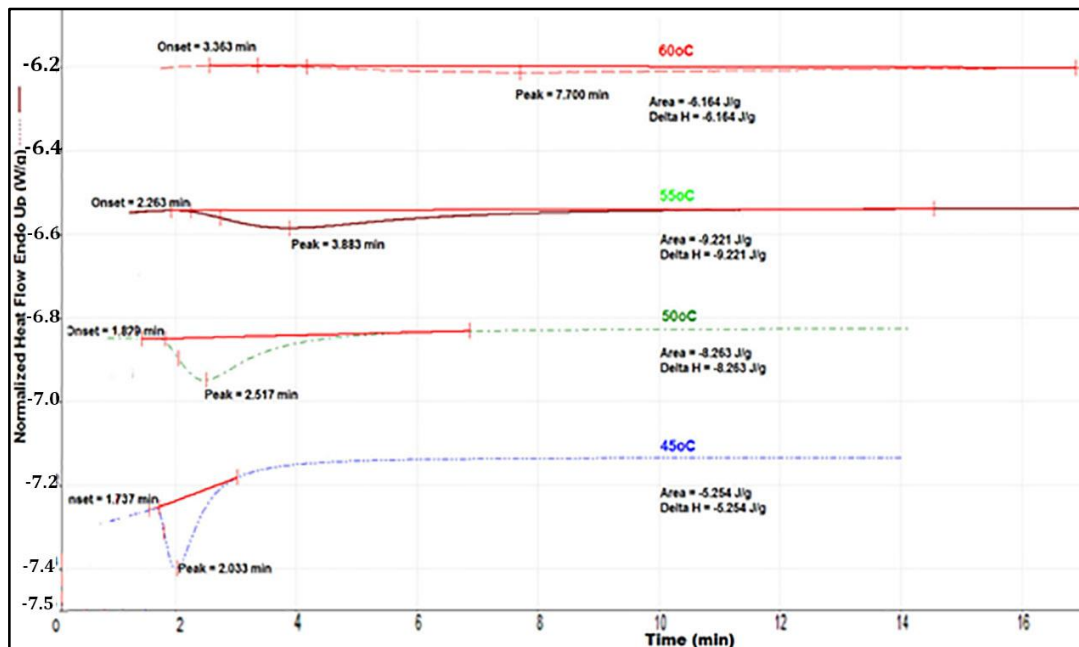


Figure 4-8 Isothermal DSC traces for 30PVDF/PC unsalted gel from 45–60°C. The data here are offset. The data are offset and combined from different data files.

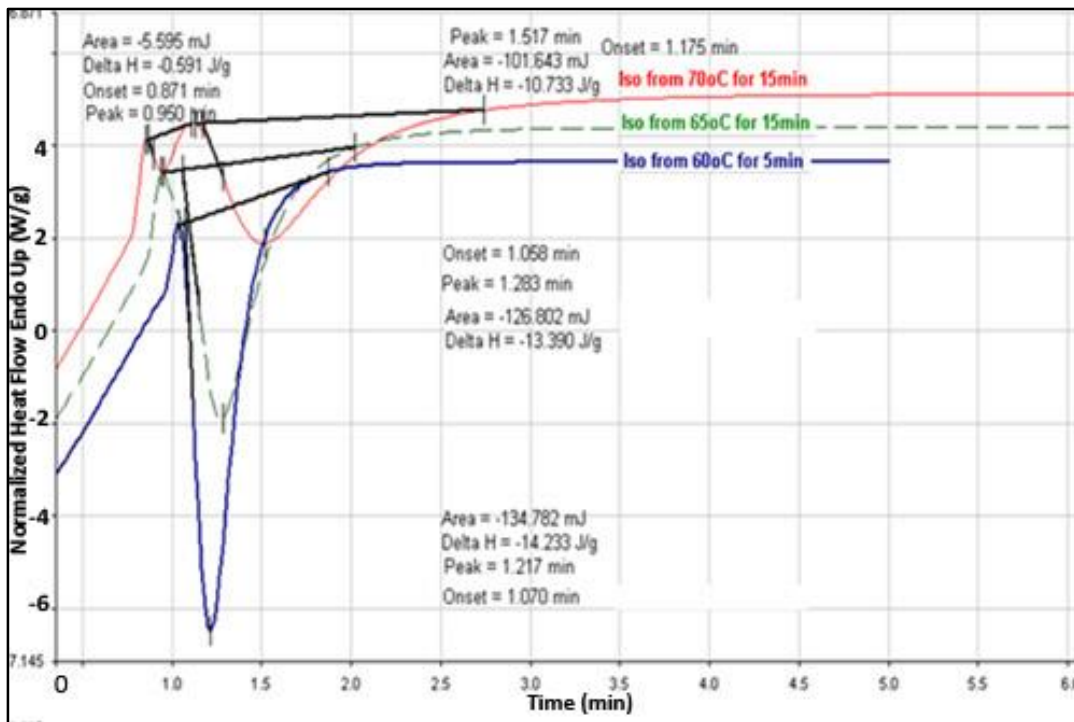


Figure 4-9 Isothermal DSC traces for 30PVDF/PC/LiBF₄ 1M salted gel from 60-70°C. The data are offset and combined from different data files.

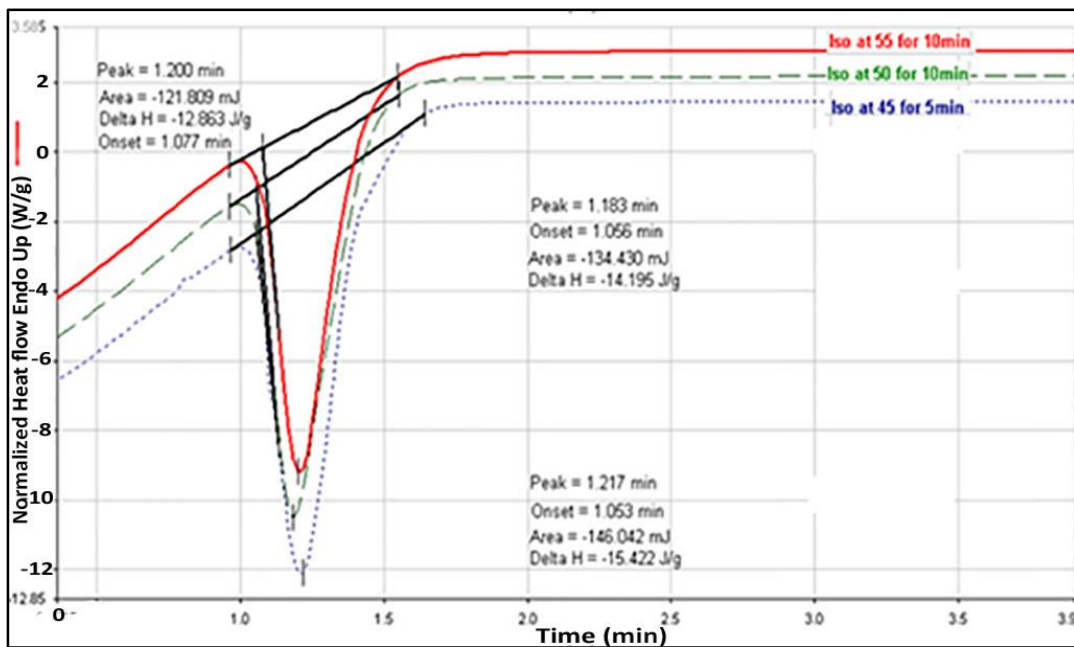


Figure 4-10 Isothermal DSC traces for 30PVDF/PC/LiBF₄ 1M salted gel from 45-55°C. The data are offset and combined from different data files.

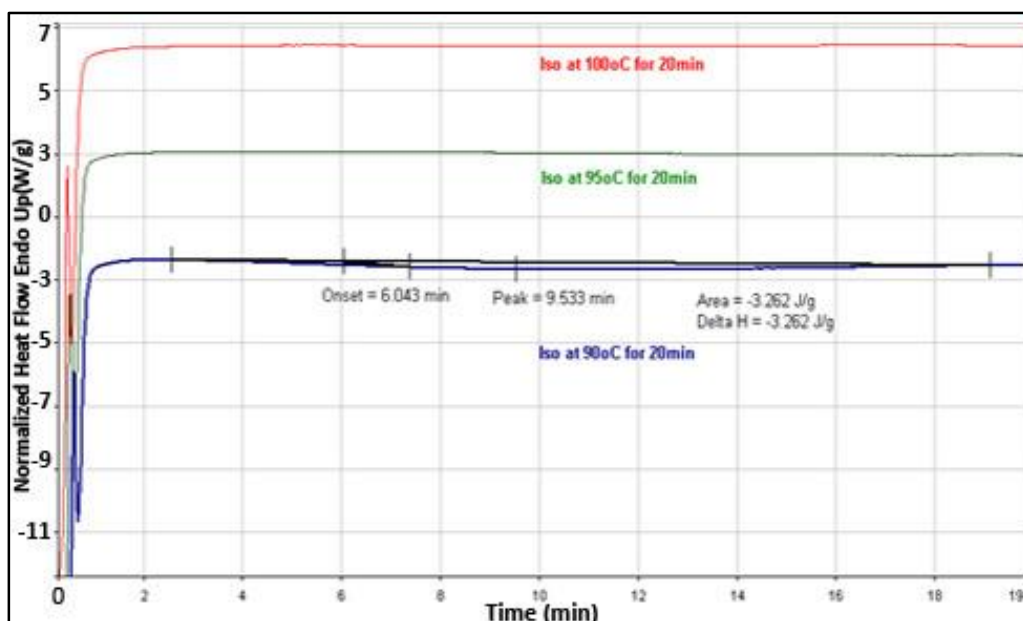


Figure 4-11 Isothermal DSC traces for 30PVDF/PC/LiBF₄ 1M salted gel from 90-100°C. Note that there is no crystallisation observed at 95°C or above. The data are offset and combined from different data files.

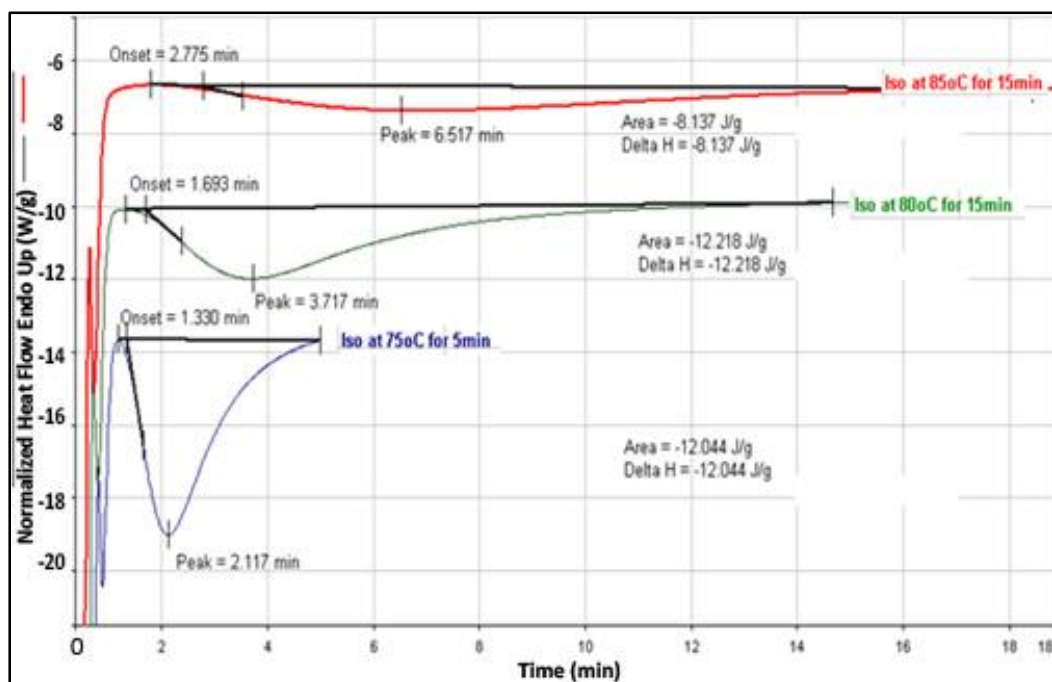


Figure 4-12 Isothermal DSC traces for 30PVDF/PC/LiBF₄ 1M salted gel from 75-85°C. The data are offset and combined from different data files.

Table 4-2 Onset times and areas of crystallisation peaks under isothermal conditions. The dashes show an isothermal experiment has been undertaken, but that no crystal peak has been observed.

Isothermal temp	Unsalted gel		Salted gel	
	Crystallisation time (onset)	$ \Delta H $	Crystallisation time (onset)	$ \Delta H $
	mins	J/g	mins	J/g
30	1.75	10.105	1.033	16.511
35	1.627	9.17	1.035	17.166
40	1.521	9.541	1.047	15.786
45	1.649	5.104	1.053	15.422
50	1.731	7.286	1.056	14.195
55	2.04	8.244	1.077	12.863
60	2.903	1.728	1.07	14.233
65	5	0.662	1.058	13.39
70	-	-	1.175	10.733
75	-	-	1.33	12.044
80			1.693	12.218
85			2.775	8.137
90			6.043	3.262
95			1.033	16.511
100			1.035	17.166

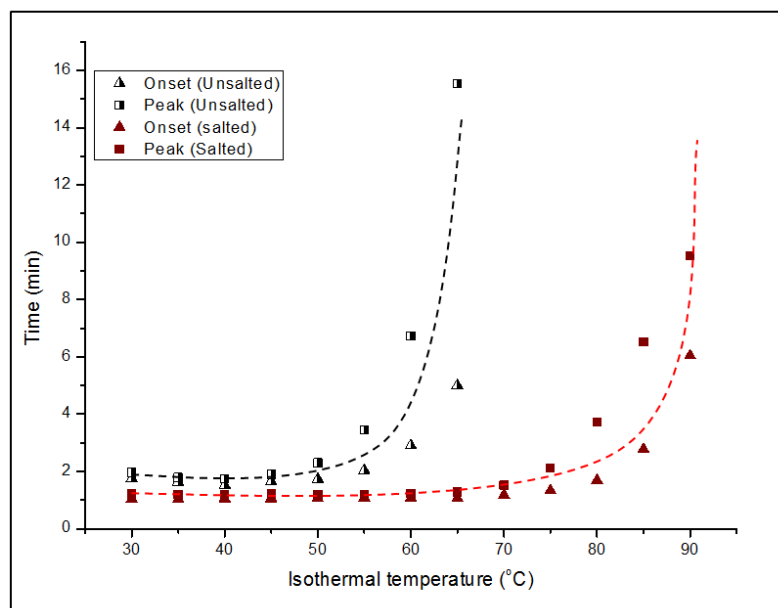


Figure 4-13 Time to initial crystallisation under isothermal conditions for 30%PVDF/PC unsalted gels and 30%PVDF/PC/LiBF₄ 1M salted gels, as determined by DSC.

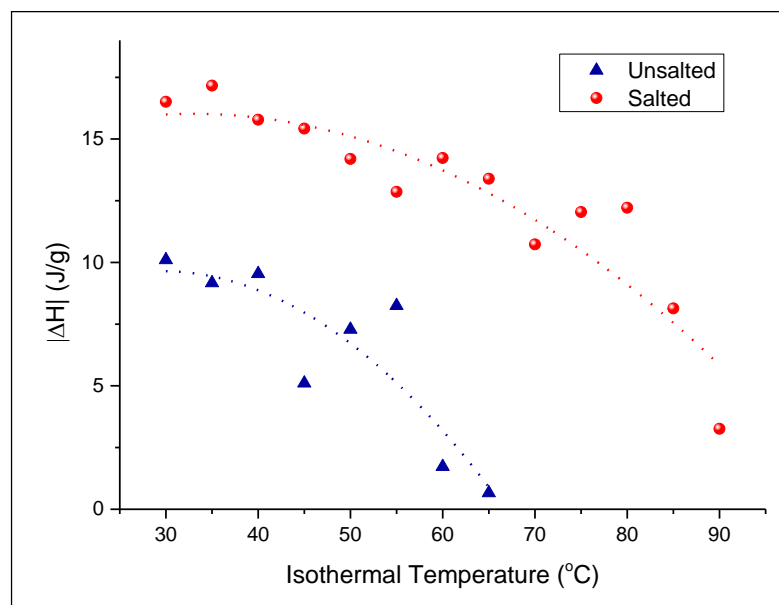


Figure 4-14 Heat of fusion of crystallisation plotted as a function of the isothermal crystallisation temperature.

4.2.3 Comparing crystallisation and gelation

Figure 4-15 shows a comparison between gelation time and crystallisation time for unsalted gel as a function of isothermal temperature, while Figure 4-16 shows a similar comparison for salted gel. The two figures show that crystallisation occurs faster than gelation at some temperatures. The unsalted gel took much longer to gel at 90°C, and no gelation was observed above this temperature. For the salted gel, gelation took place at significantly higher temperatures than crystallisation, and took longer than it to occur. However, the gelation times for salted gel were low in comparison to those for unsalted gels. Thus, gelation can occur at higher temperatures than crystallisation, suggesting that gelation can take place without noticeable crystallisation. According to Okabi et al. [42], rapidly cooling molten solutions of PVDF gels to 30°C can contribute to the formation of high amounts of spherulites.

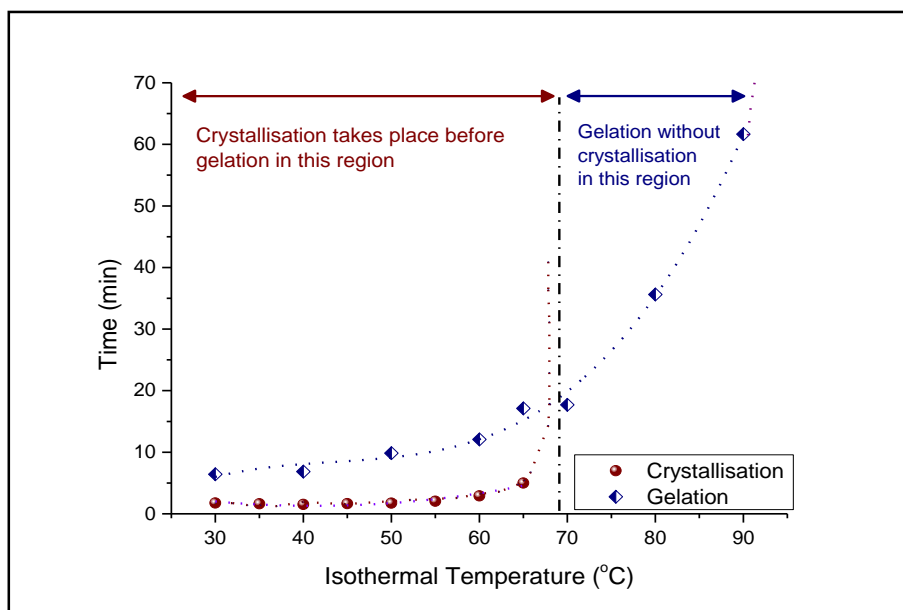


Figure 4-15 Time to initiate crystallisation and gelation for 30%PVDF/PC unsalted gels. The onset of crystallisation is determined by the DSC peak. The onset of gelation is determined by $F' = F''$.

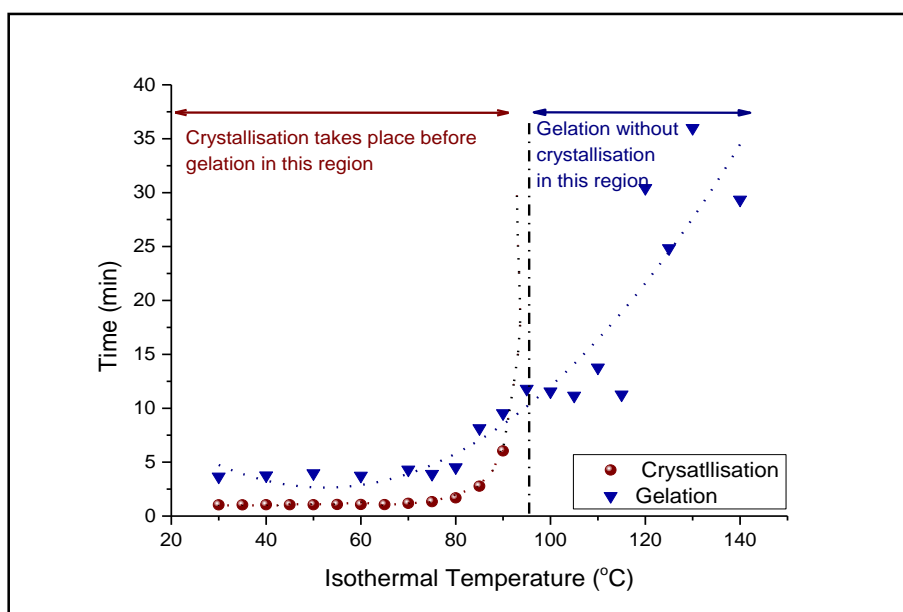


Figure 4-16 Time to initiate crystallisation and gelation for 30%PVDF/PC/LiBF₄ 1M gels. The onset of crystallisation is determined by the DSC peak. The onset of gelation is determined by $F' = F''$.

4.2.4 Subsequent melting temperature

Samples that were isothermally crystallised (see section 4.2.2) were then heated again from each isothermal crystallisation temperature until the molten peaks were obtained for each point. Figure 4-17 shows the subsequent melting behaviour after isothermal crystallisation for salted and unsalted gels. The general trend found was that the melting points increased with increasing crystallisation temperature in both types of gels. In salted gels, T_m is obviously higher than in unsalted gels. For unsalted gels, the highest crystallisation temperature at which subsequent melting was seen was 70°C, whereas for salted gels it was 95°C. Figure 4-18 shows that ΔH drops rapidly as these maximum temperatures are approached.

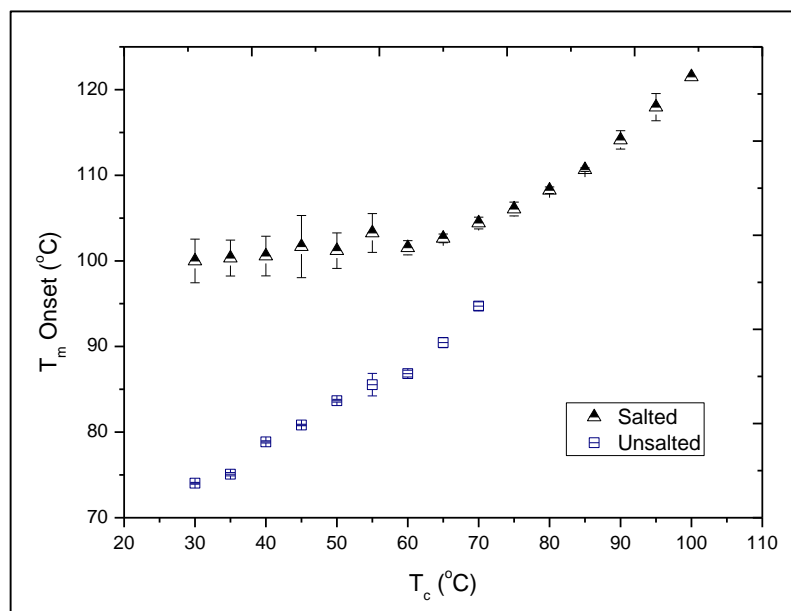


Figure 4-17 Subsequent melting points plotted as a function of isothermal crystallisation temperature for 30%PVDF/PC unsalted gels and 30%PVDF/PC/LiBF₄ 1M salted gels.

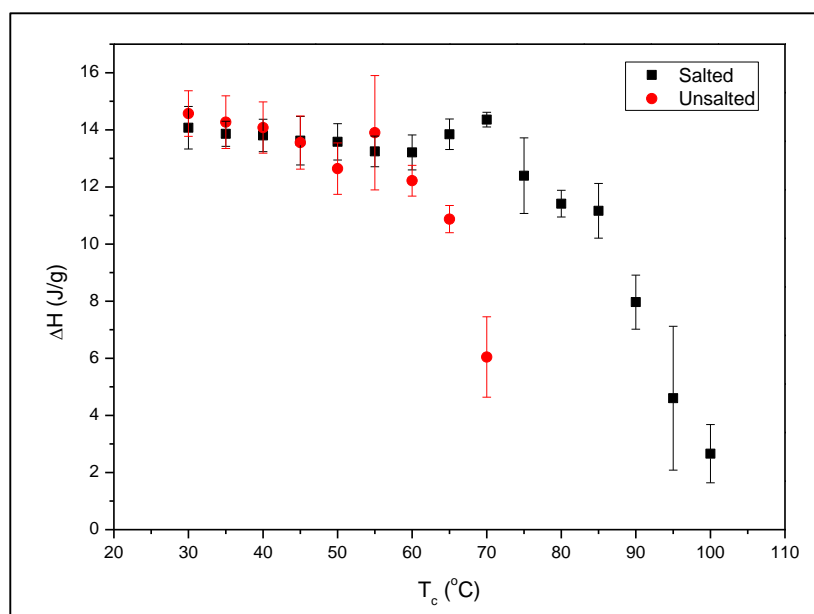


Figure 4-18 Heat of fusion of the melting peak following isothermal crystallisation at T_c for 30%PVDF/PC unsalted gels and 30%PVDF/PC/LiBF₄ 1M salted gels.

4.2.5 Isothermal optical microscopy

Hot-stage optical microscopy was used to observe the effect of salt on the gel structure of 30PVDF/PC unsalted gel and 30PVDF/PC/LiBF₄ 1M salted gel upon gelation from molten solution. Figure 4-19 and Figure 4-22 show the optical micrographs ascertained when the salted and the unsalted gels respectively were heated from room temperature to 160°C, at which temperature the whole structure disappeared. Figure 4-20 shows the optical micrographs obtained when the salted gel was cooled from 160°C to 110°C, with no spherulites being detected within this temperature range. This result concurs with those obtained using the DSC machine and DMTA measurements, in which no crystallisation was found to occur within this temperature range for the salted gel. Figure 4-21 shows that salted gel can form gel by both crystallisation and phase separation at 50°C. Figure 4-23 shows that gelation occurred independently of crystallisation when

unsalted gel was cooled from 160°C to 80°C, and did so by forming annular structures that are thought to be the result of a type of early meta-stable phase separation. However, significantly different structures were seen in the unsalted gel when it was cooled from 160°C to 50°C, as shown in Figure 4-24. In this case, the structure exhibited a similar behaviour to that of the salted gel, with crystallisation and phase separation taking place simultaneously in both. However, the spherulitic structures were bigger and formed more slowly in the unsalted gel than in the salted gel at 50°C.

4.2.6 Combining DMTA and optical microscopy

The combined data from DMTA and optical microscopy confirm the shape of the phase diagram shown in Figure 2-8. For 30PVDF/PC unsalted gel, it can be deduced from DMTA that the binodal line is crossed at above $T_2=90^\circ\text{C}$, and the crystallization curve is crossed around $T_3=70^\circ\text{C}$.

The different structures formed in the distinct temperature regions are shown by the optical microscopy. Figure 4-23 shows isothermal phase separation at 80°C without crystallization for an unsalted gel, the view between crossed polarisers confirming the conclusion that no crystallisation has taken place. However, Figure 4-24, with its bright images between crossed polarisers, gives evidence of spherulitic structures formed at the lower temperature of 50°C. Salted samples show similar distinct regimes, seen in Figure 4-20 and Figure 4-21 respectively. The finer structure of the salted samples can also be seen in contrast to the coarser structure of the unsalted samples, providing evidence that the salt has a nucleating effect.

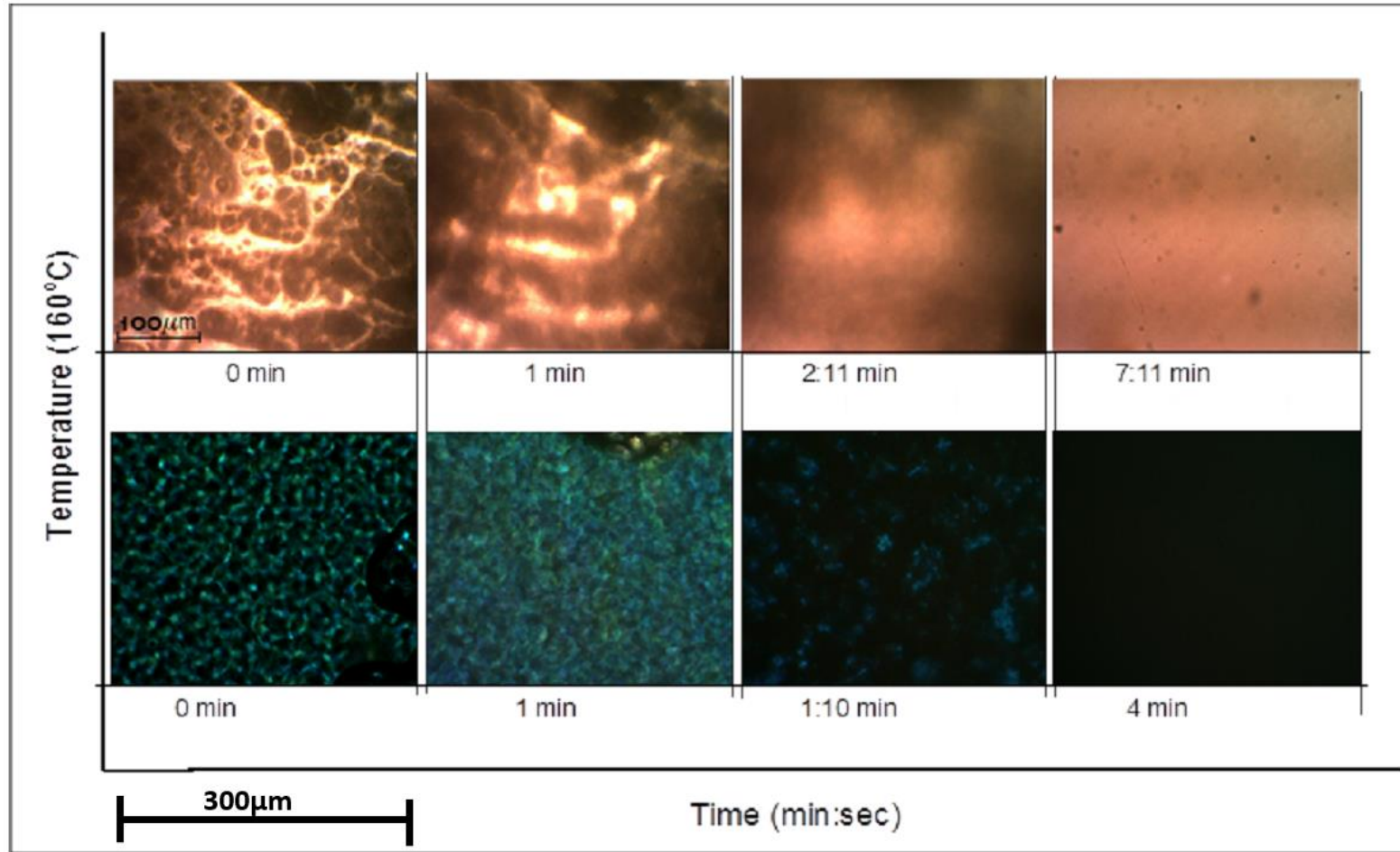


Figure 4-19 Optical Micrographs of heating from room temperature to 160°C for 30PVDF/PC/LiBF₄ 1M salted gel showing structure evolution isothermally. (The top are normal micrographs while below the crossed-polariser micrographs).

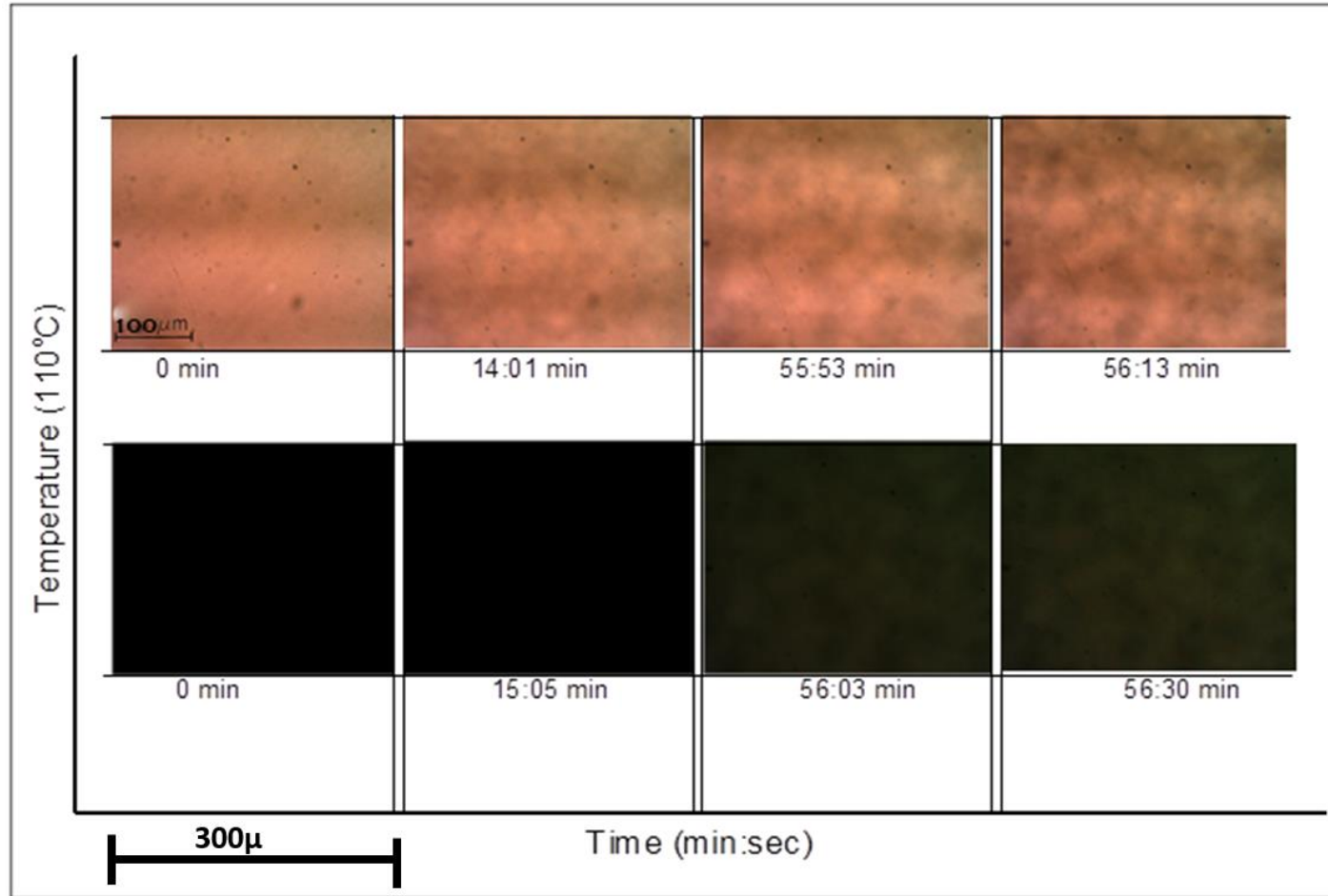


Figure 4-20 Optical Micrographs of cooling from 160°C to 110°C for 30PVDF/PC/LiBF₄ 1M salted gel showing no crystallisation occurs at this point. (The top are normal micrographs while below the crossed-polariser micrographs).

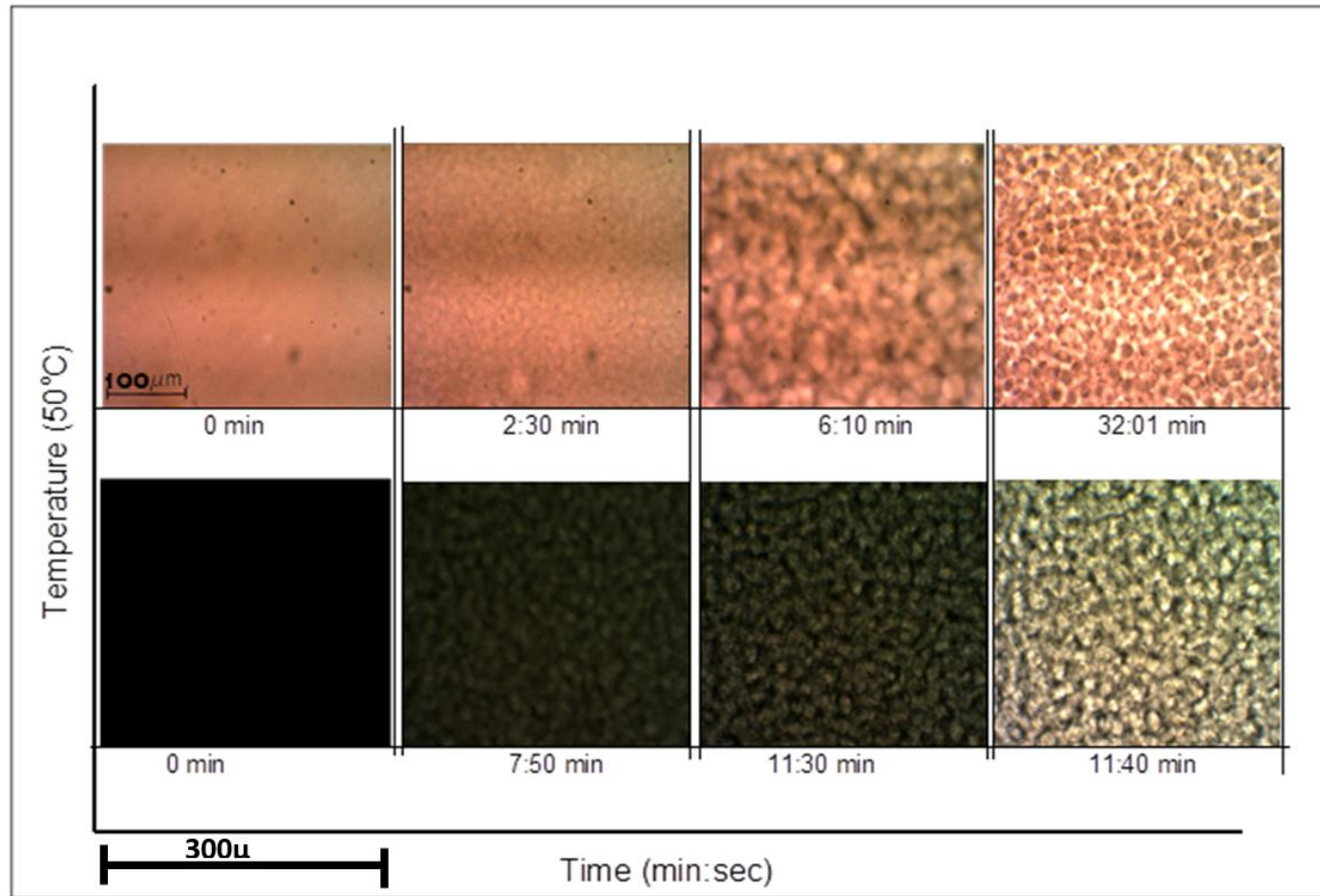


Figure 4-21 Optical Micrographs of cooling from 160°C to 50°C for 30PVDF/PC/LiBF4 1M salted gel showing gelation occurs via crystallisation. (The top are normal micrographs while below the crossed-polariser micrographs).

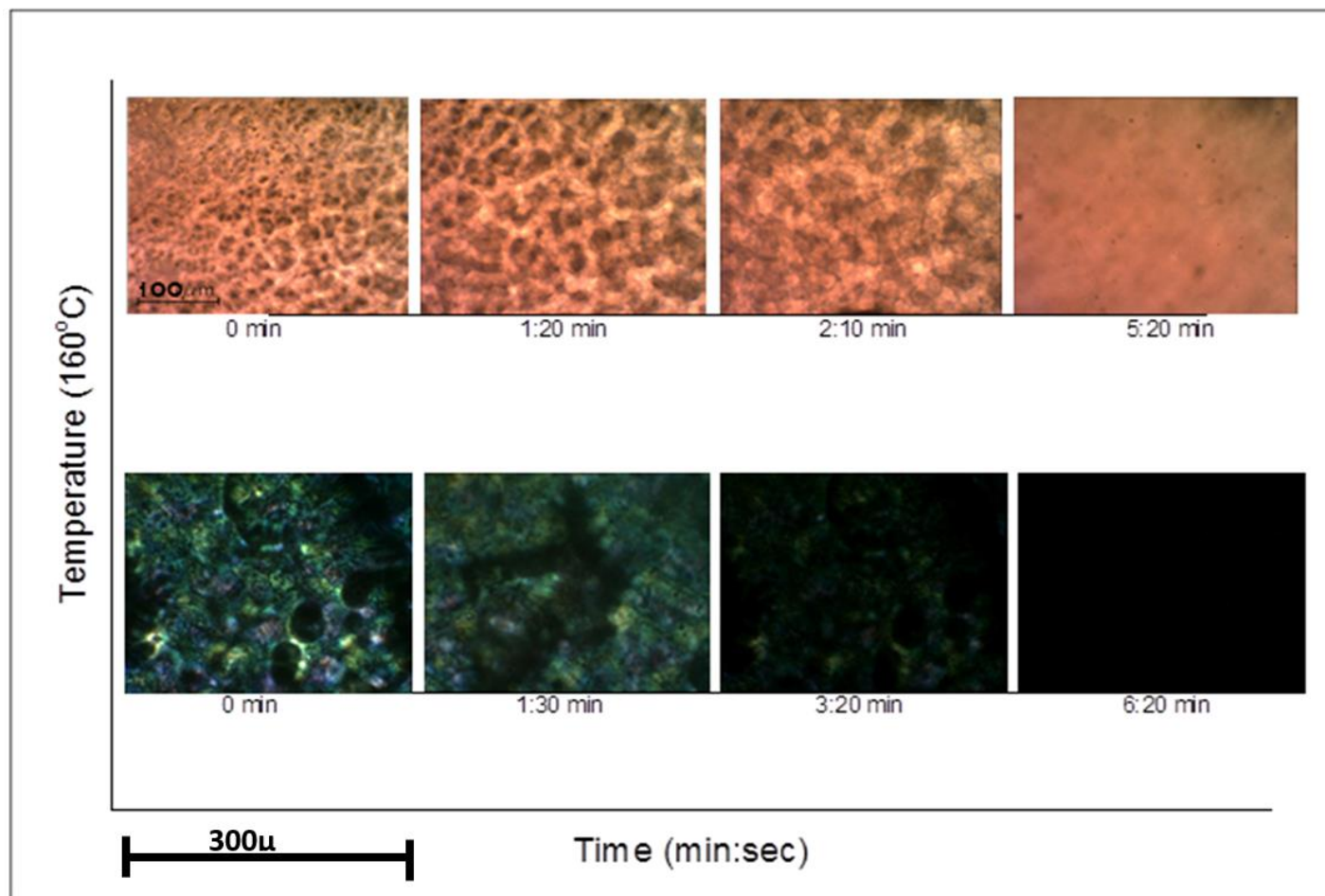


Figure 4-22 Optical Micrographs of heating from room temperature to 160°C for 30PVDF/PC unsalted gel, showing structure evolution isothermally. (The top are normal micrographs while below the crossed-polariser micrographs).

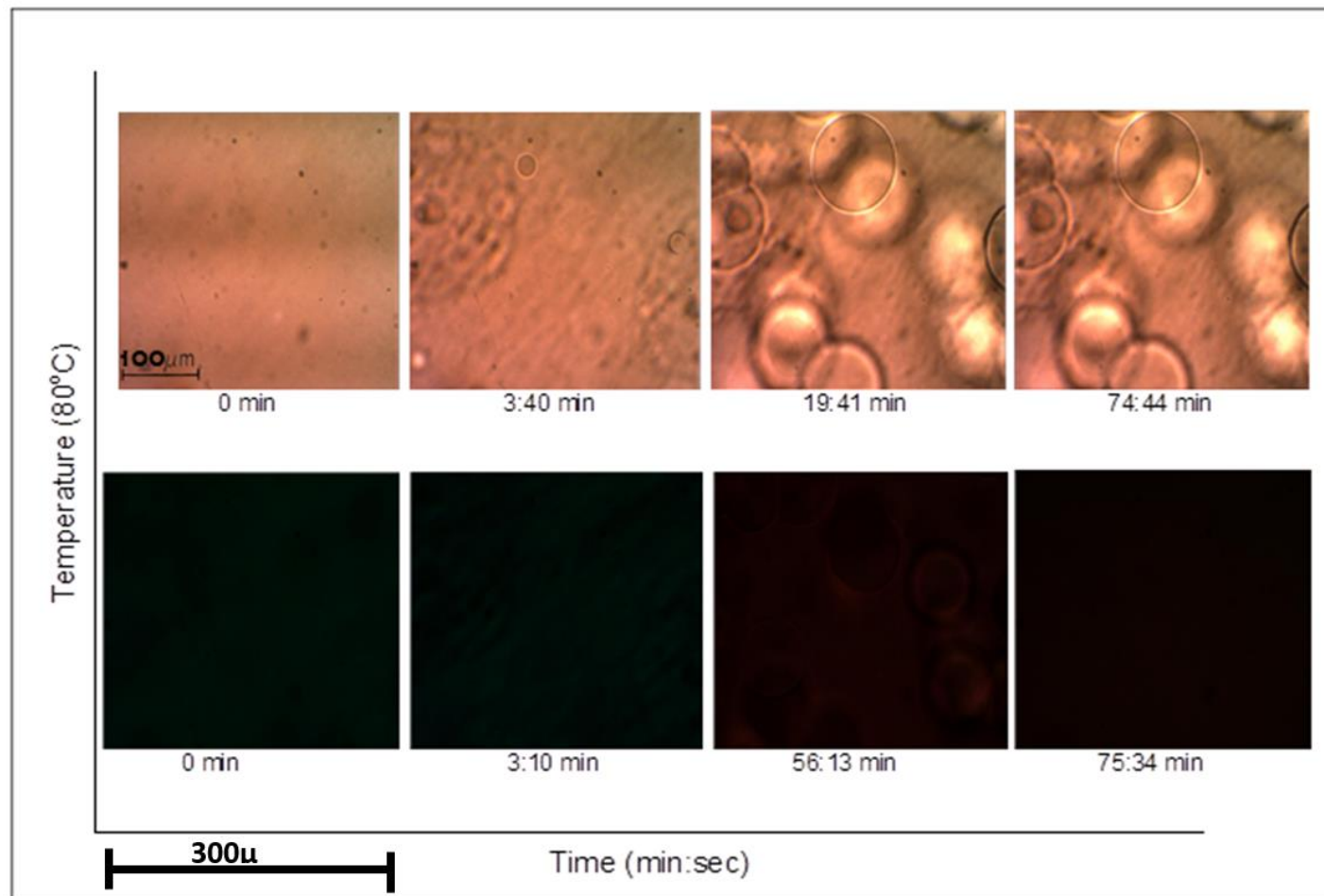


Figure 4-23 Optical Micrographs of cooling from 160°C to 80°C for 30PVDF/PC unsalted gel showing low phase separation but no crystallisation this point. (The top are normal micrographs while below the crossed-polariser micrographs).

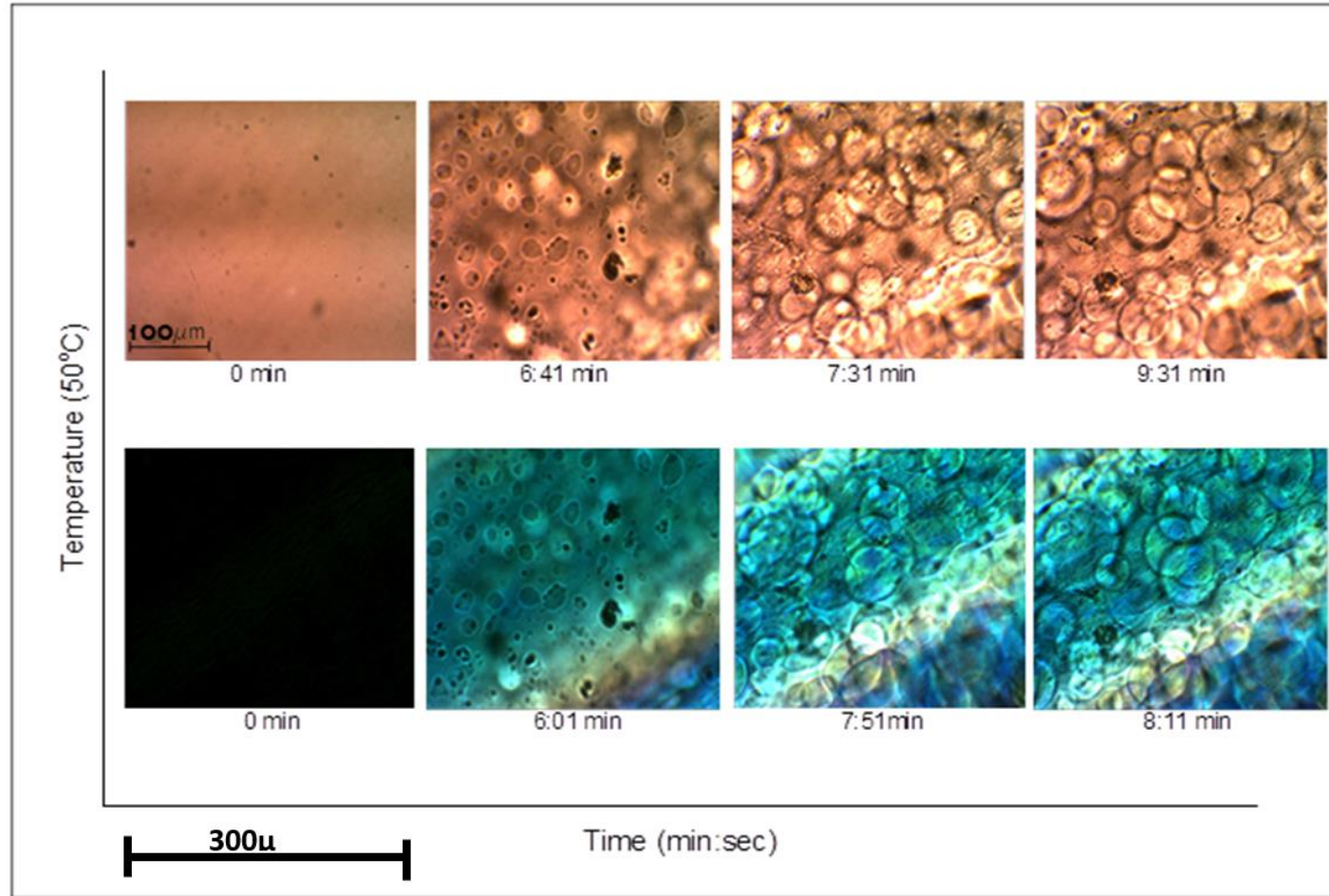


Figure 4-24 Optical Micrographs of heating from room temperature to 160°C for 30PVDF/PC unsalted gel, showing structure evolution isothermally. (The top are normal micrographs while below the crossed-polariser micrographs).

4.3 Discussion and conclusions

This chapter presented the results obtained through using a number of techniques to investigate isothermal gelation in two types of PVDF-based gels 30PVDF/PC and 30PVDF/PC/LiBF₄ 1M. The results reveal several facts and allow us to draw a number of conclusions:

1. Gelation under isothermal conditions takes longer at higher temperatures (see Figure 4-6), and this concords with the findings of Cho et al. [41]. Salted samples gel faster than unsalted samples at corresponding isothermal temperatures. The subsequent melting temperature (see Figure 4-17) shows that salted gels have higher melting points at any given isothermal temperature, and the faster gelation of salted samples could thus be explained by a higher degree of super-cooling.
2. Figure 4-15 and Figure 4-16 show that there is a temperature window in which gelation occurs without crystallisation for both salted and unsalted samples. We assume that gelation occurs via liquid-liquid phase separation within this window; whilst at the lower temperatures in which crystallisation was observed, we assume that gelation occurred via solid-liquid phase separation. This structural difference is confirmed by the optical microscopy observations shown in Figure 4-19 to Figure 4-24.
3. Figure 4-14, shows that the degree of crystallinity increases as isothermal temperature decreases, and also that the presence of salt increases the degree of crystallinity although it may again be that the

degree of super cooling determines the degree of crystallisation.

Chapter5. The Effects of Gel Composition

5.1 Introduction

In chapter 2, it was seen that the melting point of the polymer solution is depressed when solvent is added to the polymer because of changes in the intermolecular forces that affect their interaction parameters. This chapter will now examine and discuss the effect of all the gels' components on their melting points, including their polymer contents, solvent qualities and salt concentrations. Flory interaction and Hansen solubility parameters represent the key solutions for the thermodynamic behaviours of these gels that will be discussed. The main aim of this chapter is to provide a better understanding of the thermal stability of these gels that are essential for rechargeable batteries.

5.2 The polymer concentration effect

5.2.1 Gel melting points

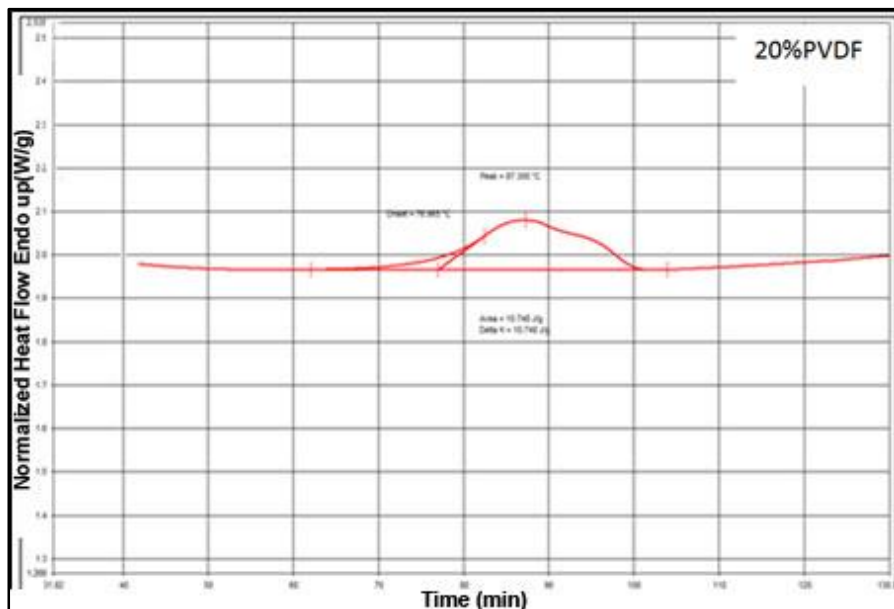
The effects of polymer concentration were studied through preparing and testing polymer gel samples of PVDF/PC unsalted and PVDF/PC/LiBF₄ 1M salted gels, with PVDF concentrations of between 20–40 percent total sample weight. The PC mass was kept at 7g in all the samples, and the salt mass was calculated in the way outlined in chapter 3. All the gel samples were made in the glove box, as also mentioned in chapter 3.

Melting points were obtained by heating samples using the DSC at a heat rate of 10°C/min until endothermic peaks were detected. The onset values of these peaks were then taken as the measured onset melting points. Figure 5-1, Figure 5-2 and Figure 5-3 show the DSC traces for the unsalted gels within the range of PVDF concentrations, while Figure 5-4, Figure 5-5 and Figure 5-6 show similar DSC traces for the salted gel samples within the same range.

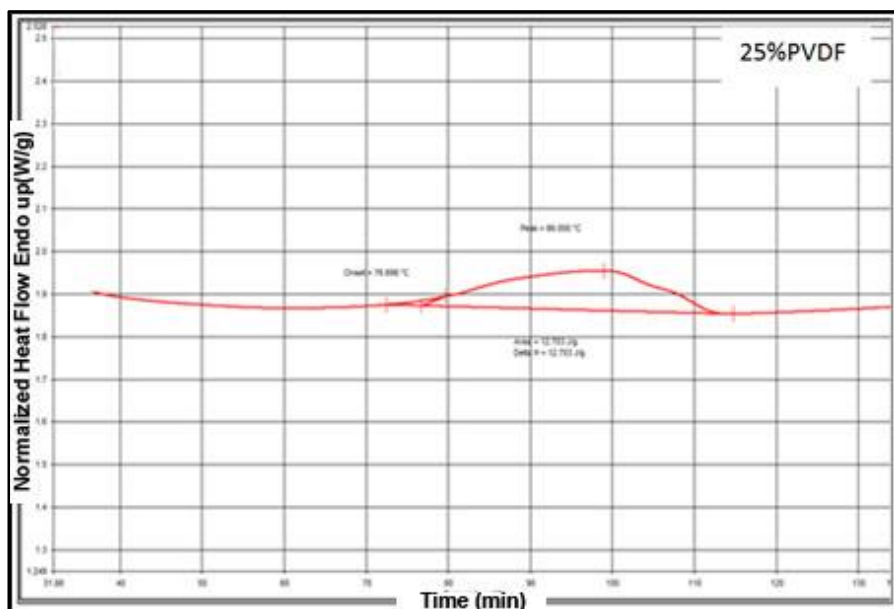
Table 5-1 summarises the results obtained using the DSC measurements for both salted and unsalted gels. As can be seen in the figures, the heating curve remains straight until the melting point is reached, at which point an endothermic transition can be seen to occur through the appearance of a positive peak. This peak represents the melting behaviour of the gel, where the crystal structure is being lost by the breaking of the crystals. This operation requires extra thermal energy, which presents as the nominated endothermic peak.

Figure 5-7 plots the melting points that were obtained against the polymer concentrations for both salted and unsalted gels. It shows that melting points slightly increased when the concentration of the polymeric solution was increased with further polymer additions. However, the presence of salt in the gel system had a significant effect on melting points. Figure 5-8 shows how the heat of fusion from the melting peaks increased when the polymer concentration in the solution was increased. At low polymer concentrations, the presence of salt appears to have a more significant effect on the heat of fusion than the polymer concentration has. However, at

high polymer concentrations, the salt has a less dominant effect. Figure 5-9 shows that the degree of crystallinity of PVDF in salted gel decreases when the concentration of PVDF in the gel is increased, while the unsalted gel shows little change when the PVDF concentration is increased.

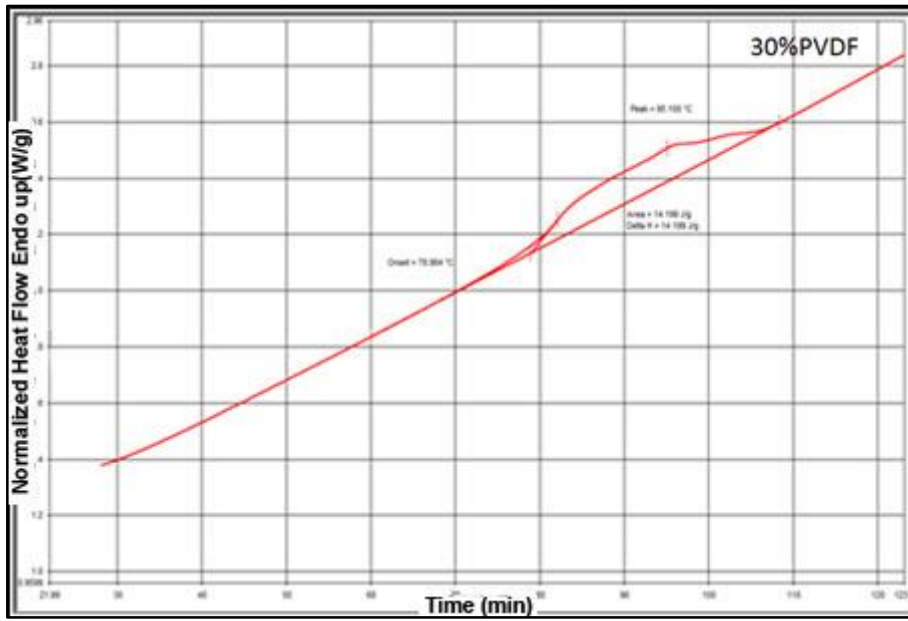


(a)

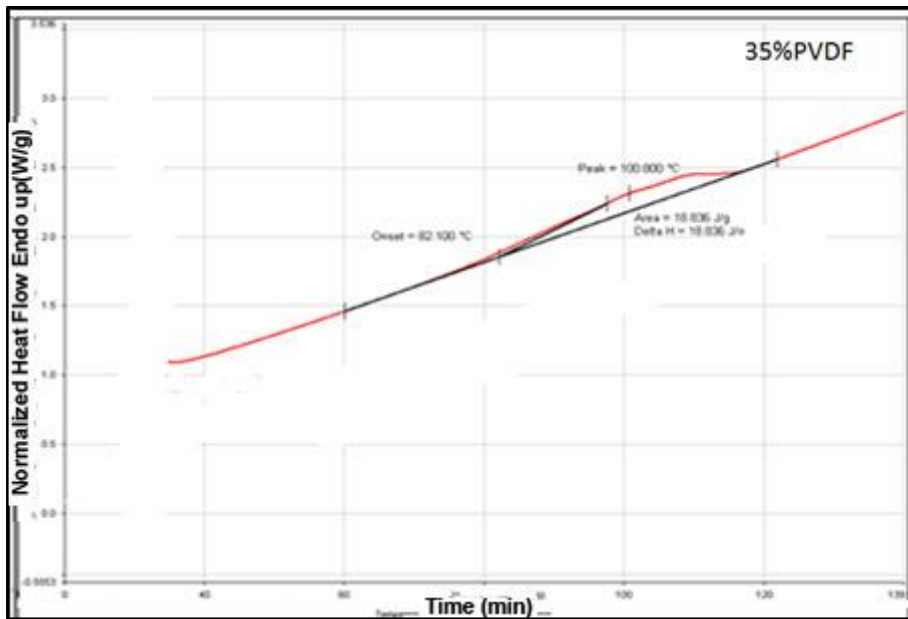


(b)

Figure 5-1 Heating (10°C/min) DSC traces for unsalted gel from (a) 20PVDF/PC and (b) 25PVDF/PC.



(a)



(b)

Figure 5-2 DSC traces for unsalted gel from (a) 30PVDF/PC and (b) 35PVDF/PC.

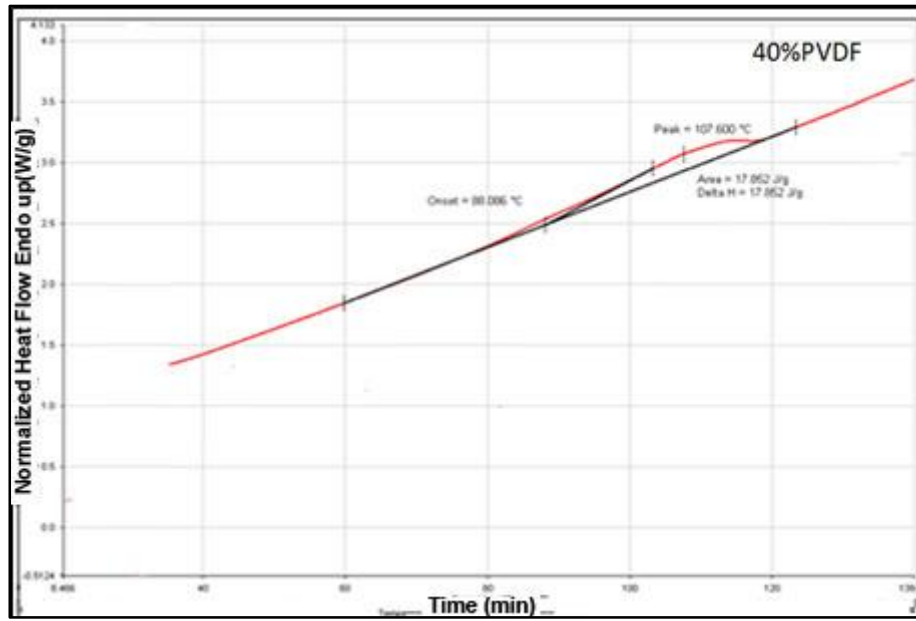
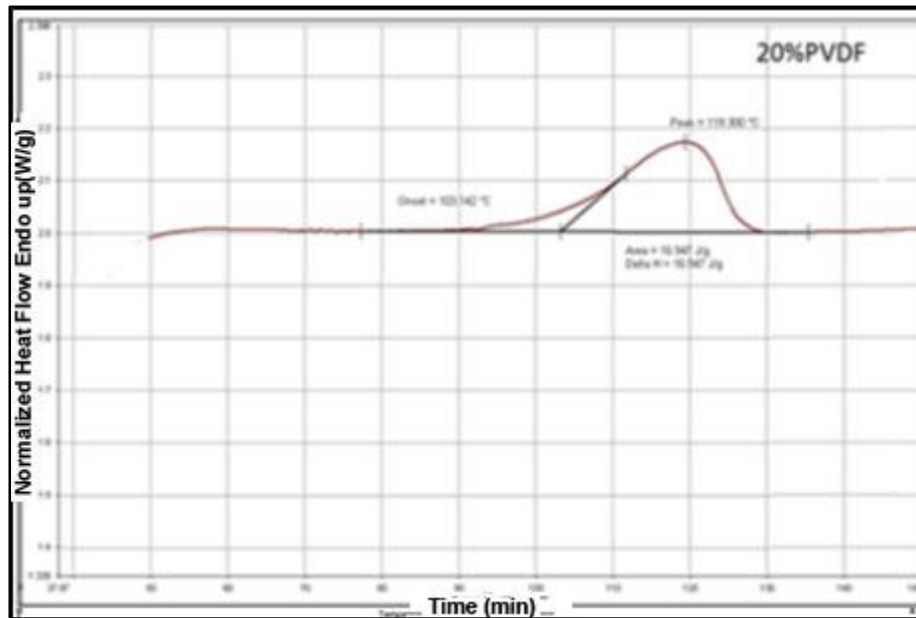
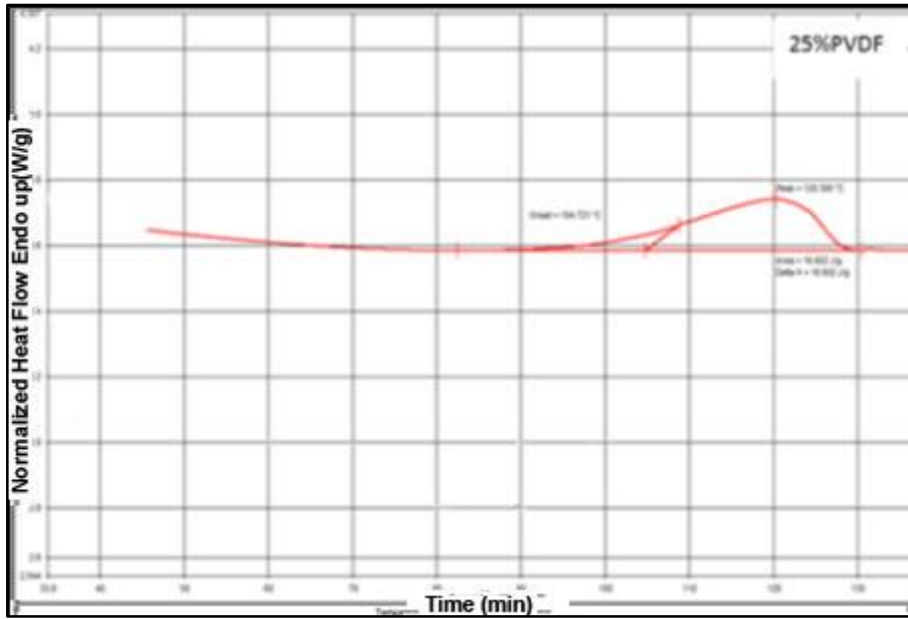


Figure 5-3 DSC traces for unsalted gel from 40PVDF/PC.

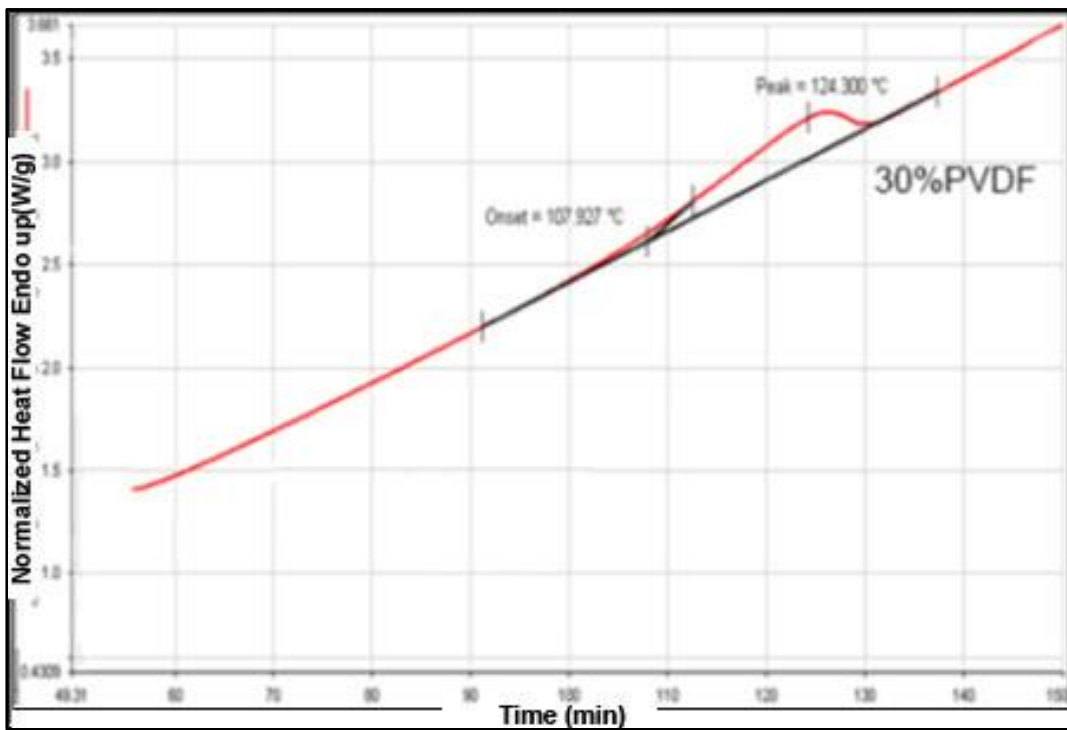


(a)

Figure 5-4 DSC traces for salted gel from 20PVDF/PC/LiBF4 1M.

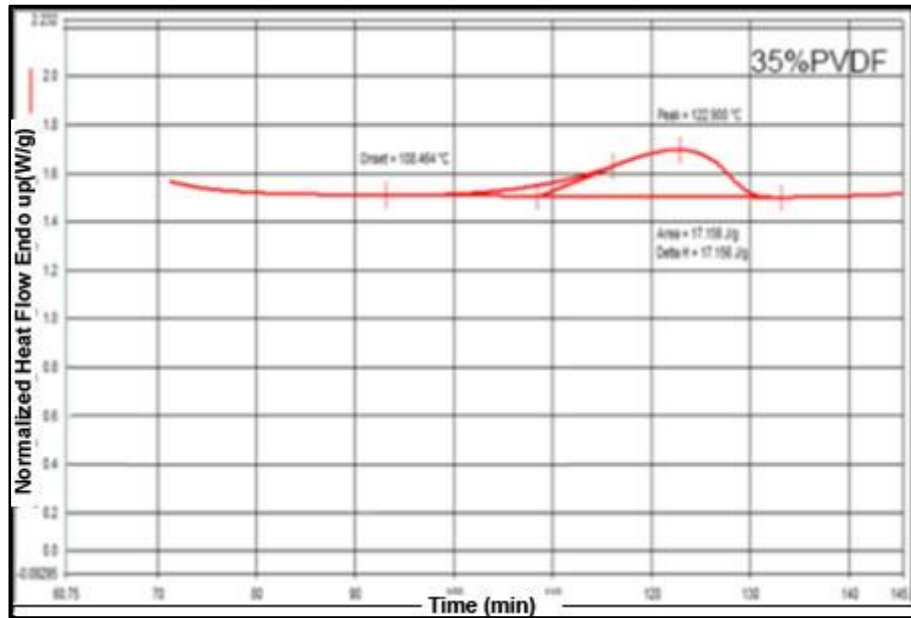


(a)

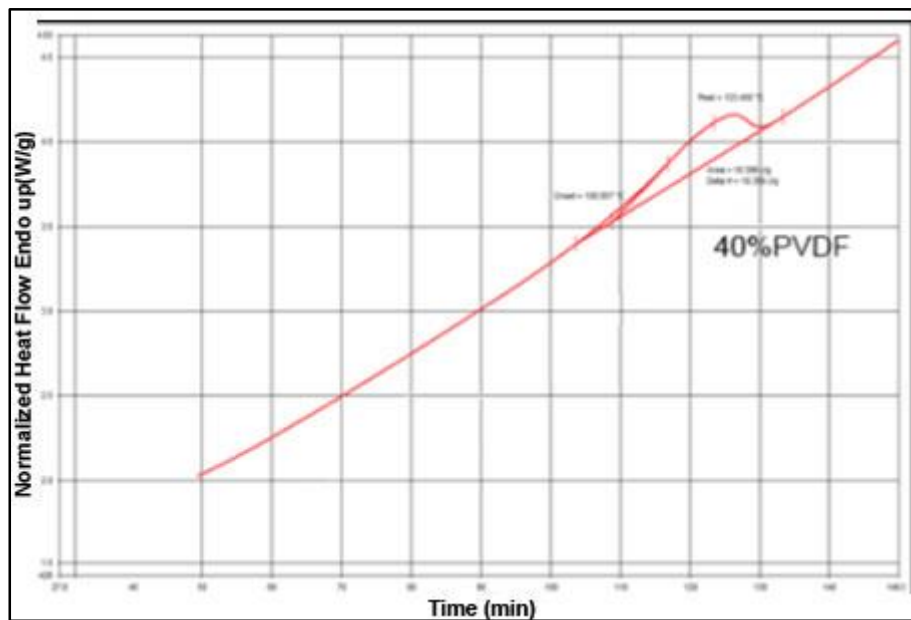


(b)

Figure 5-5 DSC traces for salted gel from (a) 25PVDF/PC/LiBF₄ 1M and (b) 30PVDF/PC/LiBF₄ 1M.



(a)



(b)

Figure 5-6 DSC traces for salted gel from (a) 35PVDF/PC/LiBF₄ 1M and (b) 40PVDF/PC/LiBF₄ 1M.

Table 5-1 The effect of PVDF concentration on the melting point of PVDF/PC/LiBF₄ 1M salted gel and PVDF/PC unsalted gel.

PVDF (Wt%)	v_{PC}^*	Unsalted		Salted	
		T_m (°C)		T_m (°C)	
		Onset	Peak	Onset	Peak
20	0.856	77.03	88.80	103.16	117.72
25	0.817	77.87	99.08	104.61	119.93
30	0.776	79.21	95.67	107.28	122.20
35	0.734	82.98	98.83	108.40	122.35
40	0.690	88.81	107.2	109.80	124.06

* v_{PC} is PC volume fraction

According to Ying et al. [142], the reduction in melting points at low polymer concentrations can be attributed to the change in the morphological structure of PVDF caused by the diluent effect, while the considerable increase in melting points with the addition of electrolyte salt is due to its strong interaction with the lithium ion gel system, which affects its structure and causes morphological changes in the PVDF gel system. However, Figure 5-7 shows that the salt affects the PVDF gel's melting point more than the diluent agent (the solvent). An increase in melting point that accompanies an increase in PVDF concentration has also been reported by other researchers [41]. The interaction of LiBF₄ with the gel system is not well understood in the literature, however, and there is not yet any theory that can predict its interaction. However, the interaction between PVDF and PC can be predicted using the melting point depression theory

(see chapter 2). As illustrated in chapter 2, the Flory interaction parameter χ_F is a measure of polymer-solvent interactions, which can provide enough information about the solubility behaviour for different solutions. Table 5-1 includes one of the required parameters for the melting point depression equation, which is the solvent volume fraction (i.e. PC volume fraction) v_{PC} . The other parameters will be provided in the next section.

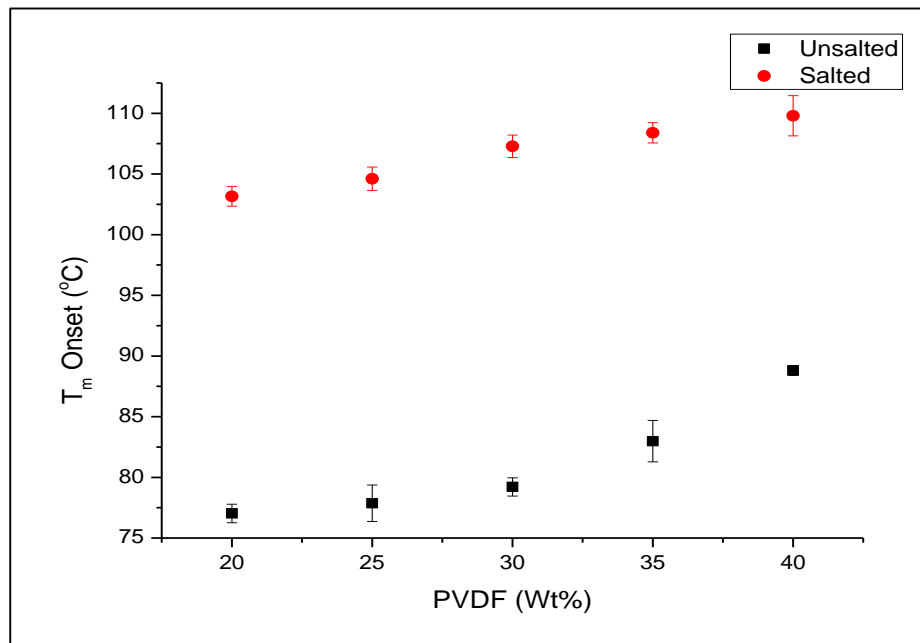


Figure 5-7 Melting temperature as a function of PVDF concentration for PVDF/PC unsalted and PVDF/PC/LiBF₄ 1M salted gels.

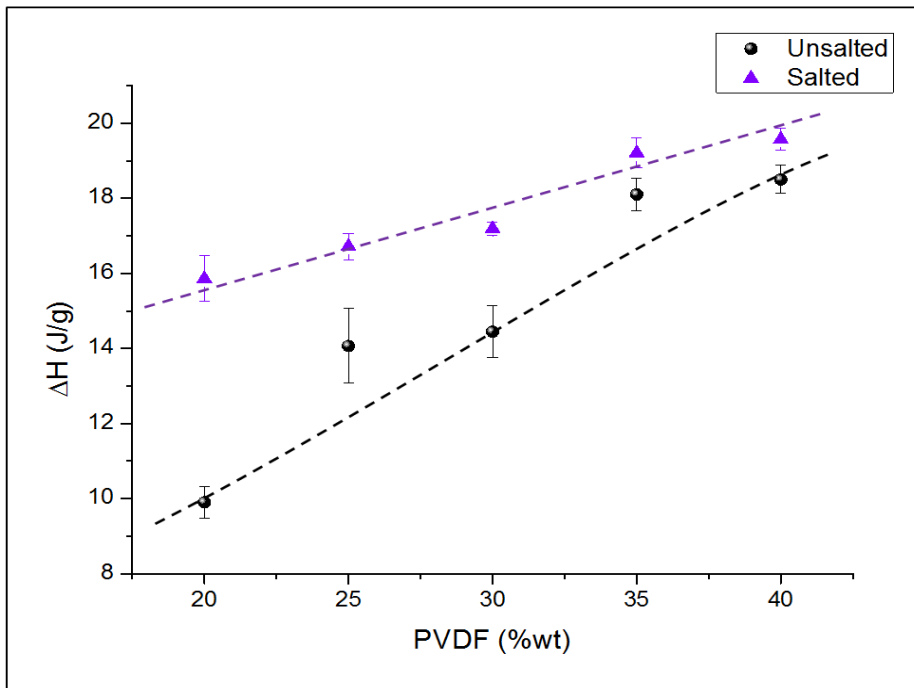


Figure 5-8 Heat of fusion plotted as a function of PVDF concentration for PVDF/PC and PVDF/PC/LiBF₄ 1M.

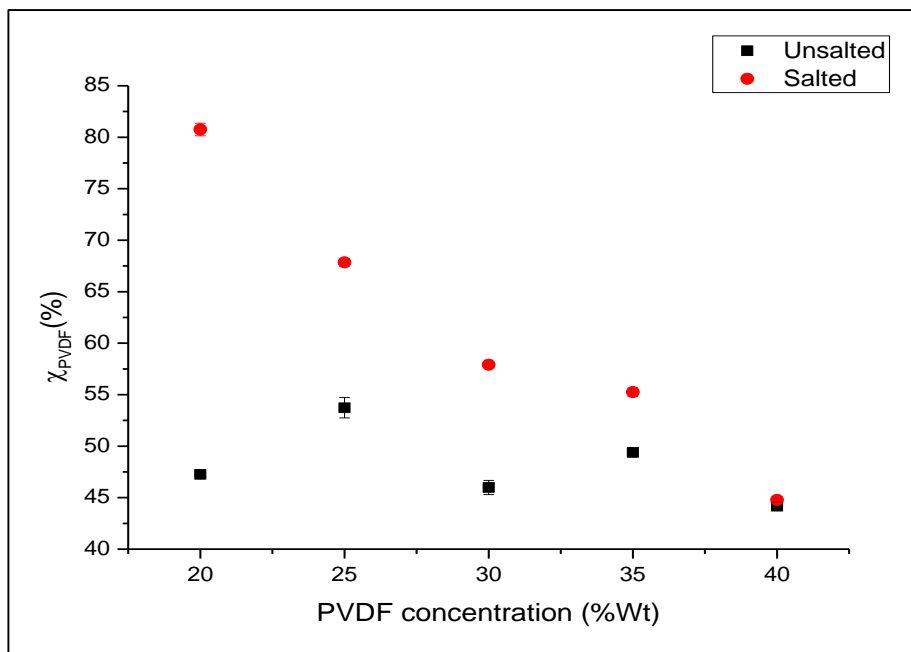


Figure 5-9 Degree of crystallisation of the polymer in the gel as a function of PVDF content for PVDF/PC and PVDF/PC/LiBF₄ 1M

Thermodynamic interpretation of the effect of polymer concentration on the melting depression

The results provided in section 5.2 concord well with those of other research in this area. Shimizu et al. [143] reported similar findings about gel melting points in relation to PVDF concentrations. They related the increase in melting point with the increase in polymer content to the difference in solubility parameters between PVDF and the solvent. Table 5-2 shows the solubility parameters for PVDF, PC and another solvent (diethyl carbonate DEC), which also have an effect on the gel properties, as will be discussed in the coming sections. Since we are studying the effects that these components have on the melting temperature of the polymer gel, we need to predict their effects at temperatures above room temperature (normally on the corresponding melting temperatures). Therefore, applying melting depression theory to this discussion may help in interpreting the effects of polymer content on the melting point by enabling us to calculate the interaction parameter, χ_F , between the polymer and the solvent.

Table 5-2 shows that the polarity solubility parameter (δ_p) of PC is noticeably higher than that of DEC, and closer to that of the PVDF. This may explain why PC is a good solvent for PVDF. Moreover, the difference between $\delta_{p(\text{PVDF})}$ and $\delta_{p(\text{PC})}$ is negative (i.e. $\delta_{p(\text{PVDF})} - \delta_{p(\text{PC})} < 0$), while the difference between $\delta_{p(\text{PVDF})}$ and $\delta_{p(\text{DEC})}$ is positive ($\delta_{p(\text{PVDF})} - \delta_{p(\text{DEC})} > 0$), which indicates that PVDF may spontaneously dissolve in PC. However, it is not only the polarity that plays a role in dissolving the PVDF, as hydrogen bonding and polydispersion energies also contribute to this operation, even though their contribution to the process is smaller.

Table 5-2. Hansen solubility parameters at room temperature.

Material	δ_d	δ_p	δ_h	δ_t
	MPa ^{1/2}			
PVDF ^[144]	17.2	12.5	9.2	23.2
PC ^[145]	20.0	18.0	4.1	27.3
DEC ^[145]	16.6	3.1	6.1	17.9

Equation 2-23 related melting depression to the interaction parameter and solvent volume fraction. Therefore, rearranging this equation to solve it with respect to the Flory interaction parameter can provide a good prediction for the interaction between the polymer and solvent. The melting point depression equation is given by:

$$\frac{1}{T_m} - \frac{1}{T_m^o} = \frac{RV_{pol}}{\Delta H_f^o V_{solv}} (v_{solv} - \chi_F v_{solv}^2) \quad \text{Equation 5-1}$$

Rearranging the above equation gives us:

$$\chi_F = \frac{1}{v_{solv}} - \left[\frac{1}{T_m} - \frac{1}{T_m^o} \right] \cdot \frac{\Delta H_f^o V_{solv}}{RV_{pol} \cdot v_{solv}^2} \quad \text{Equation 5-2}$$

This can provide χ_F values according to the parameters given in the equation. In Equation 5-2, T_m represents the observed melting temperatures of the diluted polymer under investigation, while T_m^o represents the melting temperature of the pure polymer. The T_m^o of PVDF was measured by Welch and Miller [146] to be 178°C (451.15K), while

Rosenberg et al. [147] reported its value to be 177°C (450.15K). As this latter value is very close to Welch and Miller's value, 178°C will be taken as the value for T_m° . Welch and Miller also measured the fusion heat of the pure polymer to be 3407.14 J/mol, and the gas constant, R , to be 8.3145 J/mol. K. Thus, as noted above, apart from the measured melting temperature and the solvent volume fraction (which are given empirically), almost all the other parameters are constants and can be acquired from the relevant literature. However, the molar volumes of the solvent and the polymer are dependent on the temperature, since their densities change with the temperature when mass is constant. Therefore, the temperature-dependent parameters need to be calculated at the experimentally determined melting points from Figure 5-7, and Table 3-3 shows some relevant properties of the polymer and the solvents in the study. The molar volume V is the ratio between molar mass M and the density of the substance ρ . It can be obtained using the following equation:

$$V = \frac{M}{\rho} \quad \text{Equation 5-3}$$

Thus, we need to be aware of the temperature at which we are calculating the molar volume. Table 5-3 shows the density variation of PVDF with temperature according to Welch and Miller [146], who suggest the following relationship:

$$\rho = a - bT$$

Equation 5-4

where b and a are the slope and the intercept with y-axis respectively. The data in Table 5-3 shows the densities in ranges between 180–200°C (PVF₂ being the name given to PVDF in the older literature). However, the temperatures at which melting depression should be calculated are less than the values that are shown in Table 5-1 above. Therefore, acquiring ρ within that range of temperatures requires an extrapolation from the data presented in Table 5-3 to the experimentally acquired melting points shown in Table 5-1. By plotting Equation 5-4 within the given range and extrapolating the linear function up to the required temperature, as shown in Figure 5-10, we can then calculate ρ . The corresponding ρ values have been acquired using this extrapolation, and are summarised in Table 5-4.

Table 5-3 PVDF density and linear parameters [Welch and Miller data][146]

Constants in the Density Relation ^a			
$\rho = a - bt$			
Material	$a, \text{ g cm}^{-3}$	$10^3 b, \text{ g cm}^{-3} \text{ deg}^{-1}$	Measurement range, °C
DMPH	1.2101 ± 0.0002	0.953 ± 0.002	22–140
DMAc	0.9605 ± 0.0002	0.946 ± 0.002	22–144
PVF ₂	1.706 ± 0.009	1.23 ± 0.05	180–200

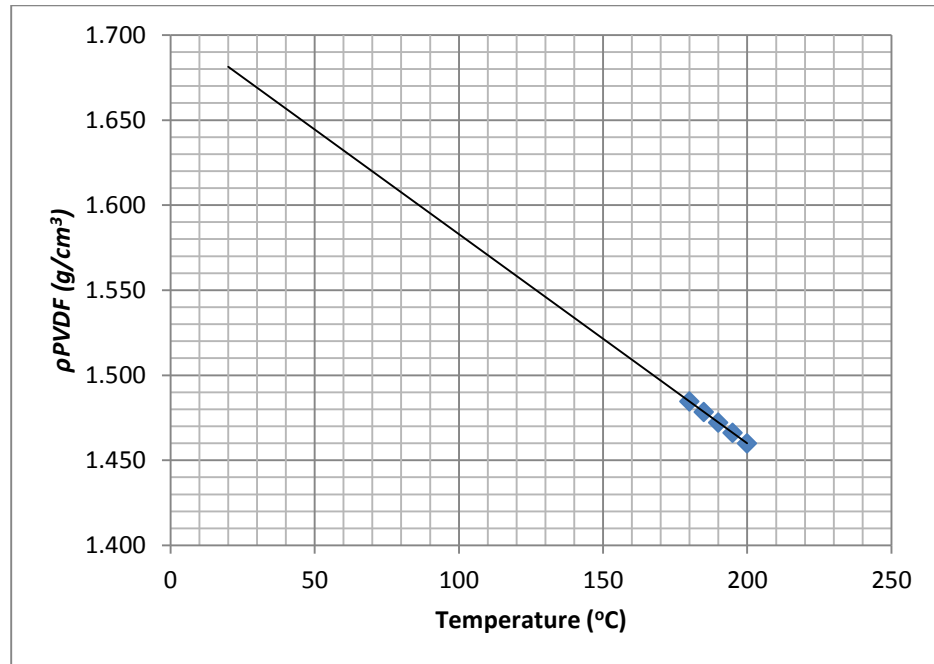


Figure 5-10 PVDF densities plotted as a function of temperatures at a range from 180–200°C. Note that the data has been extrapolated from room temperature measurements, which gives the densities within the experimental melting points.

The density and molar volume of PC can now be found in a similar way that it was for PVDF. To ascertain these values, we need to find how density varies with temperature for PC. Using Barthel [118], we can plot an extrapolated curve as shown in Figure 5-11 to acquire the desired densities of PC.

Table 5-5 shows the extrapolated densities and their corresponding molar volumes according to the measured melting temperatures. All the required variables for Equation 5-2 have now been acquired, and the equation can thus be applied to obtain the interaction parameter as a function of the volume fraction of the polymer (see Table 5-6).

Table 5-4 PVDF densities and molar volumes in relation to melting temperatures, acquired from the density extrapolated plot provided by Welch and Miller.

Measured melting Point (°C)		ρ (g/cm ³)		M_{PVDF} (g/mole)	V_{PVDF} (Cm ³ /mole)	
Unsalted	salted	Unsalted	salted		Unsalted	salted
77.03	103.16	1.61	1.58	64.04	39.69	40.48
77.87	104.61	1.61	1.58	64.04	39.71	40.52
79.21	107.28	1.61	1.58	64.04	39.75	40.60
82.98	108.4	1.61	1.58	64.04	39.86	40.64
88.81	109.8	1.60	1.57	64.04	40.04	40.68

Figure 5-12 shows how the interaction parameter varies with different concentrations of PVDF. From the figure, it can be seen that, in the unsalted gel, less potential was needed to dissolve the polymer in the solvent—i.e. the PC is a good solvent in this context. However, the values of the interaction parameter were higher for the salted gel, indicating that much more energy would be needed to dissolve the two components. Moreover, the interaction between the polymer and the solvent in the unsalted gel shows that its behaviour is unchanged when the polymer concentration of the solution is increased, unlike in the salted gel, which shows a positive increase with increasing PVDF concentration. Although there is a slight increase in the interaction parameter with increased polymer concentration in the unsalted gel, the significant difference in the values of the interaction parameter between the salted and unsalted gels confirms that the difference in melting point curves of the two gels can be directly attributed to the interaction parameter, and that the salt has a greater interaction with PC than with PVDF [148, 149].

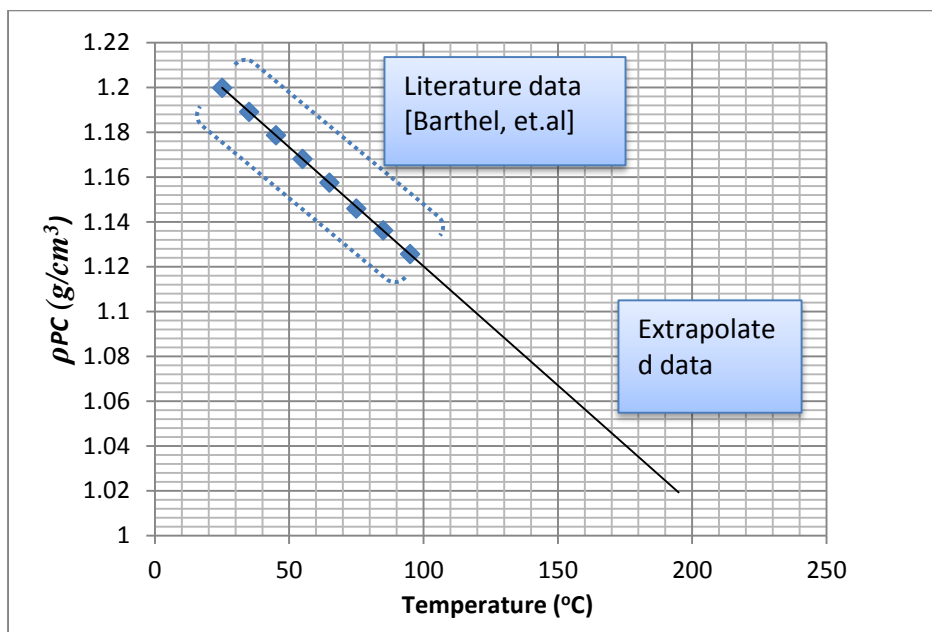


Figure 5-11 Density of PC plotted as a function of the temperature [118]. Note the extrapolated data used to find out ρ value at the experimental melting points.

Table 5-5 PC densities and their corresponding molar volumes at the measured melting temperatures.

Measured melting Point ($^{\circ}\text{C}$)		ρ (g/cm^3)		M_{PC} (g/mole)	V_{PC} (Cm^3/mole)	
Unsalted	salted	Unsalted	salted		Unsalted	salted
77.03	103.16	1.14	1.11	102.09	89.42	91.73
77.87	104.61	1.14	1.11	102.09	89.49	91.86
79.21	107.28	1.14	1.11	102.09	89.61	92.11
82.98	108.4	1.14	1.11	102.09	89.94	92.21
88.81	109.8	1.13	1.11	102.09	90.45	92.34

Table 5-6 Flory interaction parameters for salted and unsalted gels, as obtained from the melting depression equation.

PVDF (%Wt)	χ_F	
	Unsalted	Salted
20	0.363	0.613
25	0.349	0.628
30	0.335	0.657
35	0.347	0.669
40	0.387	0.682

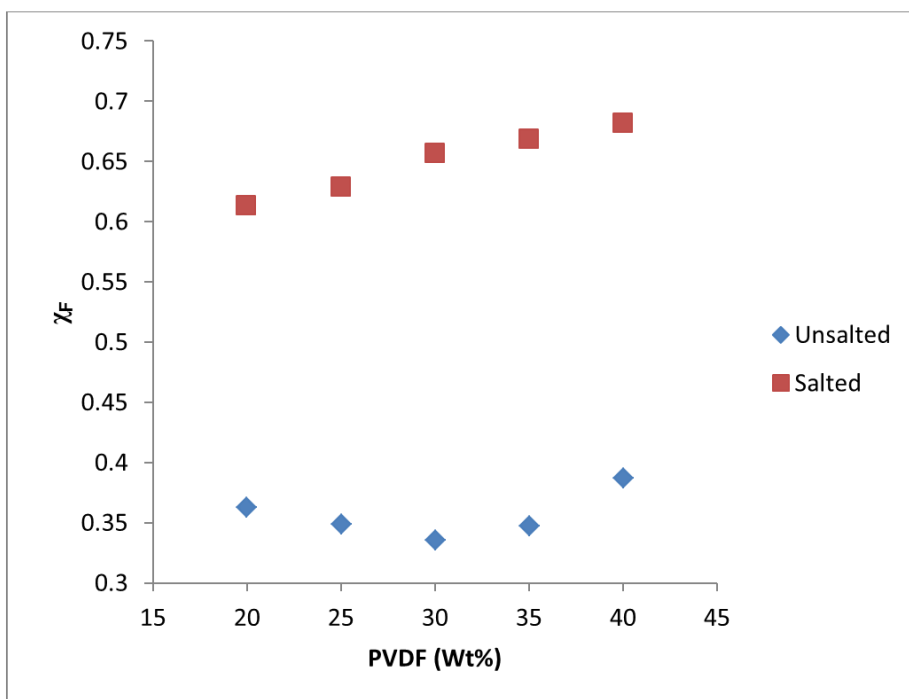


Figure 5-12 Flory interaction parameters plotted as a function of the PVDF content for the unsalted and salted gel.

5.2.2 Ionic conductivity

Figure 5-13 shows how ionic conductivity decreases with increasing polymer content. This is to be expected, as the volume fraction of the liquid electrolyte is reduced while tortuosity is increased. This behaviour can also

be attributed to the increase in the viscosity of the electrolyte system, which decreases charge carrier mobility. However, this behaviour accords with Whang et al.'s [150] findings that ionic conductivity is dependent upon the diluent agent.

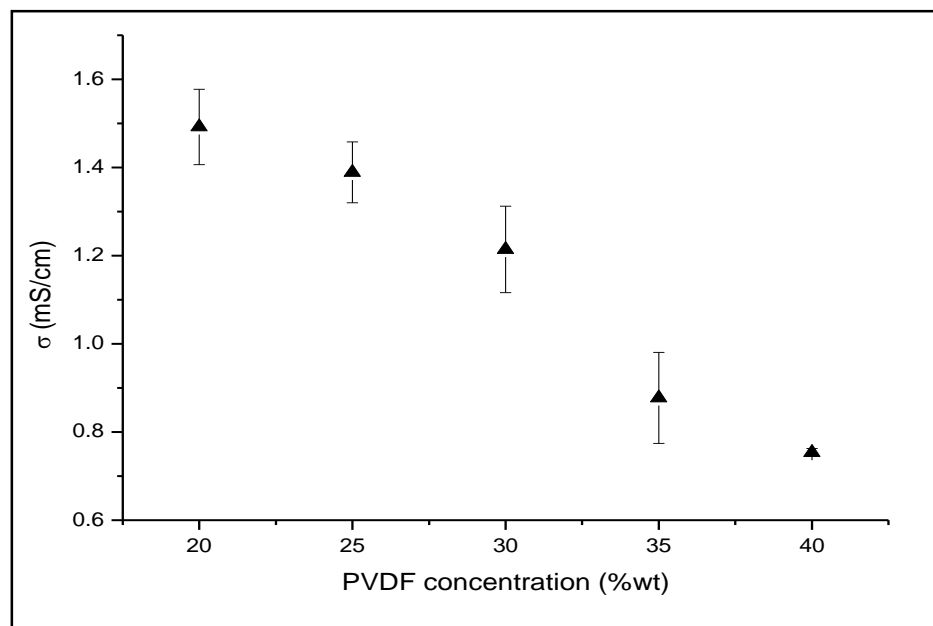


Figure 5-13 Room temperature ionic conductivity versus PVDF concentration for PVDF/PC/LiBF₄ 1M gels. The samples were made in the glove box and slow-cooled.

5.3 Effect of solvent quality

5.3.1 Gel melting points

This section discusses how mixing different ratios of solvents composed of propylene carbonate (PC) and diethyl carbonate (DEC) effects solvent quality,, taking into account that the total solvent volume must be kept constant (5.834ml). The current gel has the form 30PVDF/PC:DEC unsalted gel and 30PVDF/PC:DEC/LiBF₄ 1M, with different PC:DEC ratios.

DEC is considered to be a poor solvent for PVDF due to the difference in their solubility parameters (see Table 5-2). However, its low viscosity is considered to be a virtue in polymer gel electrolytes because it facilitates ion mobility. Figure 5-14 shows that the melting point of the gel increases with DEC content throughout the whole composition. The rise in melting point is likely attributable to the change in solvent quality affecting the Flory-Huggins interaction parameter. As DEC is a poor solvent, the thermodynamics of mixing may thus be the key behind the change in its melting point. Different mixes of the solvents will have different effects on PVDF due to the differences in solubility parameters, and the thermodynamics of mixing will now be discussed in order to examine the solvent's effect on the heat of mixing.

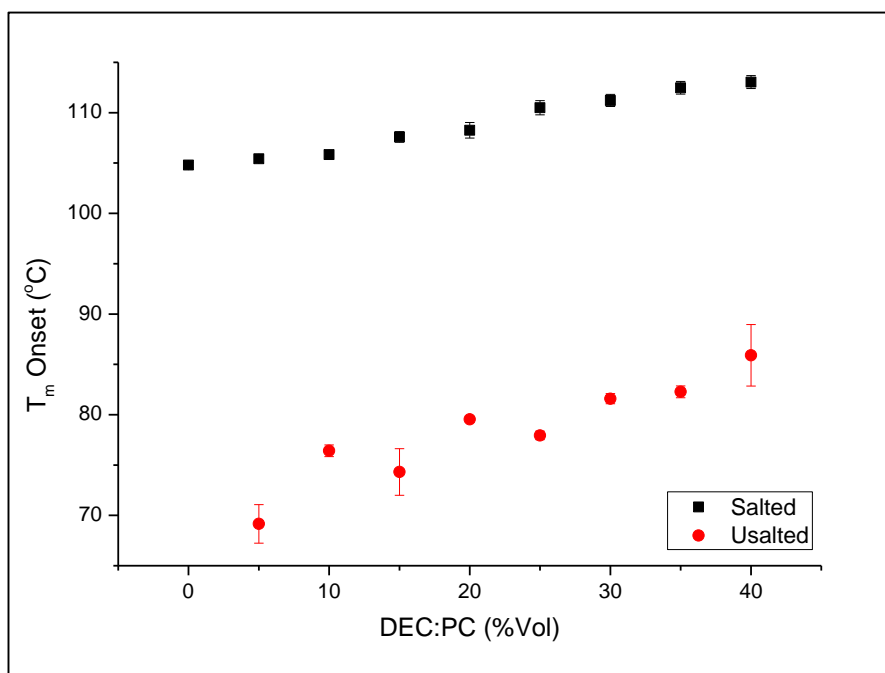


Figure 5-14 Melting temperature (onset) versus DEC:PC ratio (percentage ratio of DEC to PC) in 30%PVDF/PC:DEC/LiBF₄ 1M salted and 30%PVDF/PC:DEC unsalted gels.

5.3.2 Thermodynamics of mixing

The change in melting point may be related to the thermodynamic changes that occur during mixing when the gel is prepared, so it is essential to investigate how this affects the gel. The enthalpy of mixing provides a good method for approaching this task, and can be estimated with another form of the melting point depression utilising the Flory-Huggins theory, as shown in chapter 2. The enthalpy of mixing ΔH_{mix} has been estimated for each solvent with PVDF, using the following equation:

$$\Delta H_{mix} = V \cdot (\delta_{Solvent} - \delta_{Polymer})^2 \cdot v_{solvent} v_{Polymer} \quad \text{Equation 5-5}$$

V is the volume of the mixture (and was calculated for each solvent individually, i.e. for PVDF/PC $V=V_{PVDF}+V_{PC}$), while v_i is the volume fraction of the species i . The information in Table 5-2, and Table 5-7 was used to estimate ΔH_{mix} from the above equation, and the values of ΔH_{mix} that were obtained were plotted as a function of the melting points that were acquired empirically from 30PVDF/PC:DEC unsalted gel (see Table 5-7). Figure 5-15 shows that the ΔH_{mix} change was positive for both solvents due to the effect of squaring in Equation 5-5, and this was the case regardless of the differences between the solubility parameters of PVDF and PC, on the one hand, and PVDF and DEC on the other. However, the difference in solubility parameters can produce a noticeable change to the enthalpy of mixing, and this was confirmed for this case when the Flory-Huggins

interaction parameter was predicted using Equation 5-6 (see chapter 2) and plotted against temperature, as shown in Figure 5-16. The figure shows that higher values of χ_F are produced between PVDF and DEC than between PVDF and PC, which indicates that the energy needed to break the polymer structure apart is greater when DEC is added than when PC alone is added. On the other hand, Figure 5-15 suggests that adding DEC has a similar effect on the enthalpy of mixing between DEC and PVDF. However, PC seems to reduce the enthalpy of mixing when the temperature is increased. The Flory interaction parameter plotted in Figure 5-16 shows a slight decrease with increasing temperature, although this decrease is too small in comparison with the effect of solvent quality. DEC displays poor solvent behaviour when it interacts with PVDF, whilst PC exhibits theta solvent behaviour when it interacts with PVDF, with its χ_F values approaching 0.5.

$$\chi_F = \frac{V_{solvent}}{RT} (\delta_{solvent} - \delta_{polymer})^2 \quad \text{Equation 5-6}$$

Table 5-7 PC: PVDF/PC:DEC imperial parameters used to estimate heat of mixing.

PVDF Mass (g)	PC:DEC Volume Ratio	V_{PC} (cm ³)	V_{DEC} (cm ³)	V_{PVDF} (g)	U_{PC}	U_{DEC}	U_{PVDF}	T_m (Onset)
								°C
3	100:00	5.834	0.000	1.685	0.765	0.000	0.235	69.16
3	95:05	5.542	0.292	1.685	0.725	0.038	0.237	74.31
3	90:10	5.250	0.583	1.685	0.685	0.076	0.239	76.42
3	85:15	4.959	0.875	1.685	0.644	0.114	0.242	77.94
3	80:20	4.667	1.167	1.685	0.604	0.151	0.245	79.55
3	75:25	4.375	1.458	1.685	0.564	0.188	0.248	81.59
3	70:30	3.792	2.042	1.685	0.487	0.262	0.251	82.27
3	65:35	3.500	2.333	1.685	0.448	0.299	0.254	85.90

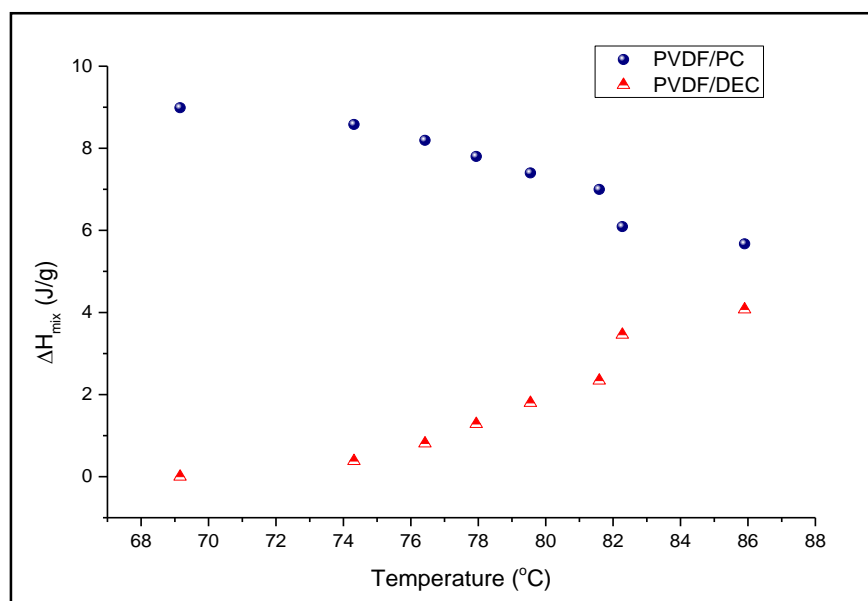


Figure 5-15 Heat of mixing predicted for 30PVDF/PC and 30PVDF/DEC, showing the thermodynamic interactions between each solvent and the polymer.

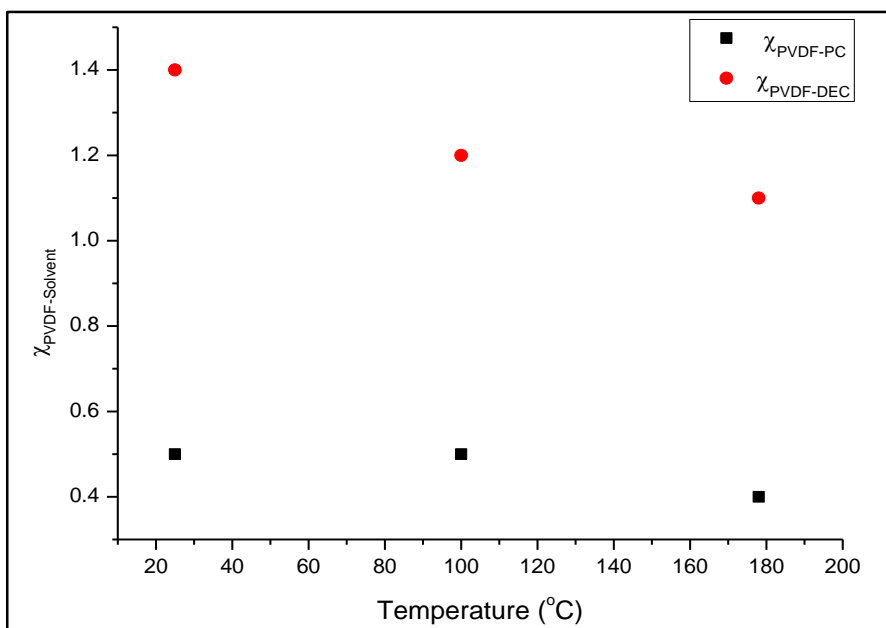


Figure 5-16 Interaction parameter plotted as a function of temperature for PVDF-PC and PVDF-DEC.

5.3.3 The effect of solvent composition on ionic conductivity

Figure 5-17 shows the decrease in ionic conductivity that occurs when the DEC fraction is increased in a PC:DEC solvent in both liquids and gels. The fall in ionic conductivity is attributed to the reduced dielectric constant of the solvent (for PC, $\epsilon=64.92$; for DEC, $\epsilon=2.82$ [151]), which results in a lower dissociation of the salt, meaning that there are less free ions available for conduction. However, this reduction in ionic conductivity is not as severe as it could be, since DEC has a lower viscosity than PC, which allows for greater ionic mobility, as shown in Equation 5-7:

$$\sigma = \frac{nq^2}{6\pi\eta r} \quad \text{Equation 5-7}$$

where n is the concentration of free ions, q is the charge on each ion, r is

the radius of each ion, and η is the viscosity of the liquid electrolyte.

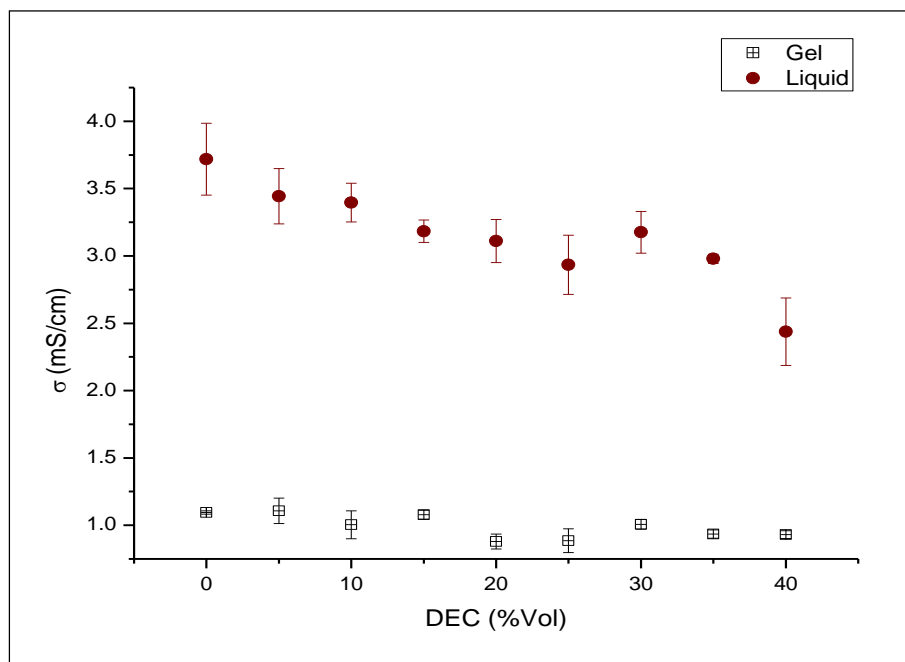


Figure 5-17 Room temperature ionic conductivity versus DEC content (percentage of total solvent) in PC:DEC/LiBF₄ 1M liquids and 30%PVDF/PC:DEC/LiBF₄ 1M gels.

5.4 The effect of salt

5.4.1 Gel melting points

5.4.1.1 Effect of salt concentration

Figure 5-18 shows the rise in melting points produced by increasing the salt concentration in the PGEs. The reasons for this increase in melting point are not fully understood, but may be due to the salt's effects on the solvent quality or to interactions between the polymer and the salt. The increase in melting point that is produced with the addition of salt may also be attributed to the increase in spherulitic structures, which can be enhanced by promoting more nucleation activities.

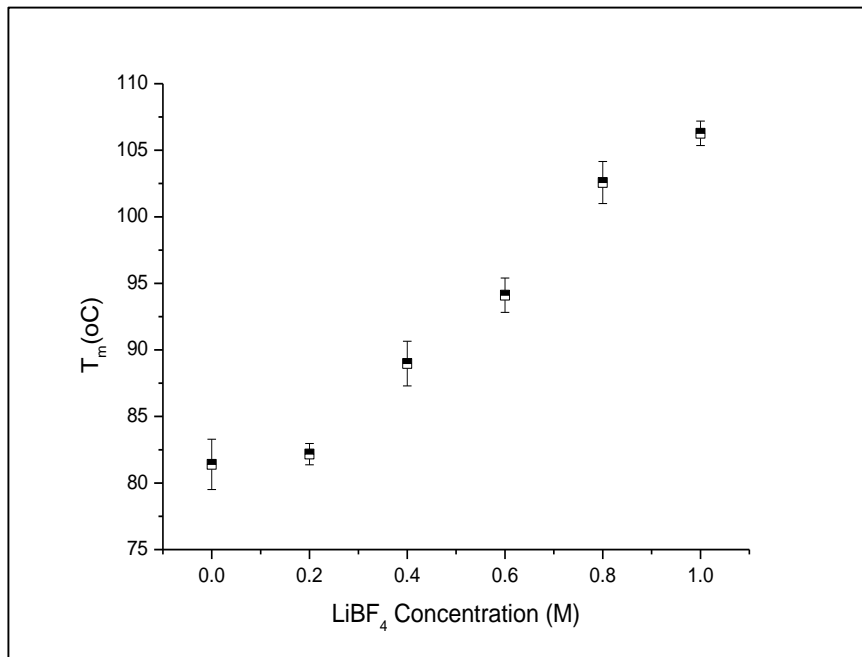


Figure 5-18 Melting temperature (onset) versus salt concentration for 30%PVDF/PC/ LiBF_4 gels.

5.4.1.2 The effect of salt nature

Figure 5-19 shows that the types of salt used has no significant effect on the melting point of the gels, although a slight increase is seen when LiBOB is used in comparison with LiBF_4 .

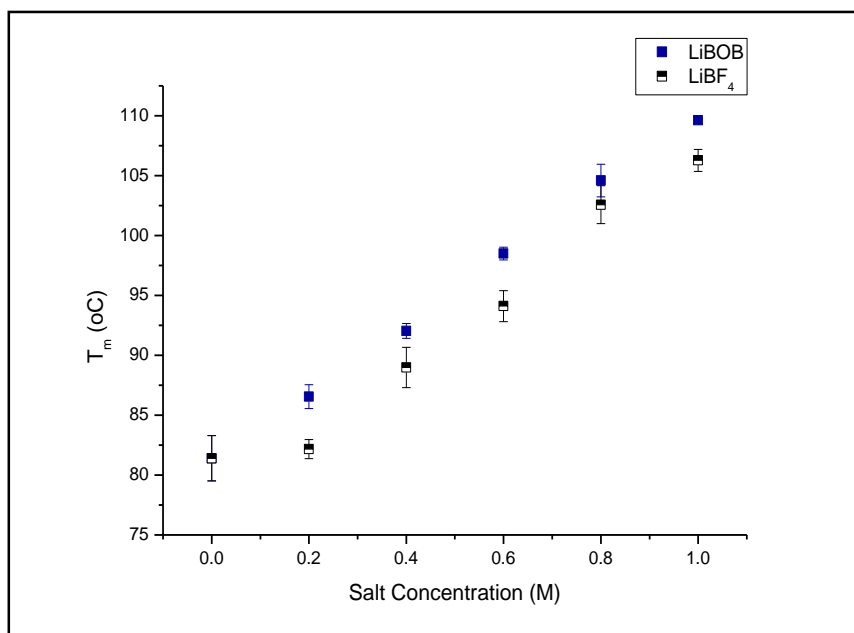


Figure 5-19 Melting point as a function of the salt concentration for 30%PVDF/PC/LiBF₄ and 30%PVDF/PC/LiBOB. To compare the effect of two types of salts on the melting point of PVDF-based gels.

5.4.2 Ionic conductivity

5.4.3 The effects of salt concentration

Figure 5-20 shows how the ionic conductivity of liquids and gels varies with salt concentration at room temperature. The maximum ionic conductivity is attributed to the result of competition between increasing free ion concentration and increasing viscosity, as shown in Equation 5-7.

5.4.3.1 The effects of salt nature

Figure 5-21 shows that LiBOB-based gels give higher ionic conductivities than LiBF₄-based gels. This is likely due to the easier dissociation that can occur in LiBOB gels because of the role that the large BOB anion plays in reducing the electrostatic force between the anion and the cation. This

leads to easier splitting in the presence of a good solvent, rendering higher numbers of Li^+ ions, thus increasing ionic conductivity.

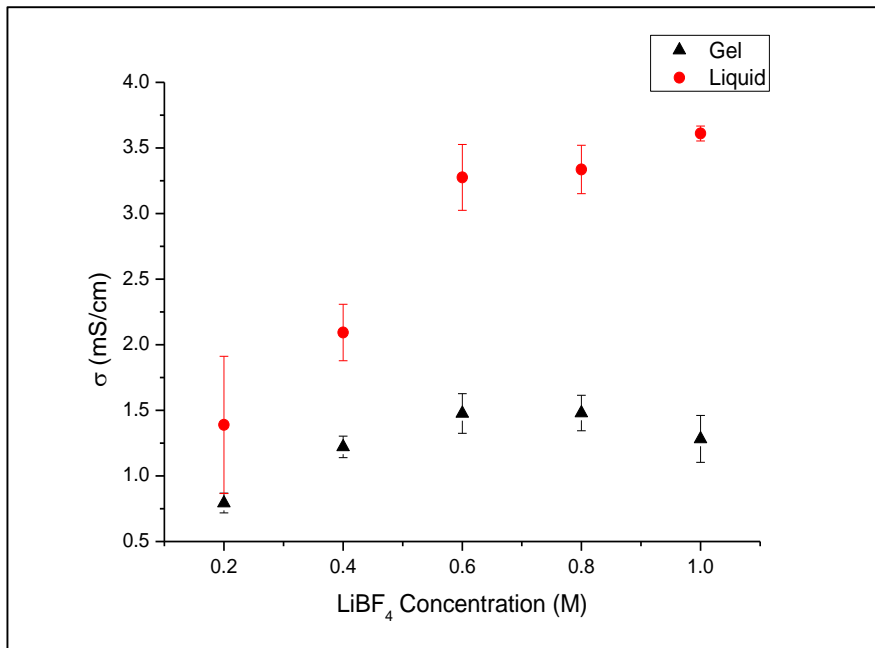


Figure 5-20 Room temperature ionic conductivity versus salt concentration for PC/LiBF₄ liquids and 30%PVDF/PC/LiBF₄ gels.

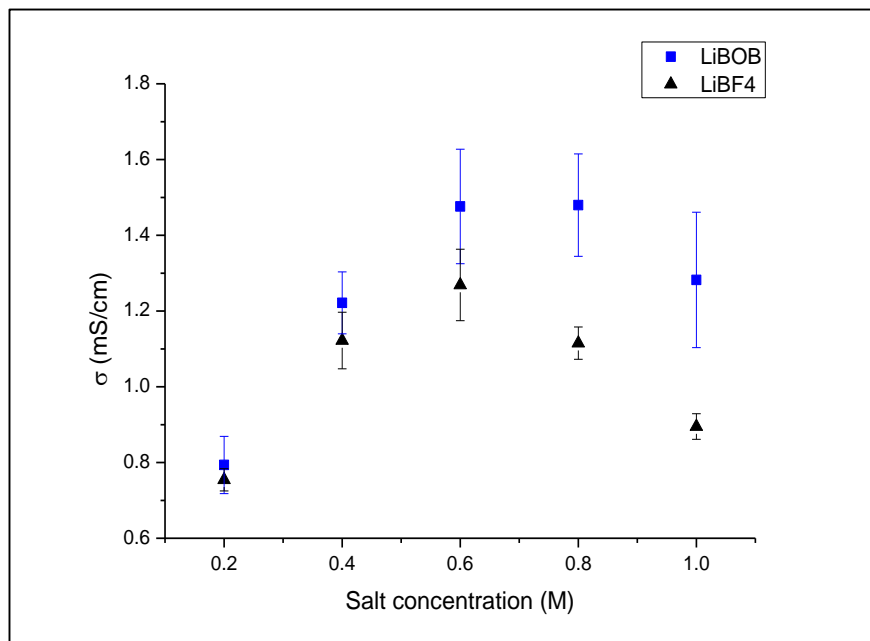
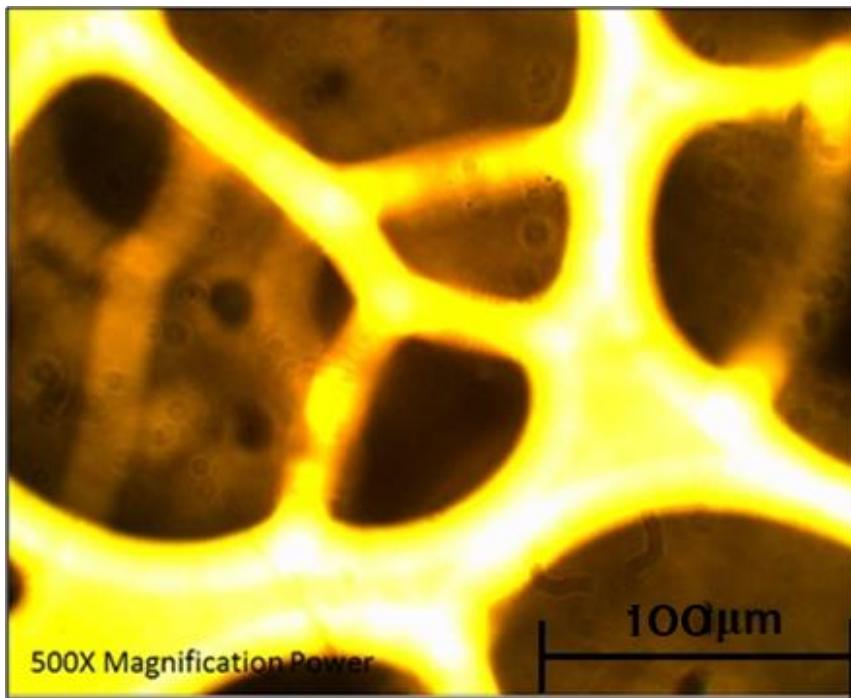


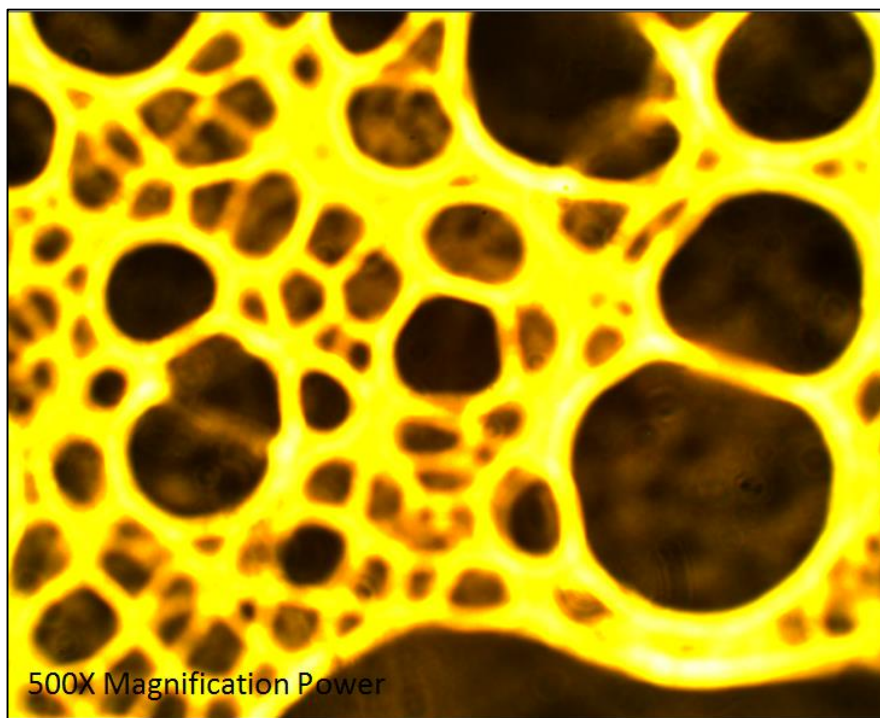
Figure 5-21 Comparison of ionic conductivity values in the salted gel samples, depending on the salt type.

5.4.4 The effects of gel composition on pore size

The effect that salt addition has on the pore size of the sample gels was investigated using optical microscopy. The details regarding the preparation and measurement of the samples using optical microscopy were provided in section 3.9.5. Figure 5-22(a) shows a room temperature optical micrograph for the unsalted gel samples, while Figure 5-22(b) shows a micrograph for the salted ones. The two figures show that salt addition has a significant effect on pore size. This may be due to the nucleation effect being accelerated by the presence of salt, and hence reducing the size of liquid pockets.



(a)



(b)

Figure 5-22 Room temperature optical micrographs illustrating the effect of salt on pore size for (a) 30PVDF/PC (unsalted gel) and (b) 30PVDF/PC/LiBF₄ 1M (salted gel). Both optical spectrographs used a magnification power of 500X.

5.4.5 Wide-angle x-ray scattering

The preparation and measuring procedures for WAXS samples were provided in section 3.9.4. Figure 5-23 shows room temperature WAXS crystallographic curves for the 30PVDF/PC unsalted gel and the 30PVDF/PC/LiBF₄ salted gel. Comparing between the two curves in the figure shows that adding salt to the gel reduces the three peaks found in the unsalted gel to one peak. To study this behaviour in more depth, these results were compared with the corresponding DSC curves produced from melting temperature measurements for independent unsalted and salted samples. Figure 5-24 provides a comparison of the melting temperature curves for unsalted and salted gels. Despite the different measurements used in the tests and the different test conditions, the curves produced using the different techniques showed similar behaviours, with the unsalted gel producing three peaks while the salted gel produced only one. Both curves were subjected to accurate analysis including curve and peak fitting, which resulted in the data summarised in Table 5-8 for the WAXS Figure 5-25 and DSC trace analyses.

The analysed data from WAXS showed three peaks in the unsalted gel at 16.2°, 20.5° and 27.6°, which were related to the planes of spaces of 5.455°A, 4.341°A and 3.230°A, respectively. In the salted gel, the single peak was detected at 20.7°, which corresponded to 4.285°A. Using the Scherer equation, it was found that the crystal size of the gel is reduced to about half its original size when the salt is added to the unsalted gel (see Table 5-8). This reduction in crystal size in the salted gels concords with the finer crystal patterns that were observed in the optical micrographs in

chapter 4 (see section 4.2.5).

The DSC analysis detected two embedded peaks in addition to the main peak in the unsalted gel, with a $\pm 7^{\circ}\text{C}$ difference from the main peak. In contrast with the unsalted peaks, the DSC analysis on the salted gel confirmed the presence of only one peak. Therefore, unsalted gel is thought to have different crystallising phases, while salted gel has only one. Satabathy [113] and Gregoreo [112] studied PVDF crystal forms, and reported crystallographic positions similar to those found in the current research (see Table 3-2). They related the peak they observed at 20° to β and γ phases with corresponding crystal planes of 200 and 110 for β and 101 for γ . Furthermore, they reported that α -phase could be found at 18.8° , 19.9° and/or 26.6° , which correspond to the crystal planes at 202, 110 and 021 respectively.

Abbrent et al. [152] found similar changes in the PVDF gel structure when lithium salt was added to it to those observed in the current research. They found that the non-polar phase α in the unsalted gel was converted to the polar phase β (20°) when salt was added. Therefore, our unsalted gel may have been crystallised in α form and converted to β form when the salt was added.

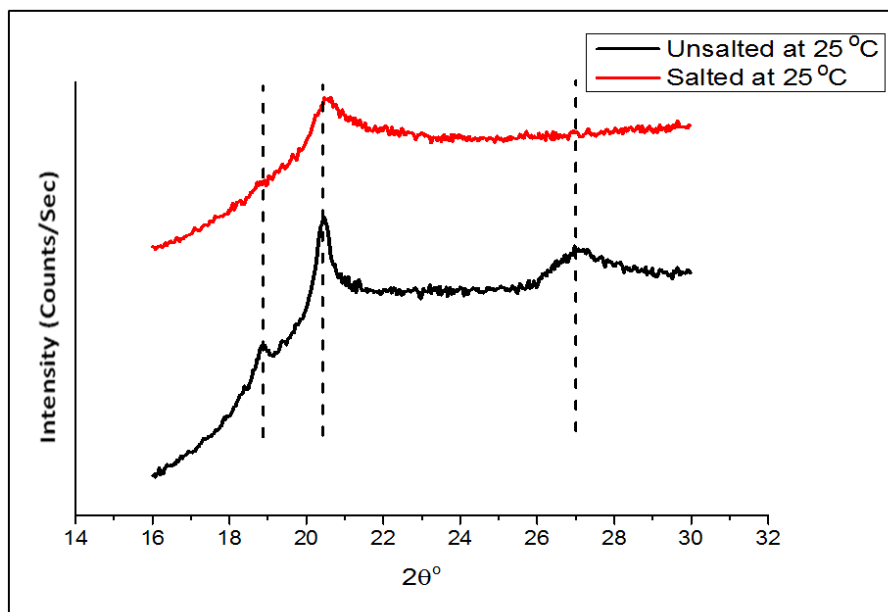


Figure 5-23 WAXS patterns for 30PVDF/PC/LiBF₄ 1M salted gel and 30PVDF/PC unsalted gel. The dotted lines in the graph are provided to compare the peaks found in the unsalted gel with the lack of peaks in the salted one.

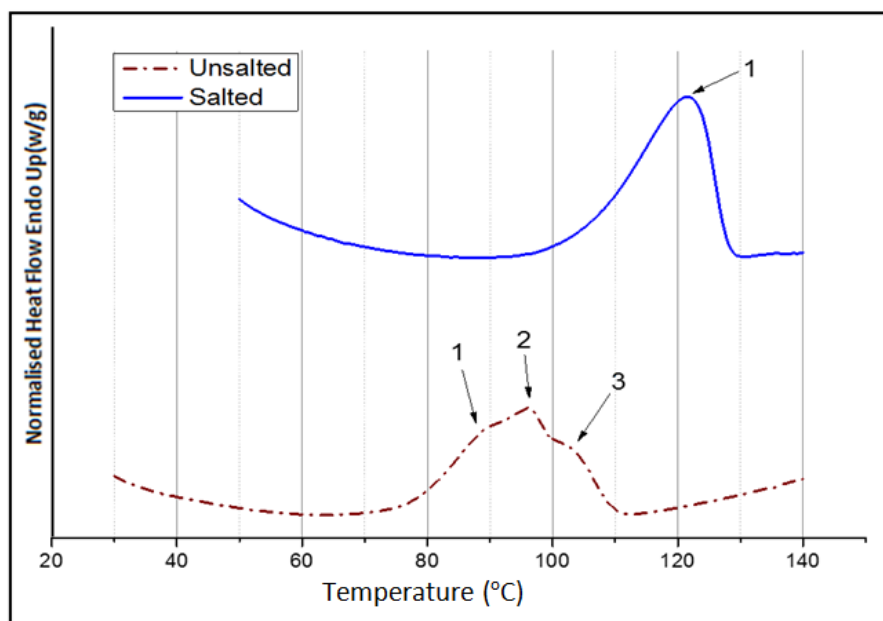
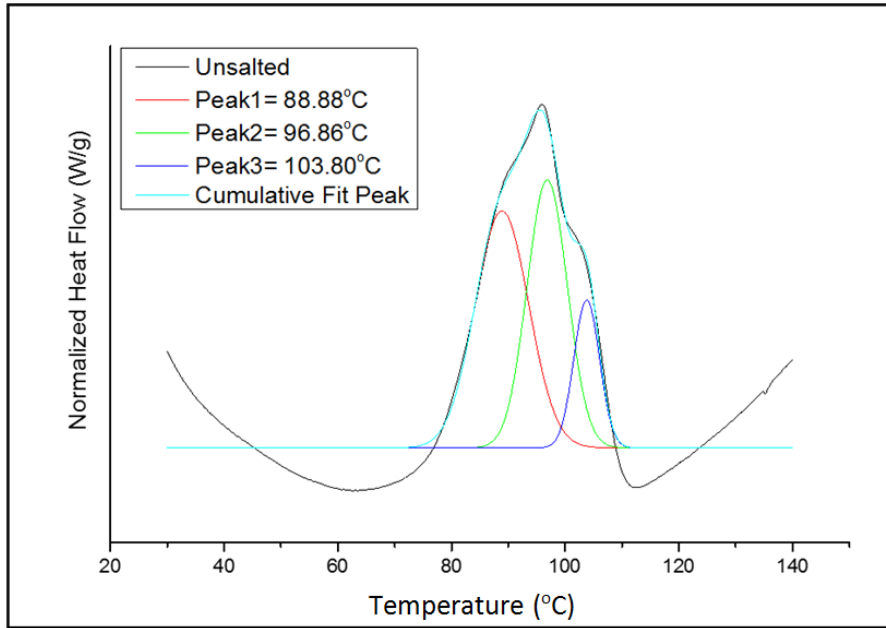
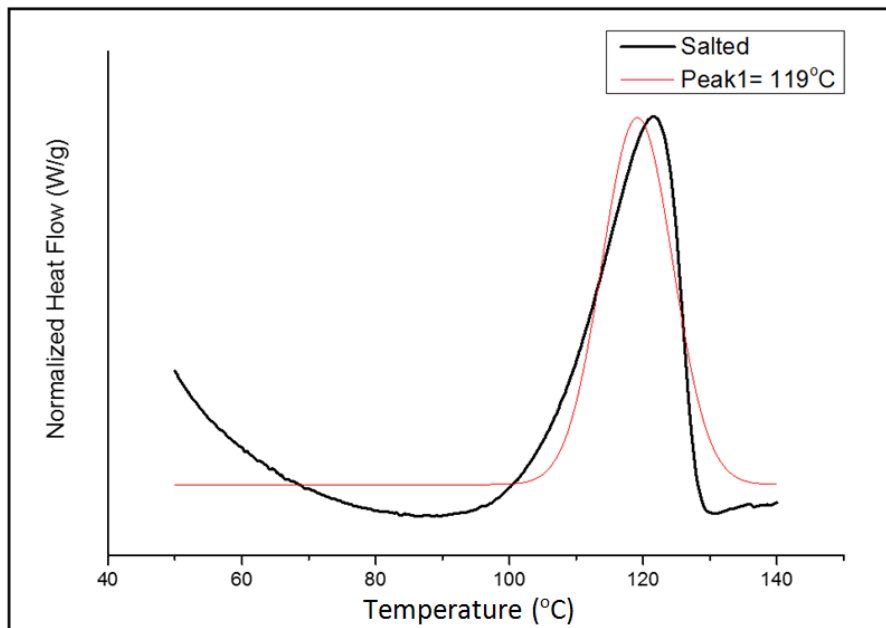


Figure 5-24 A comparison of the melting curves in the salted and unsalted gels, showing the multi peaks that are present in the unsalted gel with the single peak in the salted gel.



(a)



(b)

Figure 5-25 A comparison between (a) unsalted and (b) salted fit peaks, showing the three peaks that were found in the unsalted gel compared to the single peak that was found in the salted gel.

Table 5-8 Crystal sizes found through WAXS for 30PVDF/PC unsalted gel and 30PVDF/PC/LiBF₄ 1M salted gel.

Unsalted			Salted		
2 θ ^o	d (°A)	Crystal size (nm)	2 θ ^o	d (°A)	Crystal size (nm)
16.2	5.455	7±0.092	-	-	-
20.5	4.341	60±0.016	20.7	4.285	34.410±0.091
27.6	3.230	12±0.114	-	-	-

5.5 Discussion and conclusions

The effects of gel composition on the PVDF gel's properties were discussed in this chapter. The results from different techniques were informative, providing a good level of understanding regarding gel properties (mainly in relation to melting point depression behaviour) under different conditions. Several conclusions can be drawn:

1. Figure 5-7 clearly shows that the melting point of the gel increases with increasing polymer concentration. This concurs with the well-established effect that diluent has in causing melting point depression [148, 153]. The addition of salt generates a marked increase in the melting point of the gel (~25°C), which may be caused by the salt's effect on the Flory interaction parameter increasing the interaction energy, resulting in poorer solubility. A significant increase in the melting temperature of the gel produced by the addition of salt was also reported by Shimizu [143] for gels containing less than 14%wt PVDF in PC. This has a much lower

polymer concentration than the gel investigated in this thesis, but there is no other discussion of the salt's effect on gel melting point behaviour in the literature.

2. Figure 5-8 and Figure 5-9 show that PVDF is approximately 50% crystalline at all polymer concentrations in unsalted samples. However, in salted samples, the salt noticeably increases the crystallinity of PVDF at low PVDF concentrations, but has a much more negligible effect at higher polymer concentrations. This may suggest that the salt has a large effect in nucleating crystals and encouraging the polymer to crystallise at low PVDF concentrations, whereas the polymer overlap is enough to initiate crystallisation but too much to give mobility at high PVDF concentrations, allowing so much of the polymer to crystallise.
3. Figure 5-14 shows that there is a steady increase in the gel melting point when the proportion of DEC in the gel is increased, although not such a marked increase as that seen with the addition of salt. This can be explained with reference to solubility parameters, as the difference in the solubility between PVDF and DEC is greater than that between PVDF and PC. This is supported by the heat of mixing theoretically predicted (see Figure 5-15).
4. Figure 5-17 shows that there is a slight reduction in ionic conductivity with the incorporation of DEC. This is due to DEC's lower dielectric constant than PC being offset by its significantly lower viscosity.
5. Figure 5-18 shows that a significant increase in gel melting

temperature occurs when salt is added to it (as was discussed in chapter 4), and Figure 5-19 shows the slight increase in thermal stability that LiBOB possesses in comparison to LiBF₄.

6. Figure 5-20 shows the effect that increasing salt concentration has on ionic conductivity, which reaches a maximum at around 0.8M in 30PVDF/PC/LiBF₄ gel. This maximum level is a result of the competing factors of an increased number of free ions and the increase of the gel's viscosity. Figure 5.22 shows the slight advantage that LiBOB has over LiBF₄ here.
7. Optical microscopy (see Figure 5-22) revealed a difference in the pore size of salted and unsalted gels, with salted gels having smaller pores. This again shows that salt has a nucleating effect on many crystals, and concords with the findings provided in Figure 5-23 and Figure 5-24, which show that the salted gel has a much finer structure.

Chapter6. Conclusions and Future Work

6.1 Introduction

The primary objective of this work was to study the gelation mechanism and the gel properties for a type of material that is widely employed within the commercial world PVDF-based gel electrolytes in order to acquire a better understanding of the thermodynamics and kinetics of PVDF gels. This has been achieved by using different techniques, chosen for their suitability for measuring particular properties and activities.

This thesis has engaged with a variety of subjects in essential fields relating to the study of PVDF gelation, examining widely used solvents such as propylene PC carbonate and diethyl carbonate DEC together with the contributions of highly efficient lithium-based electrolyte salts such as lithium trifluoroborate LiBF_4 and lithium bisoxalatoborate LiBOB. Five techniques were used to measure the different gel contents and to determine their characteristics: differential scanning calorimetry (DSC), dynamic mechanical thermal analysis (DMTA), wide-angle x-ray scattering (WAXS), optical microscopy, and ionic conductivity. Using these techniques within different conditions helped to provide answers to key questions that were formerly unanswered. DSC, for example, was used to investigate two different behaviours: to compare between the isothermal crystallisation of salted and unsalted gels from molten solutions in order to identify the effect of salt on isothermal gelation activity; and to determine the effect of gel composition on melting point behaviour via heating gel samples of different

contents and comparing the observed endothermic melting peaks. Creating variations in gel composition included making qualitative and quantitative changes to gel elements, such as polymer concentration, solvent quality, salt concentration and salt quality.

DMTA was used to determine gelation behaviour in a similar way to DSC using high temperatures to produce molten samples in order to remove the thermal history, and then cooling them rapidly to a given temperature in order to observe gelation isothermally. This was done in order to determine whether gelation takes place via crystallisation or via liquid-liquid phase separation. Optical microscopy was used to validate prior results and to clarify the gel structure visually. Lastly, ionic conductivity was measured for each composition to determine the effect of each composition on ionic conductivity, and hence to discover how different gel structures can affect the gel's ionic conductivity. Overall, the results from this study have yielded a variety of important conclusions, which are summarised in the following sections.

6.1.1 Phase separation and crystallisation behaviour

Gelation from molten solutions can be described through two windows, depending on the temperature at which isothermal gelation or crystallisation can take place. The low temperature window was mainly found at $40^{\circ}\text{C} \leq T_{\text{iso}} < 70^{\circ}\text{C}$ for the unsalted gel and $40^{\circ}\text{C} \leq T_{\text{iso}} < 100^{\circ}\text{C}$ for the salted gel. Within this window, gelation is thought to take place via crystallisation, since crystallisation takes place before gelation here. The other window can be found at temperatures well above the nominated

range (i.e. above 70°C for the unsalted gel and 100°C for the salted gel). Within this range of temperatures, no crystallisation can be detected, but gelation is obviously observed, indicating that a liquid-liquid phase separation is occurring. Optical micrographs supported this finding, showing clear structural patterns at 50°C, but no specific crystal structures at higher temperatures—at 80°C for the unsalted gel and 110°C for the salted gel.

The addition of lithium salts increased nucleation activity over growth within the low temperature profiles, as was evidenced by the rapid crystallisation at this range.

Super-cooling also had a significant effect on the subsequent melting temperature and re-crystallisation of both salted and unsalted gels. However, the addition of salt competed with this effect, producing significantly higher crystallisation over the super-cooling behaviour.

6.1.2 The effect of gel composition

The effect of the electrolyte salt does not seem to be limited to isothermal gelation, with the melting point measurements showing that it provided good thermal stability for the salted gel samples. The presence of salt may change gel morphology—as was observed through the WAXS crystallographs, which showed that adding salt to the gel caused obvious modifications to the PVDF polymorphs. Increasing the salt concentration also increases ionic conductivity, but within a limit of concentration, over which increases in viscosity may suppress the mobility of charge carriers

despite their increase in numbers, thus leading to a reduction in ionic conductivity.

Polymer concentration also has a negative effect on ionic conductivity, but progressively increases the gel's melting point. The increase in polymer content may cause tortuosity and greatly increase viscosity, hindering charge carrier mobility and causing the ionic conductivity to drop. An increase in polymer concentration also appears to cause a decrease in the gel's nucleation and growth, which can be concluded from observing its negative effect on crystallisation. When the gel's polymer concentration increases, it reduces chain mobility and hence decreases the possibilities for more nuclei to form and grow. However, adding salt appears to overcome the addition of the polymer, which is shown by the occurrence of increased crystallisation over the polymer addition. The effect of salt on crystallisation is supported by the optical micrographs, which show that adding salt to the gel system considerably reduces pore size, indicating that the addition of salt greatly promotes nucleation.

Mixing a poor solvent with a good solvent in the gel system significantly enhances thermal stability, whilst preserving ionic conductivity. This preservation of ionic conductivity provides good evidence that there is competition between the high dielectric constant that the good solvent possesses on one hand (which helps in salt dissociation and frees the mobile ions), and the low viscosity that the poor solvent provides on the other (which increase the mobility of the free ions inside the polymer matrix). The noticeable enhancement of thermal stability can be attributed to the Flory Huggins interaction parameter, which affects solubility

parameters.

6.2 Future Work

As stated above, Chapter 4 showed that there are two temperature windows for different gelation mechanisms, and chapter 5 showed the effects that gel composition has on the usefulness of its properties. Given these findings, further work that investigated the effect of gelation temperature on the mechanical and electrical properties of these gels would be of particular worth.

References

1. Agrawal, R.C. and G.P. Pandey, Solid polymer electrolytes: materials designing and all-solid-state battery applications: an overview. *Journal of Physics D: Applied Physics*, 2008. **41**(22): p. 223001.
2. Ian M. Ward, H.V.S.A.H., Polymer gel electrolytes: Conduction mechanism and battery applications, in *Ionic interactions in natural synthetic macromolecules*, A.C.a.A. Perico, Editor 2012, John Wiley & Sons, Inc. p. 817–840.
3. Voice, A.M., et al., Thermoreversible polymer gel electrolytes. *Polymer*, 1994. **35**(16): p. 3363–3372.
4. S.S. Sekhon, P., S.A. Agnihorty, in: B.V.R. Chowdari, K. Lal, S.A. Agnihotry, N. Khare, P.C. Srivastava, S. Chandra, *Solid State Ionics, Science and Technology*, 1998.
5. Zhang, Q.M., V. Bharti, and G. Kavarnos, Poly(Vinylidene Fluoride) (PVDF) and its Copolymers, in *Encyclopedia of Smart Materials 2002*, John Wiley & Sons, Inc.
6. Junkyoung Lee, Y.K., Dong Hack Suh, Changjin Lee, Ionic conductivity and electrochemical properties of cross-linked poly[siloxane-g-oligo(ethylene oxide)] gel-type polymer electrolyte. *Electrochimica Acta*, 2004. **50**: p. 351–356.
7. Barthel, J. and F. Feuerlein, Dielectric-Properties of Propylene Carbonate and Propylene Carbonate Solutions. *Journal of Solution Chemistry*, 1984. **13**(6): p. 393–417.
8. Ward, I.M., et al., Separator-free rechargeable lithium ion cells produced by the extrusion lamination of polymer gel electrolytes. *Journal of Power Sources*, 2006. **162**(2): p. 818–822.

9. Costa, C.M., et al., Poly(vinylidene fluoride)-based, co-polymer separator electrolyte membranes for lithium-ion battery systems. *Journal of Power Sources*, 2014. **245**: p. 779–786.
10. Watanabe, M., et al., High lithium ionic conductivity of polymeric solid electrolytes. *Die Makromolekulare Chemie, Rapid Communications*, 1981. **2**(12): p. 741–744.
11. Jiang, Z., B. Carroll, and K.M. Abraham, Studies of some poly(vinylidene fluoride) electrolytes. *Electrochimica Acta*, 1997. **42**(17): p. 2667–2677.
12. Kataoka, H., et al., Conduction Mechanisms of PVDF-Type Gel Polymer Electrolytes of Lithium Prepared by a Phase Inversion Process. *The Journal of Physical Chemistry B*, 2000. **104**(48): p. 11460–11464.
13. Song, J.Y., Y.Y. Wang, and C.C. Wan, Review of gel-type polymer electrolytes for lithium-ion batteries. *Journal of Power Sources*, 1999. **77**(2): p. 183–197.
14. A. M. Voice, G.R.D., I. M. Ward, Structure of poly (vinylidene fluoride) gel electrolytes. *Polymer Gels and Networks*, 1997. **5**: p. 123–144.
15. Ouano, A.C. and J.A. Carothers, Dissolution dynamics of some polymers: Solvent-polymer boundaries. *Polymer Engineering & Science*, 1980. **20**(2): p. 160–166.
16. Huggins, M.L., Solutions of Long Chain Compounds. *The Journal of Chemical Physics*, 1941. **9**(5): p. 440–440.
17. Flory, P.J., Thermodynamics of High Polymer Solutions. *The Journal of Chemical Physics*, 1942. **10**(1): p. 51–61.
18. Hansen, C.M., HANSEN SOLUBILITY PARAMETERS A User's Handbook. 2nd ed2007: Taylor & Francis Group.

19. Fenton, D.E., J.M. Parker, and P.V. Wright, Complexes of Alkali-Metal Ions with Poly(Ethylene Oxide). *Polymer*, 1973. **14**(11): p. 589–589.
20. DF. Shiver, P.G.B., Nature of polymer electrolytes, in *Solid state electrochemistry*, P.G. Bruce, Editor 1995, Cambridge University Press. p. 95.
21. Wieczorek, W., et al., Effect of Salt Concentration on the Conductivity of PEO-Based Composite Polymeric Electrolytes. *The Journal of Physical Chemistry B*, 1998. **102**(44): p. 8725–8731.
22. Fontanella, J.J., et al., Electrical Relaxation in Pure and Alkali Metal-Thiocyanate Complexed Poly(Ethylene Oxide) 1983: Defense Technical Information Center.
23. Croce, F., et al., Nanocomposite polymer electrolytes for lithium batteries. *Nature*, 1998. **394**(6692): p. 456–458.
24. Weston, J.E. and B.C.H. Steele, Effects of inert fillers on the mechanical and electrochemical properties of lithium salt-poly(ethylene oxide) polymer electrolytes. *Solid State Ionics*, 1982. **7**(1): p. 75–79.
25. Yang, C.-M., et al., Gel-type polymer electrolytes with different types of ceramic fillers and lithium salts for lithium-ion polymer batteries. *Journal of Power Sources*, 2006. **156**(2): p. 574–580.
26. Capuano, F., F. Croce, and B. Scrosati, Composite Polymer Electrolytes. *Journal of The Electrochemical Society*, 1991. **138**(7): p. 1918–1922.
27. Osada, Y., *Gels Handbook* 2001: Acad. Press.
28. T. Iijima, Y.T.a.N.E., Quasi-solid organic electrolytes gelatinized with poly methylmethacrylate and their applications for lithium batteries. *Denki Kagaku*, 1985. **53**.

29. Appetecchi, G.B., F. Croce, and B. Scrosati, Kinetics and stability of the lithium electrode in poly(methylmethacrylate)-based gel electrolytes. *Electrochimica Acta*, 1995. **40**(8): p. 991–997.
30. Watanabe, M., et al., Ionic conductivity of hybrid films based on polyacrylonitrile and their battery application. *Journal of Applied Polymer Science*, 1982. **27**(11): p. 4191–4198.
31. Watanabe, M., et al., Ionic conductivity of hybrid films composed of polyacrylonitrile, ethylene carbonate, and LiClO₄. *Journal of Polymer Science: Polymer Physics Edition*, 1983. **21**(6): p. 939–948.
32. Appetecchi, G.B. and B. Scrosati, A lithium ion polymer battery. *Electrochimica Acta*, 1998. **43**(9): p. 1105–1107.
33. Kuwahara, N., et al., Phase separation in an unstable system polydimethylsiloxane-diethyl carbonate. *Physical Review A*, 1982. **25**(6): p. 3449–3452.
34. Lal, J. and R. Bansil, Light-scattering study of kinetics of spinodal decomposition in a polymer solution. *Macromolecules*, 1991. **24**(1): p. 290–297.
35. Lee, K.-W.D., P.K. Chan, and X. Feng, Morphology development and characterization of the phase-separated structure resulting from the thermal-induced phase separation phenomenon in polymer solutions under a temperature gradient. *Chemical Engineering Science*, 2004. **59**(7): p. 1491–1504.
36. Southall, J.P., et al., Ionic conductivity and viscosity correlations in liquid electrolytes for incorporation into PVDF gel electrolytes. *Solid State Ionics*, 1996. **85**(1-4): p. 51–60.
37. Ward, I.M., et al., NMR studies of ionic mobility in polymer gel electrolytes for advanced lithium batteries. *Journal of Power Sources*, 1999. **81**: p. 700–704.

38. Williamson, M.J., H.V.S. Hubbard, and I.M. Ward, NMR measurements of self diffusion in polymer gel electrolytes. *Polymer*, 1999. **40**(26): p. 7177–7185.
39. Hubbard, H.V.S.A. and I.M. Ward, POLY 285-Polymer gel composition studies using T1 NMR. Abstracts of Papers of the American Chemical Society, 2008. **235**.
40. Kim, B.S., et al., Thermoreversible gelation of poly(vinylidene fluoride) in propylene carbonate. *Journal of Macromolecular Science-Physics*, 2004. **B43**(4): p. 741–754.
41. Cho, J.W., H.Y. Song, and S.Y. Kim, Thermoreversible gelation of poly(vinylidene fluoride) in γ -butyrolactone solution. *Polymer*, 1993. **34**(5): p. 1024–1027.
42. Tazaki, M., et al., Crystallization and gelation of poly(vinylidene fluoride) in organic solvents. *Journal of Applied Polymer Science*, 1997. **65**(8): p. 1517–1524.
43. Hong, P.D. and C.M. Chou, Phase separation and gelation behaviors in poly(vinylidene fluoride)/tetra(ethylene glycol) dimethyl ether solutions. *Polymer*, 2000. **41**(23): p. 8311–8320.
44. Mal, S., P. Maiti, and A.K. Nandi, On the Gelation Rates of Thermoreversible Poly(vinylidene fluoride) Gels. *Macromolecules*, 1995. **28**(7): p. 2371–2376.
45. Zhang, P., et al., Effect of SSIE structure of Cu-exchanged β and γ on the selectivity for synthesis of diethyl carbonate by oxidative carbonylation of ethanol: A comparative investigation. *Catalysis Today*, 2010. **149**(1–2): p. 202–206.
46. Abe, T., et al., Sensitivity to Ultraviolet-Light of Tobacco Mosaic-Virus Modified by Cetyltrimethylammonium Bromide. *Microbiology and Immunology*, 1981. **25**(11): p. 1129–1138.

47. Almdal, K., et al., Towards a phenomenological definition of the term 'gel'. *Polymer Gels and Networks*, 1993. **1**(1): p. 5–17.
48. Sperling, L.H., Gel and Gelation, in *Introduction to Physical Polymer Science*, 2005, Wiley. p. 478–479.
49. Rogovina, L.Z., V.G. Vasil'ev, and E.E. Braudo, Definition of the concept of polymer gel. *Polymer Science Series C*, 2008. **50**(1): p. 85–92.
50. Aharoni, S.M. and S.F. Edwards, Gels of rigid polyamide networks. *Macromolecules*, 1989. **22**(8): p. 3361–3374.
51. Totosaus, A., et al., A review of physical and chemical protein-gel induction. *International Journal of Food Science and Technology*, 2002. **37**(6): p. 589–601.
52. Chen, C.-Y., et al., Phase-Separation-Induced Gelation of Poly(9,9-dioctylfluorene)/Methylcyclohexane Solution. *Macromolecules*, 2010. **43**(9): p. 4346–4354.
53. Chakrabarty, K., T.A.P. Seery, and R.A. Weiss, Characterization of Ionomer Solutions. 1. Phase Behavior and Gelation of Sulfonated Polystyrene Ionomers in Decalin. *Macromolecules*, 1998. **31**(21): p. 7385–7389.
54. Osada, Y. and A. Khokhlov, *Polymer Gels and Networks 2001*: Taylor & Francis.
55. Darras, O. and R. Séguéla, Crystallization-induced gelation of ethylene/1-butene copolymers over a wide crystallinity range. *Colloid and Polymer Science*, 1995. **273**(8): p. 753–765.
56. Rubinstein, M. and R.H. Colby, *Polymer Physics 2003*: OUP Oxford.
57. Cahn, J.W., Phase Separation by Spinodal Decomposition in Isotropic Systems. *The Journal of Chemical Physics*, 1965. **42**(1): p. 93–99.

58. Lin, D.-J., et al., Effect of salt additive on the formation of microporous poly(vinylidene fluoride) membranes by phase inversion from LiClO₄/Water/DMF/PVDF system. *Polymer*, 2003. **44**(2): p. 413–422.
59. van de Witte, P., et al., Phase separation processes in polymer solutions in relation to membrane formation. *Journal of Membrane Science*, 1996. **117**(1–2): p. 1–31.
60. Work, W., et al., Definition of terms related to polymer blends, composites, and multiphase polymeric materials (IUPAC Recommendations 2004). *Pure and applied chemistry*, 2004. **76**(11): p. 1985–2007.
61. Xiong, X. and S.F. Li, Dual UV-absorbing background electrolytes for simultaneous separation and detection of small cations and anions by capillary zone electrophoresis. *Electrophoresis*, 1998. **19**(12): p. 2243–51.
62. Carraher, C.E., *Seymour/Carraher's Polymer Chemistry: Sixth Edition* 2003: Taylor & Francis.
63. Höpken, J., et al., Melting, crystallization, and solution behavior of chain molecules with hydrocarbon and fluorocarbon segments. *Die Makromolekulare Chemie*, 1988. **189**(4): p. 911–925.
64. Sawyer, L.C., D.T. Grubb, and G.F. Meyers, *Polymer Microscopy* 2008: Springer.
65. Ehrenstein, G.W., *Polymeric Materials: Structure, Properties, Applications* 2001: Hanser Publishers.
66. Ehrenstein, G.W., *Polymeric materials : structure properties applications* 2000, Alemania: Hanser.
67. Cassagnau, P., et al., Application of the rubber elasticity theory to the co-crosslinking of ethylene vinyl acetate and ethylene methyl acrylate

- copolymers by transesterification. *Polymer*, 1993. **34**(9): p. 1975–1978.
68. Flory, P.J. and J. Rehner, Statistical Mechanics of Cross-Linked Polymer Networks II. Swelling. *The Journal of Chemical Physics*, 1943. **11**(11): p. 521–526.
 69. Rosenberg, B.A., *Polymer Networks* 1991, Moscow.
 70. Rogovina, L.Z., et al., The reversible network formation in polydimethyl-siloxanes with side carboxyl groups. *Makromolekulare Chemie. Macromolecular Symposia*, 1991. **45**(1): p. 53–61.
 71. Mark, J.E., B. Erman, and M. Roland, *The Science and Technology of Rubber* 2013: Elsevier Science.
 72. Roundy, D. and M. Rogers, Exploring the thermodynamics of a rubber band. *American Journal of Physics*, 2013. **81**(1): p. 20–23.
 73. Zhang, X., Z. Hu, and Y. Li, Rubber elasticity of polyacrylamide gels in high network concentration. *Polymer*, 1998. **39**(13): p. 2783–2788.
 74. E. Guth, H.M., *Chem.*, 1934. **56**(93).
 75. W. Kuhn, A., *Chem.*, 1938. **51**(640).
 76. Kuhn, W., Dependence of the average transversal on the longitudinal dimensions of statistical coils formed by chain molecules. *Journal of Polymer Science*, 1946. **1**(5): p. 380–388.
 77. Ferry, J.D., *Viscoelastic Properties of Polymers* 1980: Wiley.
 78. Mark, J.E., *Physical Properties of Polymers Handbook* 2007: Springer.
 79. Frenkel, *Acta Physicochim*, 1938. **9**: p. 235.

80. Frenkel, J., A Theory of Elasticity, Viscosity and Swelling in Polymeric Rubber-Like Substances. *Rubber Chemistry and Technology*, 1940. **13**(2): p. 264–274.
81. Flory, P.J., Statistical Mechanics of Swelling of Network Structures. *The Journal of Chemical Physics*, 1950. **18**(1): p. 108–111.
82. Sperling, L.H., Flory-Rehner Theory, in *Introduction to Physical Polymer Science* 2005, Wiley. p. 472.
83. Huggins, M.L., Some Properties of Solutions of Long-chain Compounds. *The Journal of Physical Chemistry*, 1942. **46**(1): p. 151–158.
84. Huggins, M.L., Theory of Solutions of High Polymers¹. *Journal of the American Chemical Society*, 1942. **64**(7): p. 1712–1719.
85. Flory, P.J., *Principles of Polymer Chemistry* 1953: Cornell University Press.
86. Miller-Chou, B.A. and J.L. Koenig, A review of polymer dissolution. *Progress in Polymer Science*, 2003. **28**(8): p. 1223–1270.
87. Hildebrand, J.H., *The solubility of Non-Electrolytes* 1936: New York:Reinhold.
88. Hansen, C.M., The Three Dimensional Solubility Parameter Key to Paint Component Affinities: 1.Solvents Plasicizers, Polymers and Resins. *Journal of Paint Technology*, 1967. **39**(505).
89. Hansen, C.M., *Hansen Solubility Parameters: A User's Handbook*, Second Edition 2012: Taylor & Francis.
90. Liu, Y. and B. Shi, Determination of Flory interaction parameters between polyimide and organic solvents by HSP theory and IGC. *Polymer Bulletin*, 2008. **61**(4): p. 501–509.

91. Blanks, R.F. and J.M. Prausnitz, Thermodynamics of Polymer Solubility in Polar and Nonpolar Systems. *Industrial & Engineering Chemistry Fundamentals*, 1964. **3**(1): p. 1–8.
92. Boudin, F., et al., Microporous PVdF gel for lithium-ion batteries. *Journal of Power Sources*, 1999. **81–82**(0): p. 804–807.
93. Tsuchida, E., H. Ohno, and K. Tsunemi, Conduction of lithium ions in polyvinylidene fluoride and its derivatives—I. *Electrochimica Acta*, 1983. **28**(5): p. 591–595.
94. Mohamed, N.S. and A.K. Arof, Investigation of electrical and electrochemical properties of PVDF-based polymer electrolytes. *Journal of Power Sources*, 2004. **132**(1–2): p. 229–234.
95. Eisenmenger, W., H. Schmidt, and B. Dehlen, Space charge and dipoles in polyvinylidene fluoride. *Brazilian Journal of Physics*, 1999. **29**: p. 295–305.
96. Priya, L. and J.P. Jog, Poly(vinylidene fluoride)/clay nanocomposites prepared by melt intercalation: Crystallization and dynamic mechanical behavior studies. *Journal of Polymer Science Part B: Polymer Physics*, 2002. **40**(15): p. 1682–1689.
97. Lang, S.B. and S. Muensit, Review of some lesser-known applications of piezoelectric and pyroelectric polymers. *Applied Physics A*, 2006. **85**(2): p. 125–134.
98. Lovinger, A.J., *Ferroelectric Polymers*. *Science*, 1983. **220**(4602): p. 1115–1121.
99. Layek, R.K., et al., Physical and mechanical properties of poly(methyl methacrylate) -functionalized graphene/poly(vinylidene fluoride) nanocomposites: Piezoelectric β polymorph formation. *Polymer*, 2010. **51**(24): p. 5846–5856.

100. Briber, R.M. and F. Khoury, The morphology of poly(vinylidene fluoride) crystallized from blends of poly(vinylidene fluoride) and poly(ethyl acrylate). *Journal of Polymer Science Part B: Polymer Physics*, 1993. 31(10): p. 1253–1272.
101. Park, Y.J., Y.S. Kang, and C. Park, Micropatterning of semicrystalline poly(vinylidene fluoride) (PVDF) solutions. *European Polymer Journal*, 2005. 41(5): p. 1002–1012.
102. He, L., et al., Facile and effective promotion of β crystalline phase in poly(vinylidene fluoride) via the incorporation of imidazolium ionic liquids. *Polymer International*, 2013. 62(4): p. 638–646.
103. El Mohajir, B.-E. and N. Heymans, Changes in structural and mechanical behaviour of PVDF with processing and thermomechanical treatments. 1. Change in structure. *Polymer*, 2001. 42(13): p. 5661–5667.
104. Noland, J.S., et al., Compatible High Polymers—Poly(Vinylidene Fluoride) Blends with Homopolymers of Methyl and Ethyl Methacrylate. *Advances in Chemistry Series*, 1971(99): p. 15–&.
105. Lando, J.B., H.G. Olf, and A. Peterlin, Nuclear magnetic resonance and x-ray determination of the structure of poly(vinylidene fluoride). *Journal of Polymer Science Part A-1: Polymer Chemistry*, 1966. 4(4): p. 941–951.
106. Shuford, R.J., et al., Characterization and Piezoelectric Activity of Stretched and Poled Poly(Vinylidene Fluoride) .1. Effect of Draw Ratio and Poling Conditions. *Polymer Engineering and Science*, 1976. 16(1): p. 25–35.
107. Mcgrath, J.C. and I.M. Ward, High Effective Draw as a Route to Increased Stiffness and Electrical Response in Poly(Vinylidene Fluoride). *Polymer*, 1980. 21(8): p. 855–857.

108. Matsushige, K., et al., The α - β Crystal Transformation of Poly(Vinylidene Fluoride) under Tensile and Compressional Stresses. *Polymer*, 1980. **21**(12): p. 1391–1397.
109. Doll, W.W. and J.B. Lando, The polymorphism of poly(vinylidene fluoride). II. The effect of hydrostatic pressure. *Journal of Macromolecular Science, Part B*, 1968. **2**(2): p. 219–233.
110. Lu, F.J. and S.L. Hsu, Study of the Crystallization Behavior of Poly(Vinylidene Fluoride) from the Melt under the Effect of an Electric-Field. *Macromolecules*, 1986. **19**(2): p. 326–329.
111. Prest, J.W.M. and D.J. Luca, The formation of the gamma phase from the alpha and beta polymorphs of polyvinylidene fluoride. *Journal of Applied Physics*, 1978. **49**(10): p. 5042–5047.
112. Gregorio, J.R. and M. Cestari, Effect of crystallization temperature on the crystalline phase content and morphology of poly(vinylidene fluoride). *Journal of Polymer Science Part B: Polymer Physics*, 1994. **32**(5): p. 859–870.
113. S. Satapathy, P.K.G., Santosh Pawar, K. B. R. Varma, Crystallization of Beta-phase Poly (vinylidene fluoride) films using dimethyl sulfoxide (DMSO) solvent and at suitable annealing condition. 2008.
114. Gregorio, R., Determination of the alpha, beta, and gamma crystalline phases of poly(vinylidene fluoride) films prepared at different conditions. *Journal of Applied Polymer Science*, 2006. **100**(4): p. 3272–3279.
115. Kobayashi, M., K. Tashiro, and H. Tadokoro, Molecular Vibrations of Three Crystal Forms of Poly(vinylidene fluoride). *Macromolecules*, 1975. **8**(2): p. 158–171.

116. Paramita Jaya, R. and T. Kohji, Phase-transition behavior of a crystalline polymer near the melting point: case studies of the ferroelectric phase transition of poly(vinylidene fluoride) and the β -to- α transition of trans-1,4-polyisoprene. *Polymer Journal*, 2013.
117. Dillon, D.R., et al., On the structure and morphology of polyvinylidene fluoride–nanoclay nanocomposites. *Polymer*, 2006. **47**(5): p. 1678–1688.
118. Barthel, J., R. Neueder, and H. Roch, Density, Relative Permittivity, and Viscosity of Propylene Carbonate + Dimethoxyethane Mixtures from 25 °C to 125 °C. *Journal of Chemical & Engineering Data*, 2000. **45**(6): p. 1007–1011.
119. Shiao, H.C., et al., Low temperature electrolytes for Li-ion PVDF cells. *Journal of Power Sources*, 2000. **87**(1–2): p. 167–173.
120. Moumouzias, G. and G. Ritzoulis, Viscosities and densities for propylene carbonate + toluene at 15, 20, 25, 30, and 35.degree.C. *Journal of Chemical & Engineering Data*, 1992. **37**(4): p. 482–483.
121. Zhang, S.S., et al., Effect of propylene carbonate on the low temperature performance of Li-ion cells. *Journal of Power Sources*, 2002. **110**(1): p. 216–221.
122. Tobishima, S., J. Yamaki, and T. Okada, Propylene Carbonate Ether Mixed-Solvent Electrolytes for Lithium Secondary Batteries. *Denki Kagaku*, 1985. **53**(3): p. 173–177.
123. Rivas, M.A., et al., Permittivity and density of binary systems of {dimethyl or diethyl carbonate}+ n-dodecane from from T=(288.15 to 328.15) K. *The Journal of Chemical Thermodynamics*, 2004. **36**(3): p. 183–191.

124. A. Rodríguez, J.C., A. Domínguez, and J. Tojo, Viscosities of Dimethyl Carbonate or Diethyl Carbonate with Alkanes at Four Temperatures. New UNIFAC-VISCO Parameters. *J. Chem. Eng. Data*, 2003. **48**: p. 146–151.
125. Aurbach, D., et al., The Study of Electrolyte Solutions Based on Ethylene and Diethyl Carbonates for Rechargeable Li Batteries. *Journal of the Electrochemical Society*, 1995. **142**(9): p. 2873–2882.
126. Fujii, T., M. Takehara, and M. Ue, Application of LiBOB as an Electrolyte Salt For 4 V Class Lithium Ion Rechargeable Cells.
127. Rivas, M.A., et al., Permittivity and density of binary systems of {dimethyl or diethyl carbonate}+n-dodecane from $T=(288.15\text{ to }328.15)$ K. *The Journal of Chemical Thermodynamics*, 2004. **36**(3): p. 183–191.
128. G.Mezger, T., *The Rheology Handbook*2002, Hannover, Germany: Hannoprint.
129. Menard, K.P., *Dynamic Mechanical Analysis A Practical Introduction*1999: CRC Press.
130. Pungor, E., *A Practical Guide to Instrumental Analysis*1995, Florida: Boca Raton.
131. Wunderlich, B., *Thermal Analysis*1990, New York: Academic Press.
132. Dean, A.J., *The Analytical Chemistry Handbook*1995, New York: McGraw Hill, Inc.
133. Voice, A.M., G.R. Davies, and I.M. Ward, Structure of poly(vinylidene fluoride) gel electrolytes. *Polymer Gels and Networks*, 1997. **5**(2): p. 123–144.

134. Rosenberg, Y., et al., The sol/gel contribution to the behavior of γ -irradiated poly(vinylidene fluoride). *Journal of Applied Polymer Science*, 1991. **43**(3): p. 535–541.
135. Macdonald, J.R., Impedance spectroscopy. *Annals of Biomedical Engineering*, 1992. **20**(3): p. 289–305.
136. Barsoukov, E. and J.R. Macdonald, *Impedance Spectroscopy: Theory, Experiment, and Applications* 2005: Wiley.
137. Bower, D.I., *An Introduction to Polymer Physics* 2002: Cambridge University Press.
138. Myers, H.P., *Introductory Solid State Physics*. 2nd ed 2002: CRC Press.
139. Glatter, K., *X-ray scattering* 1982: Academic Press.
140. Watt, I.M., *The principles and practice of electron microscopy* 1996, Cambridge; New York: Cambridge University Press.
141. Guojie, W. and P. Huiming, INTERACTIONS AMONG COMPONENTS AND GELATION OF PVDF-BASED GEL ELECTROLYTES. *Acta Polymerica Sinica*, 2001. **1**(6): p. 702–705.
142. Tian, L.-y., X.-b. Huang, and X.-z. Tang, Study on morphology behavior of PVDF-based electrolytes. *Journal of Applied Polymer Science*, 2004. **92**(6): p. 3839–3842.
143. Shimizu, H., et al., Sol-gel transitions of poly(vinylidene fluoride) in organic solvents containing LiBF₄. *Polymer Journal*, 2011. **43**(6): p. 540–544.
144. Bottino, A., et al., Solubility parameters of poly(vinylidene fluoride). *Journal of Polymer Science Part B: Polymer Physics*, 1988. **26**(4): p. 785–794.

145. Barton, A.F.M., CRC handbook of solubility parameters and other cohesion parameters 1983: CRC Press.
146. Welch, G.J. and R.L. Miller, Crystallization of Poly(Vinylidene Fluoride)—Equilibrium Melting-Point and Heat of Fusion of Alpha-Polymorph. *Journal of Polymer Science Part B-Polymer Physics*, 1976. **14**(9): p. 1683–1692.
147. Rosenberg, Y., et al., The sol/gel contribution to the behavior of γ -irradiated poly(vinylidene fluoride). *Journal of Applied Polymer Science*, 1991. **43**(3): p. 535–541.
148. Okabe, M., et al., The Flory-Huggins Interaction Parameter and Thermoreversible Gelation of Poly(vinylidene fluoride) in Organic Solvents. *Polymer Journal*, 2003. **35**(10): p. 798–798.
149. Abbrent, S., Lithium ion interactions in polymer gel electrolytes: Effect on structure, dynamics and morphology, 2000, Uppsala University.
150. Whang, W.-T. and C.-L. Lu, Effects of polymer matrix and salt concentration on the ionic conductivity of plasticized polymer electrolytes. *Journal of Applied Polymer Science*, 1995. **56**(12): p. 1635–1643.
151. Shiao, H.C., et al., Low temperature electrolytes for Li-ion PVDF cells. *Journal of Power Sources*, 2000. **87**(1–2): p. 167–173.
152. Abbrent, S., et al., Crystallinity and morphology of PVdF-HFP-based gel electrolytes. *Polymer*, 2001. **42**(4): p. 1407–1416.
153. Rim, P.B. and J.P. Runt, Melting-Point Depression in Crystalline Compatible Polymer Blends. *Macromolecules*, 1984. **17**(8): p. 1520–1526.